# ABRASION FAILURE OF LINING RUBBER ON AGITATOR BLADES IN THE LEACHING CIRCUIT OF MINERAL PROCESSING INDUSTRIES

# A.K.M. Shamsul Huda Akan

**Dedicated To My Parents**

# Statement of Sources

I hereby declare that this submission is, to the best of my knowledge and belief, original, except as acknowledged in the text. I also state that the material contained herein has not been previously submitted, either in whole or in part, for a degree at Central Queensland University, or any other institution.

A.K.M. Shamsul Huda Akan

# Abstract

The failure of agitator blades was an issue of major concern in the leaching circuit of the Australian Magnesium Corporation (AMC) pilot plant in Gladstone. The aim of this project was to investigate the causes of the failure of the agitator blades and to make some recommendations to help avoid the problem in the future. At the start of this thesis, a comprehensive failure analysis was carried out in order to understand the potential failure mechanisms operating in the slurry tanks. A number of potential failure mechanisms were identified and these included erosive slurry wear of the rubber and chemical and/or thermal degradation of the rubber. These failure mechanisms may also act synergistically. An experimental programme of research was planned to investigate the separate influences of slurry wear and chemical and/or thermal degradation of the rubber. The results of these tests were then used to extend our understanding of the failure of the agitator blades.

A slurry erosion test has been developed in order to quantify the erosion of bromobutyl rubber. The study investigated the effects of particle size, erosion time, slurry weight concentration and specimen velocity. Wear was measured using surface roughness measurements and scanning electron microscopy (SEM) of the worn surfaces. The degree of wear was found to increase with increased particle size, slurry weight concentration and erosion time and the wear appear to be at a maximum at a nominal angle of impact of the particles of approximately 40°. Wear appeared to decrease with increasing slurry velocities, but this may have been due to changes in particle shape. One of the key factors in the development of damage on the surface of the rubber was found to be wear of the abrading particles and the condition of the abrading particles needs to be taken into account when interpreting the results of slurry wear tests. In general the experimental results were found to be in good agreement with the predictions from the literature and a model has been developed in order to obtain a better understanding of slurry erosion.

In addition to the slurry wear tests, the chemical degradation behaviour of bromobutyl rubber was investigated by measuring hardness (shore A) and surface morphology of the rubber after exposure of the rubber to acid and water at 70°C. In acid,

the rubber hardness increased with time and whereas in water alone, the rubber hardness decreased. This indicated that the acid immersion had a hardening effect on the rubber and this may have played some part in the failure.

From this work, it is apparent that both slurry wear and exposure to acid and/or temperature have an effect on the degradation of the rubber. Particle size and shape had a major effect on damage accumulation rates, with most damage occurring with large, sharp particles. For tests where the particle size was below 3.35 mm the damage accumulation rate was insignificant. Morphological studies of the worn surfaces suggest that a major mechanism of damage was the formation of cracks which penetrated the rubber and exposed the underlying steel agitator blades to the acidic environment. Hardening of the rubber by exposure to the acid solution would have decreased the resilience of the rubber and may have increased the effect of the slurry wear on crack formation, but at this stage the coupled effects of slurry wear and chemical/thermal degradation have not been explored.

# Acknowledgements

Thanks are due to those without whose support this thesis would never have been completed. In particular to my supervisor, Professor Richard Clegg for his invaluable support, encouragement and wisdom. I am also indebted to my co-supervisor Dr. David M. Druskovich for his support and encouragement throughout my study at Central Queensland University (CQU).

My special thanks to Professor Waren Thorpe, Director, PELM Centre, Central Queensland University who approached and managed this project from Australian Magnesium Corporation (AMC).

I would also like to thank Mr. Gary Hoare for his generous help and advice during design and construction phase of the slurry erosion test apparatus and Jason Connor for his assistance and encouragement.

I am also grateful to Csabi Szeles for his generous help, support and friendship and Natalia Deeva for her assistance with SEM studies.

I must also thank to Benita Maudsley for her administrative support & assistance and Courtney Miles for his generous IT support.

Thanks to Central Queensland University and Australian Magnesium Corporation for providing financial assistance in the form of a university/industry collaborative grant.

And most importantly I extend my gratitude to my friends and family for their constant support and encouragement for the last two years, especially to my wife Sayeda and our children Qumrul, Rafiul and Hazera. Since she was born in July 2004, Hazera became a constant source of pleasure for my study. I am so much indebted to her.

# Contents

# List of Tables

# List of Figures

Chapter 1
# Introduction

Failure of materials is a common phenomenon in engineering applications. A wide range of coating materials is being used in order to prevent premature failures of equipment and components in service. Synthetic rubbers such as bromobutyl rubber have become popular as coating materials in chemical and mineral processing industries because of their low cost, chemical and wear resistance. Typical uses of bromobutyl rubbers include the lining of slurry mixing tanks, agitator shafts and blades and slurry pumps. Australian Magnesium Corporation (AMC) used coating bromobutyl rubber in order to prevent failure of agitator blades in erosive and corrosive magnesite slurries. Unexpected failures of agitator blades occurred in the leaching circuit of AMC in a period of three to eight months.

During 1997, AMC set up a demonstration plant at Gladstone, Queensland and operated for several years. The aim of the plant was to investigate the efficacy of the process for their proposed magnesium project at Stanwell near Rockhampton. One of the major issues was the high failure rate of agitator blades in the leaching circuit. The agitator blades were made of mild steel. They were coated with bromobutyl rubber in order to protect mild steel blade material from corrosive and erosive magnesium slurries. A number of premature failures of agitator blades occurred in a period of three to eight months in the service. It was observed that the failures occurred following the failure of coating bromobutyl rubber. The cost of such failures significantly affects the operational budget of mineral processing industries [1]. In order to reduce the operational costs, occurrence of these has to be reduced to an acceptable level. An understanding of wear mechanisms and wear rate of materials under various parameters are quite necessary in this case.

The life of agitator blades is largely controlled by the integrity of the bromobutyl rubber coating. Hence, the focus of this work is on the failure mechanisms of the bromobutyl rubber in magnesite slurries. It was noted that in practice, the wear of the rubber was most severe in the early stages of digestion, where the magnesite particle

1

sizes were largest and where the slurry concentration was highest. Hence, this work will particularly examine the effects of particle size, slurry concentration, erosion time and specimen velocity on the wear mechanisms of the rubber. Furthermore the experiment will give an insight into the effects of angle of impingement on wear behaviour.

## 1.1 The AMC Process

The AMC process consists of a number of major process areas including ore handling, leaching, dehydration, crystallisation, calcination and metal casting (as shown in Figure 1.1).



**Figure 1.1: Major manufacturing areas in the Australian Magnesium Corporation (AMC) [2].**

The leaching circuit is a major area in the AMC processes. It consists of bromobutyl rubber coated tanks connected through pipes in a number of stages such as mixing, purification and filtration. The equipment and components including agitator blades were coated with bromobutyl rubber. The failure of agitator blades was noticed in the slurry mixing tanks. Magnesite particles -3.5 mm in size were digested with concentrated hydrochloric acid in the slurry mixing tanks by means of rotating agitator blades. The hydrochloric acid entered the slurry mixing tank at 33% concentration and exited at 1-2% concentration. The temperature was maintained at $70^0C$ throughout the leaching circuit. Magnesite ore ($MgCO_3$) reacts with hydrochloric acid and produces

2

$MgCl_2$ and $H_2O$. Carbon dioxide gas is evolved during the reaction process. The reaction occurring in the slurry mixing tank may be represented by the following equation.

$$MgCO_3 + 2HCl = MgCl_2 + H_2O + CO_2 \qquad (1.1)$$
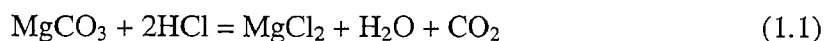
For a period in service, it was observed that the bromobutyl rubber coating had failed causing the exposure of the underlying mild steel blade material to the acidic slurry medium. Consequently, the mild steel agitator blades corroded and failed rapidly. It was postulated that the failure occurred as a result of abrasive erosion of the coating rubber with solid particles in the magnesite slurry.

## 1.2 Failure mechanisms

Failed rubber parts, slurry chemical information and magnesite ore were obtained in order to investigate the failure processes and to understand the wear mechanisms. A number of techniques, for example, Scanning Electron Microscopy (SEM) and X-ray diffraction (X-RD) were used in this investigation.

The SEM studies reported that the failure occurred as a result of progressive fatigue cracks in the rubber surface by slurry erosion. The cracks resulted from erosion due to repeated impact of slurry particles on the rubber surface. It was considered in the investigation that erosion would be further accelerated by chemical degradation of bromobutyl rubber in the acidic slurry medium. XRD showed that impurity content such as silica, which was suspected to be influencing erosion, was insignificant in the magnesite ore. Based on the outcomes of the failure analysis (refer to Chapter 3) test methods were established to determine erosion and chemical degradation of bromobutyl rubber.

## 1.3 Slurry erosion

Slurry erosion is a process by which material is removed from the layers of a surface impacted by a stream of abrasive particles in a liquid medium [3]. This is a common mode of wear in slurry handling processes. The direction and flow characteristics of impacting solid particles on the target surface in a turbulent slurry environment are quite complex. The slurry abrasive wear, commonly termed as slurry erosion, is a major

concern for numerous industries such as slurry mixing and transportation in alumina and magnesium refineries, coal washing plants and cement industries.

The common solutions for reducing slurry erosion are to minimise solid particle size, liquid flow velocity, slurry solid concentration and using the most wear resistant materials available. Until recently, the majority of research in slurry erosion has focused on empirical test methods. The work in this thesis mainly focuses on test methods. In practice, simulating the practical industrial situations in the controlled laboratory environment has been impossible. As a result, researchers tend to be turning towards computational models to obtain results for better prediction of wear in slurry process [4]. A slurry erosion model has been developed based on the modifications of an existing model. The details of this model are described in Chapter 5 of this thesis.

## 1.4 Slurry erosion test method

Standardized test methods often do not simulate practical industrial conditions. A number of these methods used by researchers in wear was studied (refer to Chapter 6). Most of them do not simulate conditions close to AMC process. Hence, the slurry erosion test method was established in order to simulate some of the practical industrial conditions in AMC process.

This test method is a modified version of slurry-pot erosion test apparatus used by Clarke [5] in his work. Bromobutyl rubber specimen wrapped around the mandrel will be rotating to cause wear of rubber while the magnesite slurry is in agitation. A detailed description with diagrams is placed in Chapter 6 of this thesis.

This method will quantify the wear of bromobutyl rubber against nominal impingement angle of attacks by magnesite particles. The test parameters include particle size, slurry concentration, and erosion time and specimen velocity. This method will also determine the wear mechanisms by examining eroded rubber specimens.

## 1.5 Rubber degradation test method

Hardness (shore A) is one of the major properties that can significantly affect the erosion of rubber. In the AMC process, erosion of bromobutyl rubber was considered to be due to the change in rubber properties. A number of ASTM standard test methods were studied to carry out tests in order to determine the rubber degradation in AMC process. None of

them were simulating AMC process conditions reasonably closely. Hence, a chemical degradation test method was established in order to simulate most of the AMC conditions.

This test method will investigate how hardness affected bromobutyl rubber in the acidic slurry environment. SEM studies and EDS analysis will be carried out to investigate surface topography, morphology and any inclusions in the rubber surface. The limitation of this test method is that it is not capable of investigating chemical changes, if occurred, in the rubber main structure. A detailed description of the method with a schematic diagram is shown in Chapter 4 of this thesis.

## 1.6 Thesis structure

This thesis consists of nine chapters and two appendices:

Chapter 1 provides a short description on topics such as AMC processes, slurry erosive wear, failure mechanisms and test methods. It also discusses the significance of the problem, aims and structure of the thesis.

Chapter 2 is literature review, particularly slurry erosive wear caused by the slurry solid particles.

Chapter 3 presents a failure analysis of the failed bromobutyl rubber coatings in the AMC process. This investigation includes the results of particle analysis, X-Ray diffraction and SEM techniques.

Chapter 4 describes the chemical degradation test method, rubber degradation results and mechanisms.

Chapter 5 describe the modelling of slurry erosive wear of rubber material in a liquid slurry medium.

Chapter 6 describes the experimental set up, design and materials selection and experimental procedures for the abrasion-erosion wear of materials especially the rubber material.

Chapter 7 described the results obtained by slurry erosion experiments. This chapter mainly focuses the results of eroded bromobutyl rubber in the light of the present and previous work.

Chapter 8 discusses the results described in chapter 7. The discussions include surface roughness of bromobutyl rubber, wear mechanisms and particle analysis.

Chapter 9 presents conclusions, limitations and future direction of this work.

## 1.7 References

1.  Gates, J.F. 2003, "Material selection for wear," A seminar handout on Materials Selection at Gladstone, Australia, pp.1-11.
2.  Internet source - Australian Magnesium Corporation's previous website.
3.  Mbabazi, J.G., Sheer, T. J., and Shandu, R., 2000, "A model to predict erosion on mild steel surfaces impacted by boiler fly ash particles", Wear, Vol. 257, pp. 612-624.
4.  Keating, A. 1999, "A model for the investigation of two-phase erosion-corrosion in complex geometries" A PhD thesis submitted to the Department of Mechanical Engineering, The University of Queensland.
5.  Clark, H. McI. 1993, "Test methods and applications for slurry erosion – A review," American Society for Testing and Materials, Philadelphia, USA, pp. 113-132.

Chapter 2

# Theory and Literature Review

## 2.1 Theory

*Wear* can be defined as a cumulative surface damage phenomenon in which material is removed from a body as small debris particles, primarily by mechanical processes. It consists of a number of processes that can take place by themselves or in combination, resulting in material removal from contacting surfaces through a complex combination of local shearing, plowing, gouging, welding and tearing [1].

A wear mode is a recognizable type of wear which occurs under a particular set of macroscopic conditions, producing characteristic physical and phenomenological manifestations by a particular microscopic mechanism or group of mechanisms [1]. A wear mode may be subdivided into three main parts, namely the following.

- Situation

- Manifestation

- Mechanism

*Situation* deals with mechanical conditions, for example, contact forces, sliding velocities and the apparent agent of damage such as abrasives. *Manifestation* involves the variation of wear rate over time, for example, an initiation period in which very little wear occurs followed by a rapid onset and acceleration of the wear rate. *Mechanism* is the fundamental microscopic process by which material is removed from the surface.

A number of commonly observed wear modes including erosive, adhesive, abrasive, corrosive and surface fatigue wear, are recognized by engineers and process scientists. In this particular study, it was thought that abrasive and erosive wear modes were likely to have occurred. Therefore, discussions were limited to abrasive and erosive wear.

## 2.1.1 Abrasive Wear

Abrasive wear is due to hard particles or protuberances that are forced against and move along a solid surface [1]. A model of abrasion process is shown in Figure 2.1. For a better understanding of the wear mode, it can be examined in terms of situation, mechanisms and manifestations.
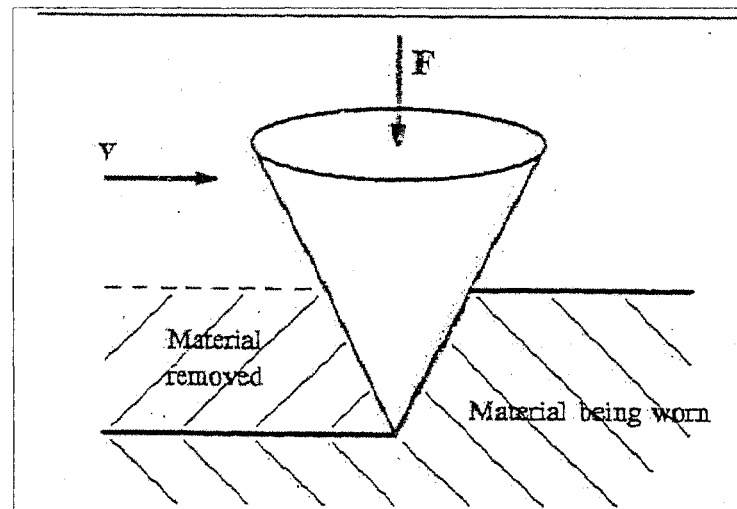


**Figure 2.1: The side view of the conical cutting tool model of abrasion process [1].**

### Situation

Usually, this occurs in situations such as ball mills, grinding on bonded abrasives and mineral transfer chutes. However, it may occur in slurry flow situations particularly at low impingement angle with high particle velocity. In this case, sliding is low and very fine scratches may be formed on the material surface. Abrasive particle size in this situation is moderate.

### Mechanisms

A number of mechanisms including micro-cutting, micro-plowing and micro-fracture may be involved. This is pictorially represented in Figures 2.2 to 2.4 using the model of metal cutting operation.

*Micro-ploughing mechanism of abrasion*
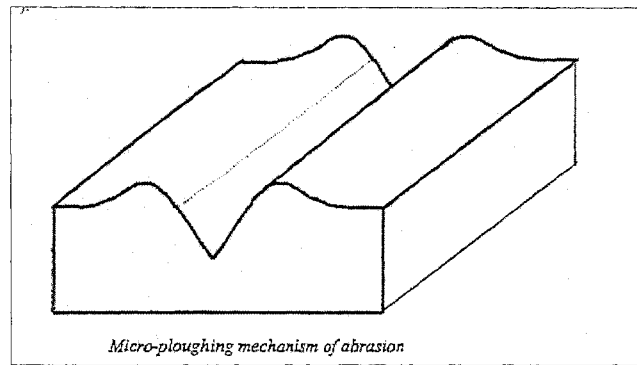
**Figure 2.2: Schematic view of micro-plowing mechanism of abrasive wear process [1].**

The micro-plowing mechanism (refer to Figure 2.2) works in a similar way to plowing of soil. The debris produced by this cutting mechanism is moved to both sides of the cutting tool [1].



*Micro-cutting mechanism of abrasion*
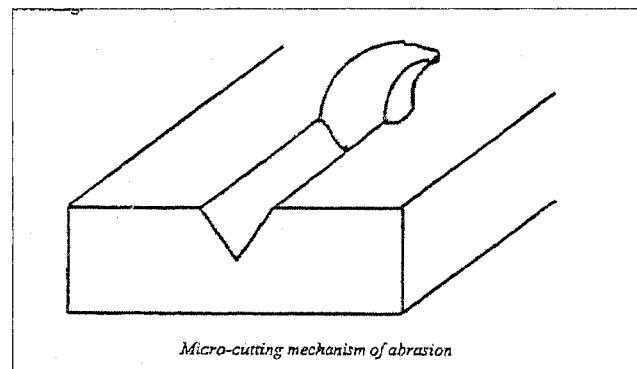
**Figure 2.3: Micro-cutting mechanisms occur as a result of abrasion wear [1].**

In this mechanism (refer to Figure 2.3), micro-chips move toward the direction of cutting which eventually can be discharged either side of the cutting tool [1].



*Micro-fracture mechanism of abrasion*
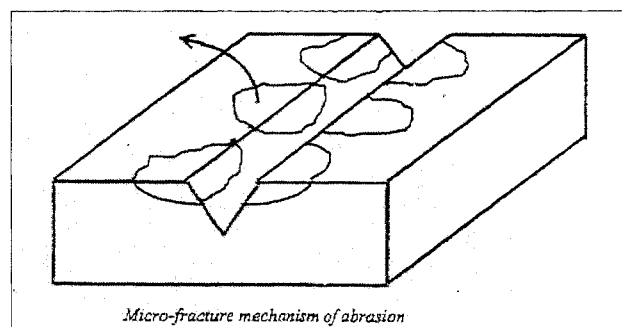
**Figure 2.4: Micro-fracture mechanism of abrasion [1].**

In the micro-fracture mechanism (refer to Figure 2.4), chips are produced by micro-fracture of the material [1].

**Manifestations**

Fine and/or rough scratches may be formed on rubber surfaces. Grooves can appear on a rubber surface when it turns into plastic.

The abrasive wear can occur in both dry and slurry media. It is typically categorized according to the type of contacts as follows

- Two-body contact, where an abrasive slides along a surface (see Figure 2.5a).

- Three-body contact, where the abrasive is caught between two surfaces (see Figure 2.5b).

The followings processes are involved in abrasive wear

- Plowing (where material is displaced from a groove to the sides).

- Micro-fatigue

- Wedge formation, the formation of a wedge in the front of an abrasive tip.

- Cutting, where a chip is removed.

- Micro cracking, where small cracks are found due to high stresses close to the abrasive [2].
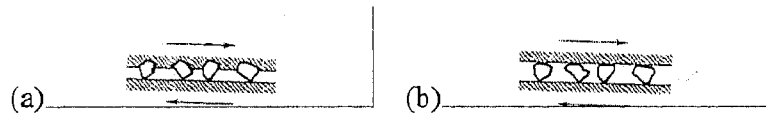
Figure 2.5: Two and three-body abrasive wear due to contact of particle and surface (a) two-body abrasion and (b) three-body abrasion [3].

## 2.1.2 Slurry Erosive Wear

Slurry erosive wear is due to the material exposed to a high velocity stream of slurry, which is a mixture of solid particles in a liquid medium [1]. This wear process can also be explained in terms of situation, mechanisms and manifestations as follows.
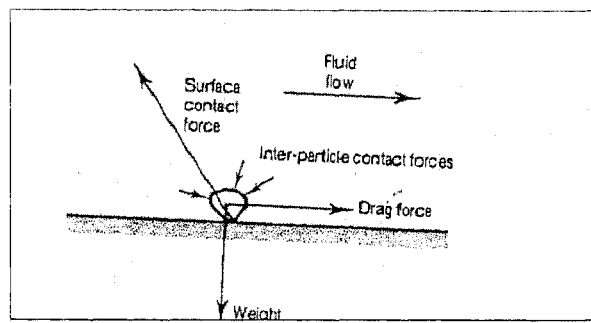
**Figure 2.6: Forces act on a particle in contact with a solid during erosion are shown in the above diagram [3].**

## Situation

In slurry flow situations, incident angles of solid particles on rubber surface vary. At a low impingement angle, it begins to merge with low stress abrasion. The contact forces may depend on particle mass, velocity and impingement angle. Sliding is low to moderate with minimum crushing of particles.
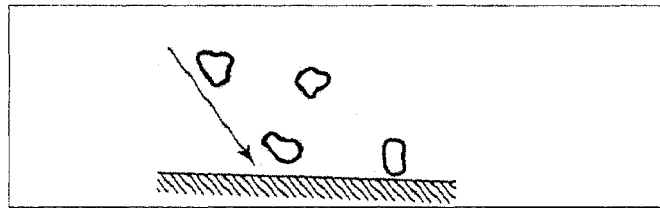


**Figure 2.7: Solid particles impacting on a material surface during erosion [3].**

## Mechanisms

Due to varying impingement angles a number of mechanisms including micro-cutting, micro-plowing and micro-fracture could be involved in the wear process. These mechanisms are associated mostly with particle velocity, impingement angle and particle size.

## Manifestations

Since slurry erosion is a slow process, the detailed damage may not appear smooth to naked eyes. The damages, however, may be observed under a microscope.

Slurry erosion can involve several wear modes, such as

- Abrasion-corrosion wear, which is the result of abrasive rubbing in the presence of a corrosive liquid.

- Crushing and grinding.

- High velocity erosion – can be destructive if the particle velocity is above 6-9 m/s.

- Low velocity erosion – occurs as a result of flow of slurry at low velocities.

- Saltation wear which is due to sediment transportation.

- Cavitation erosion – repeated nucleation, growth and violent collapse of cavities and bubbles in liquid [2].

### 2.1.3 Archard's wear model

Numerous models have been developed by researchers working in various fields of wear. Most of these models are distinguished from each other as they were based on a variety of situations, manifestations and mechanisms. Wear is a complex failure process. As a result, no universal model has yet been created. However, the model developed by Archard in 1950 is still accepted by many researchers. Though a number of his assumptions were not true in detail, the basic form of the model is still in use today [1]. The following is a derivation of Archard's model (refer to Equation 2.4).

For abrasive wear, the maximum volume of wear that can occur is given by

$$W = Ad \qquad (4.1)$$

where, $W$ is the volume of removed material, $A$ is the cross sectional area of the groove and $d$ is the sliding distance. The cross-sectional area of the groove can be expressed as

$$A = k_1 p \qquad (2.2)$$

where, $k_1$ is a shape dependent constant and $p$ is the depth of penetration, which in turn can be expressed as

$$p = k_2 L/H \qquad (2.3)$$

In Equation 4.3, $L$ is the load and $H$ is the hardness of the material and $k_2$ is another constant which is influenced by plowing/cutting, break down and rolling of the abrasive. Combining the equations 4.1, 4.2, 4.3 and 4.4 the following equation is obtained

$$W = k_3 Ld/H \hspace{3cm} (2.4)$$

where, $k_3 = k_1 \times k_2$ and $k_3$ is a wear constant.

## 2.2 Literature Review

Wear has been studied for many years and hence a great deal of information is available on the topic. A summary of wear due to slurry flows is presented in the following section.

Wear is a very complex subject. A number of failure modes can be identified for each type of wear, where each mode may result from one or more situations incorporating a number of wear mechanisms. A further complexity within the subject is to resolve the number of wear mechanisms that occur separately or simultaneously. For example, corrosive wear has four different failure modes and each mode has at least one situation with a number of mechanisms. Shook and Roco described at least eight different mechanisms for a particle to erode a surface and there are an equal number of environments that such wear can take place [29].

In studying erosion, research is primarily focused in understanding the wear mechanism and measuring wear on specific surfaces that are subjected to a slurry flow which have a varied mix of particle types and sizes. These studies may lead to good information on wear but the challenge to establish a universally accepted model on slurry erosion of materials still remains unsolved. During the last few decades, there has been significant progress in the research of slurry erosion. However, the challenge has not yet been overcome except for a few specific circumstances.

From the available published research, it is clear that a number of variables must be considered in order to evaluate wear due to slurry flow. Certainly, most of these variables do not contribute equally to wear for a particular situation and it may be quite impossible to control all of them. However, it may be possible to prevent wear by identifying and controlling the major variables responsible for wear. The following three factors should be considered for identification of major variables responsible for slurry erosive wear.

1. *The nature of the eroding particles*
2. *The fluid and concentration properties of the slurry*

*3. The nature of the wearing material*

## 2.2.1 Solid Particles

For a better understanding of slurry erosive wear, it is essential to know the nature and physical properties of solid particles impacting on material surfaces. The key factors that contribute to wear are discussed below based on the work of previous researchers.

**Particle size**

Changes in particle size affect the wear rate and many researchers have considered particle size one of major factors for wear as wear rate increases with increasing particle size (as shown in Figure 2.8) up to a threshold. Iwai and Nambu found that wear rate of elastomer materials increased with particle size up to 300 microns. The wear rate is independent of particle size above this value [4].
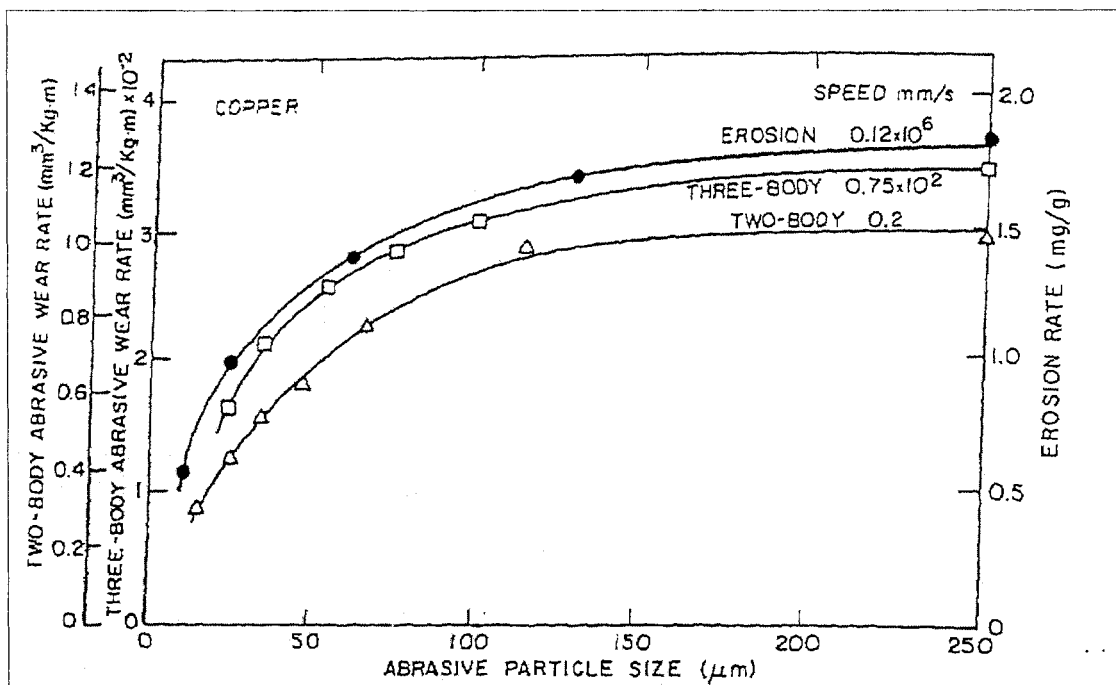


**Figure 2.8: Wear rate as a function of SiC particle size for copper in erosion and in two-body and three-body abrasion [4].**

Clark and Wong determined that impact on specimen surface under slurry erosion did not occur for particle sizes less than 34 microns in diameter as a result of a squeeze

film around the specimen surface [5]. Arnold and Hutching found the steady-state erosion rate higher with larger particles [6].

**Particle shape**

Various types of surface damage result from different shapes of particles, for example, spherical, angular and irregularly shaped particle. However, there is less information available on the effect of particle shape on wear than for particle size. Bell and Rogers claimed that the shape of the particles would partially determine the type of damage that occurred, for example, a spherical particle will produce less damage on a ductile target than an angular particle [7].

The importance of particle shape has gained increasing recognition in recent years. Kaya *et al.* described the significant role of particle shape in the applications of slurry abrasives and slurry rheology. Their investigation indicated that the shape of particles is controlled by the nature of the material, the type of comminution device used and the residence time in the grinding circuit [8]. Despite recognitions and concerns for the effect of particle shape in wear, there has not been much more study in this area. As a result, the relation between particle shape and wear is still largely unexplored.

**Particle hardness**

A harder particle may damage the surface of eroding target more than a particle having a lower hardness. The critical factors in this case are the relative hardness of the particle and wear plate. Harder particles are more effective in cutting than are softer particles.

Table 2-1: Moh's hardness of a number of particulate materials [31].

| Material | Description or composition | Hardness (Moh) |
|----------|---------------------------|----------------|
| Bauxite | Aluminium hydroxide mixture | 1.5 |
| Magnetite | $(Fe,Mg)Fe_2O_4$ | 6.0 |
| Magnesite | $MgCO_3$ | 3.5-5.0 |
| Quartz | $SiO_2$ | 7.0 |
| Limonite | $FeO(OH).nH_2O$ | 5.0-5.5 |

Klemm indicated that the presence of very small percentages of highly abrasive materials, in soft materials like coal and limestone, would cause severe abrasive damage

to materials surfaces. However, he did not develop a predictive model for the effect of hardness on wear [17]. Figure 2.9, indicates that rubber is superior to steel for most of the minerals except for limestone which shows minor difference in wear between steel and rubber.
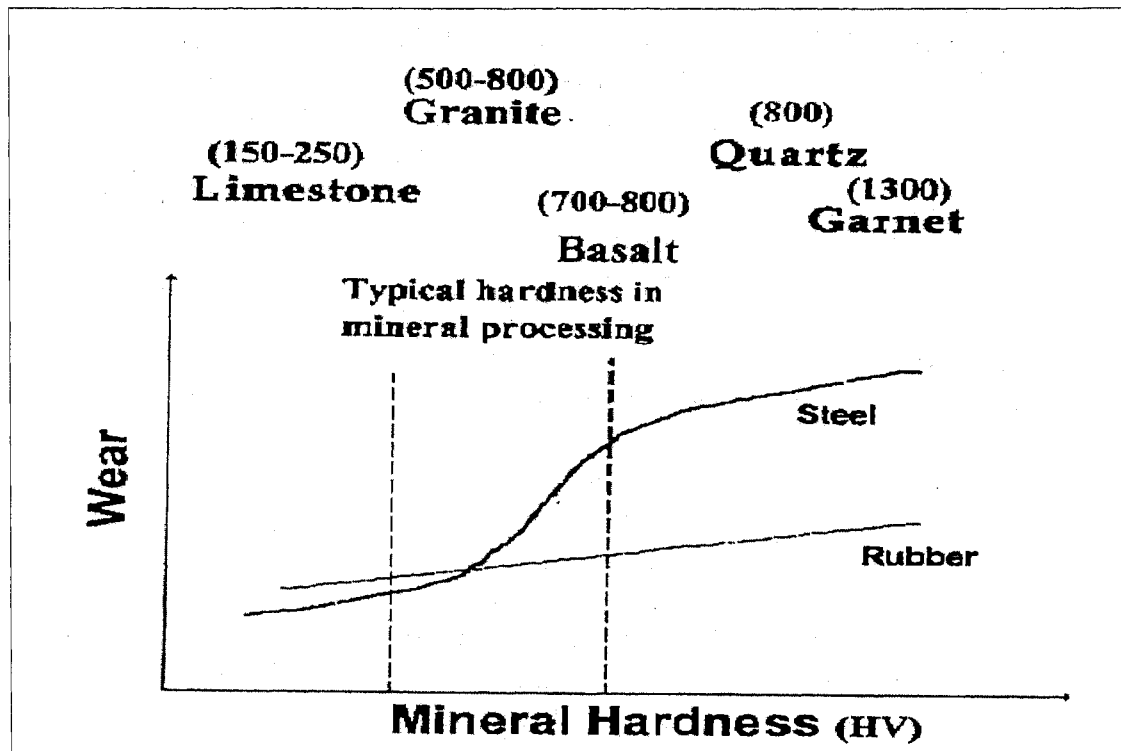


Figure 2.9: Variation in wear rate for mild steel and rubber as a function of mineral hardness [12].

Particle velocity

In most cases, slurry velocity and particle velocity will not be same. For various slurry conditions, the solid particles may have different velocity. So it is essential to distinguish fluid velocity from particle velocity while explaining the effect of velocity in slurry erosion.
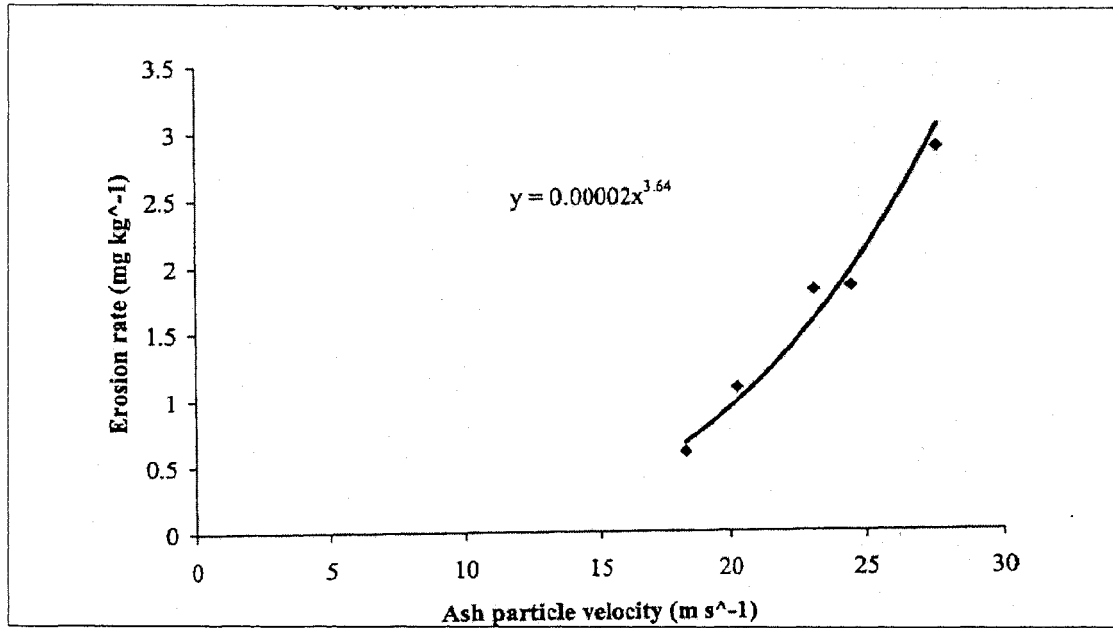
**Figure 2.10: Mild steel erosion rate at various ash particle impingement velocities [15].**

Figure 2.10 indicates that erosion rate of materials is increased with increasing particle velocity [15]. Iwai and Nambu determined the erosion rate was related to a velocity by $(v-v_0)^n$, where $v_0$ is the critical velocity, which is dependent on particle size. The exponent was said to be independent of particle size but is dependent on the eroding surface materials [4]. Roger and Bell stated the most common form of the erosion equation is $m = k\,v^n$, where m = mass eroded, v is the impact velocity and k and n are constants [7]. They used an erosion rig similar to a slurry jet and found that eroded-mass increased with increasing impact velocity of solid particles. Clark and Wong determined erosion rate is proportional to the square of particle impact velocity [5].

Bitter developed a model of slurry erosive wear for solid particles impacting on metal surfaces and considered the combined mechanisms of deformation and cutting wear [26]. He verified that the erosion rate is proportional to the particle velocity and his model is still accepted by many researchers working in the field of slurry erosion. No threshold value of velocity for particle size was determined unlike in the work of Iwai and Nambu [4]. Arnold and Hutchings found a rapid rise in the erosion rate of rubber with velocity above 70 m/s, particularly at an impact angle of 90°[6].

**Particle impingement angle**

Like particle velocity, it is important to understand the interaction between the moving solid particles and the eroding material surface in the slurry. Most researchers have emphasised the effect of the impingement angle of solid particles on eroding surfaces, particularly for metals and their alloys. Some of them agreed with the fact that the effect of impingement angle is less important for elastomeric materials under slurry flow conditions.
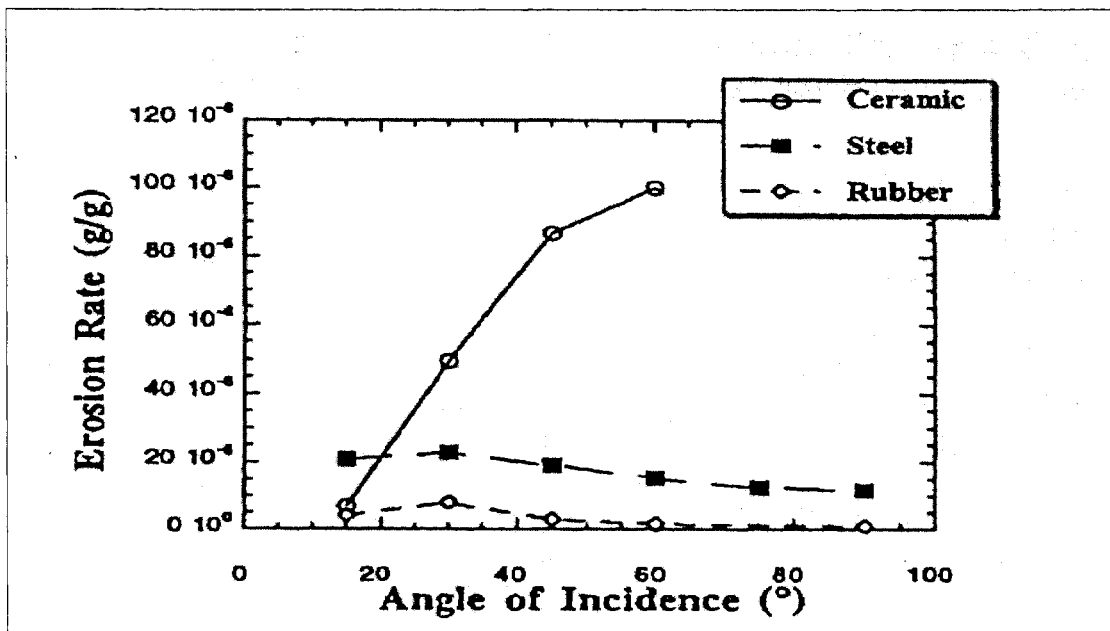


Figure 2.11: Variation in wear rate as a function of angle of incidence for erosion jet conditions in a variety of materials [12].

Clark and Wong found a peak value of cutting wear at impact angles between 20 and $25^0$ for a range of materials by a slurry erosion test method [11]. Sare *et al.* compared erosion rate of ceramic, steel and rubber versus angle of incidence and found that rubber (refer to Figure 2.11) was the most erosion-resistance material [12]. Iwai and Nambu also found the wear rate of rubber was almost independent of impingement angle [4]. Mesa *et al.* measured mass losses for martensinic stainless steel and showed that it was higher under normal impact conditions than under oblique incidence of the hard particle [18].

## 2.2.2 Slurry parameters

An understanding of slurry characteristics is necessary in order to establish how the wear is influenced by various slurry parameters. Previous research has shown that the key

slurry parameters that affect wear include slurry flow, solid concentration, slurry temperature and viscosity. Several of these slurry characteristics are discussed below.

**Slurry temperature**

The effect of slurry temperature on erosion of materials has not been extensively investigated by researchers. Generally it is known that the temperature influences the rate of reaction for chemical systems. However, there is little evidence currently available on how temperature influences the erosion of materials.
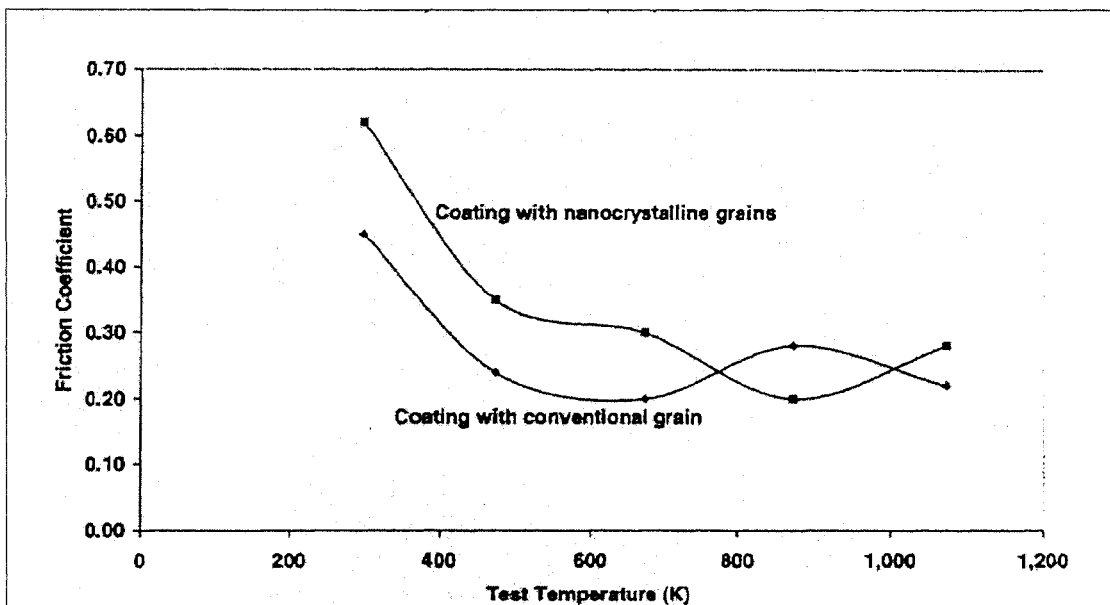


Figure 2.12: The influence of test temperature on the steady-state friction coefficient of coating with nanocrystalline grains and coating with conventional grains [9].

Mesa *et al.* analysed the effect of slurry temperature on erosion and corrosion resistance of three martensinic stainless steel from the point of view of establishing the mechanisms of mass removal from the surface. They found increasing slurry temperature led to higher mass loss, especially when testing was performed at $70^0C$, where the specific mass loss varied linearly with the test duration [18]. Evidence from SEM analysis showed the mass loss resulted from chemical mechanisms such as intergranular and pitting corrosion. But the effect of temperature on erosion mechanisms was not justified. The influence of test temperature, on the steady-state friction coefficient of two different coatings, is illustrated in Figure 2.12 which shows that the friction coefficient

decreases with temperature. The ratio of the frictional force to the normal force for a sliding body is called the coefficient of friction.

**Slurry viscosity:**

Viscosity is an important parameter in slurry flow as the movement of solid particles in any fluid may be influenced by the viscosity of the fluid.
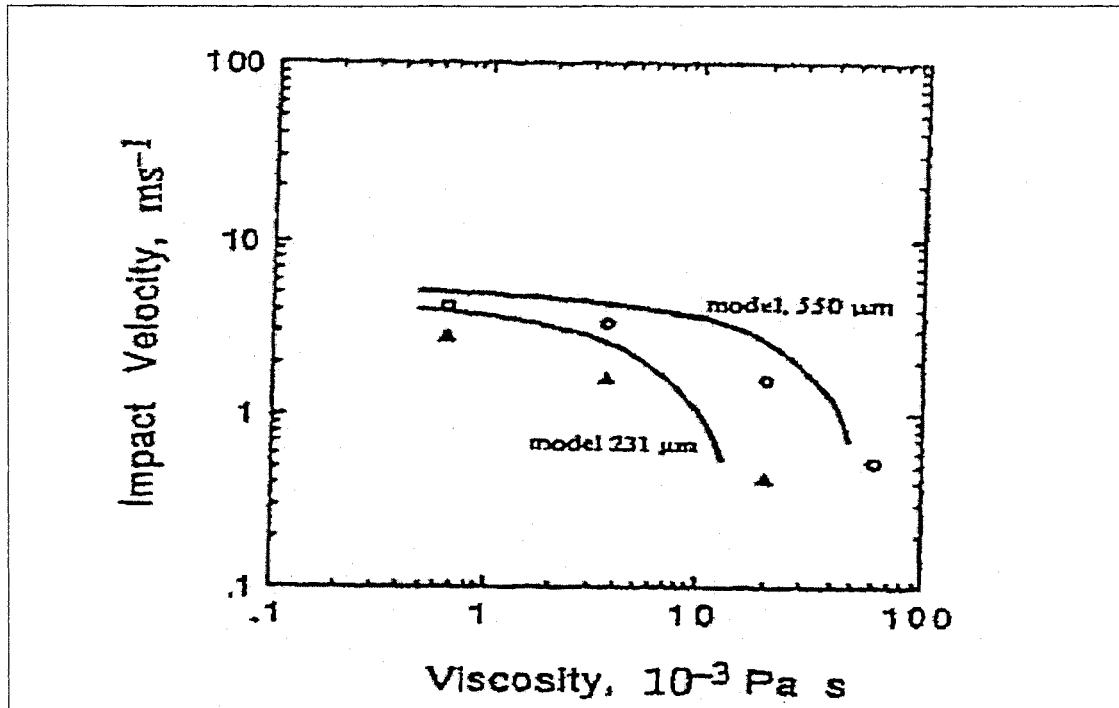


Figure 2.13: Comparison of predicted impact velocities (full lines) and experimental values (data points) for glass beads mean diameter 231 and 550 micrometer tested in water glycerin solutions [5].

Clark reviewed test methods and applications for slurry erosion that examined the effect of viscosity on relative erosion rate. He established that the effect of a viscosity up to about $10 \times 10^{-3}$ Pas is negligible but at higher viscosities both collision efficiency and impact velocity decreased dramatically leading to a prediction of no particle impact whatsoever in a suspending liquid of viscosity $50 \times 10^{-3}$ Pas or greater [19]. Clark and Burmeister found that the impact velocity of particles decreased as the viscosity of the fluid increased [20]. They used glass beads of three different mean diameters suspended in a water-glycerine mixture to verify their conclusion. Clark and Wong determined that the impact velocity of a particle decreased with increasing viscosity (refer to Figure 2.13)

and no apparent impact of particles on the surface was observed above a certain threshold value of viscosity.

## Slurry flow conditions

The particle velocity, which causes the damage on impacting on material surface, is highly influenced by the characteristics of the fluid flow in the slurry system. Many researchers in erosion have emphasised the erosion mechanism rather than the fluid mechanics aspects.
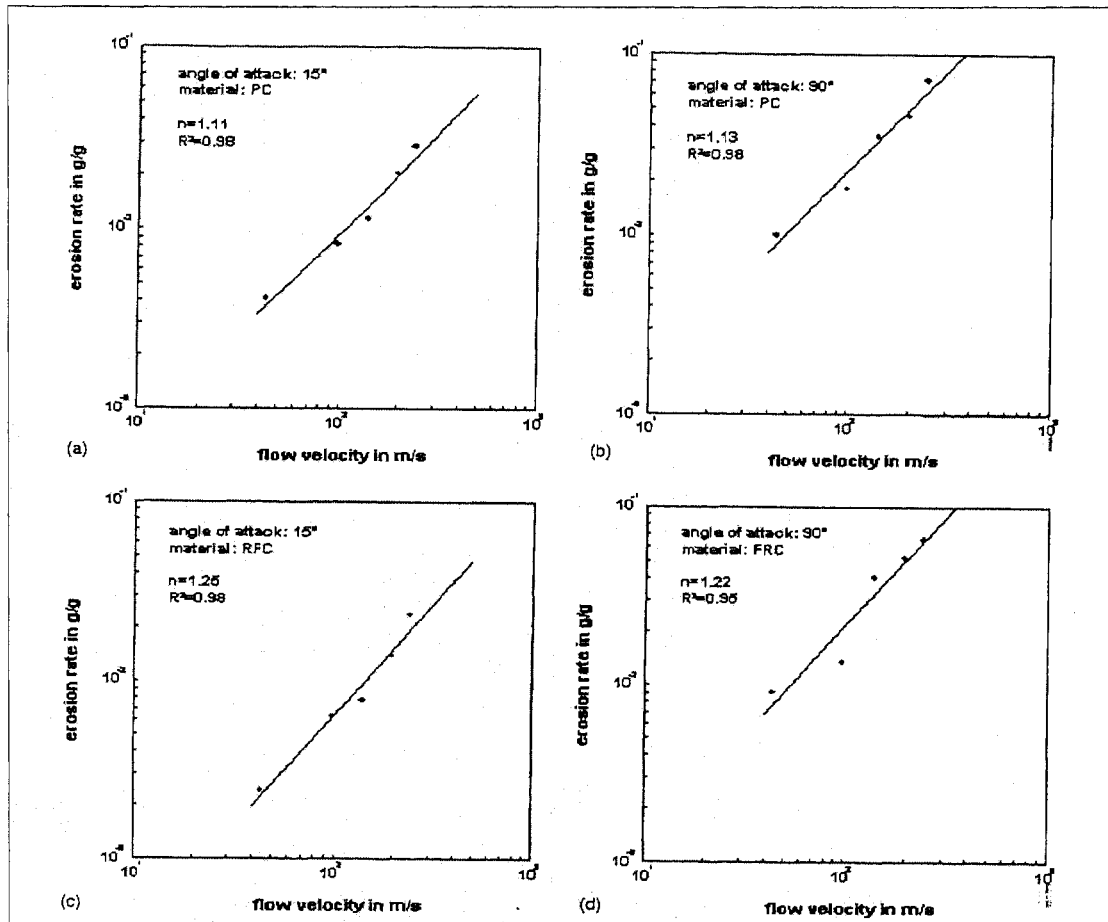


Figure 2.14: Relationship between flow velocity, angle of attack and relative erosion rate (PC denotes plain concrete and FRC denotes fibre-reinforced concrete) [14].

In some cases, the calculation of particle trajectories in a fluid stream rather than material selection has been the key to solving major erosion problems [5]. A relationship between erosion rate of materials and flow velocity of particles is shown in Figure 2.14. Pourahmadi and Humphery studied solid-fluid turbulent flow to predict erosive wear and produced a model to explain their results [21]. They commented that the viscous

interactions between the fluid and particulate phase caused reductions in the turbulent kinetic energy of both solid and particle. The model was described as.

$$E = c\frac{m_p}{p_1}q_p{}^2\int(\beta)$$  (4.5)

where, c = fraction of the number of particles cutting in an idealized manner, $m_p$ = particle mass striking the surface per unit area per unit time, $p_1$ = Vickers hardness of the wall material, $q_p$ = the magnitude of the particulate phase impact velocity, $\int(\beta)$ = a function of the particle angle of attack. However the model did not distinguish how slurry flow behaviours influenced the wear of material, whereas the work of Finnie [16], Bitter [26] and Clark [5] does.

**Slurry solids concentrations**

Studies, on how solid concentrations affect slurry erosive wear, have been done by a number of researchers. Almost all of them have agreed that erosive wear increases with increasing value of solid concentration up to a threshold and after that wear is less affected by increasing solid concentration. However, some researchers claimed the parameter as one of the less important variables of erosive wear. Consequently, the dependency of solid concentration in wear has not been clearly identified.
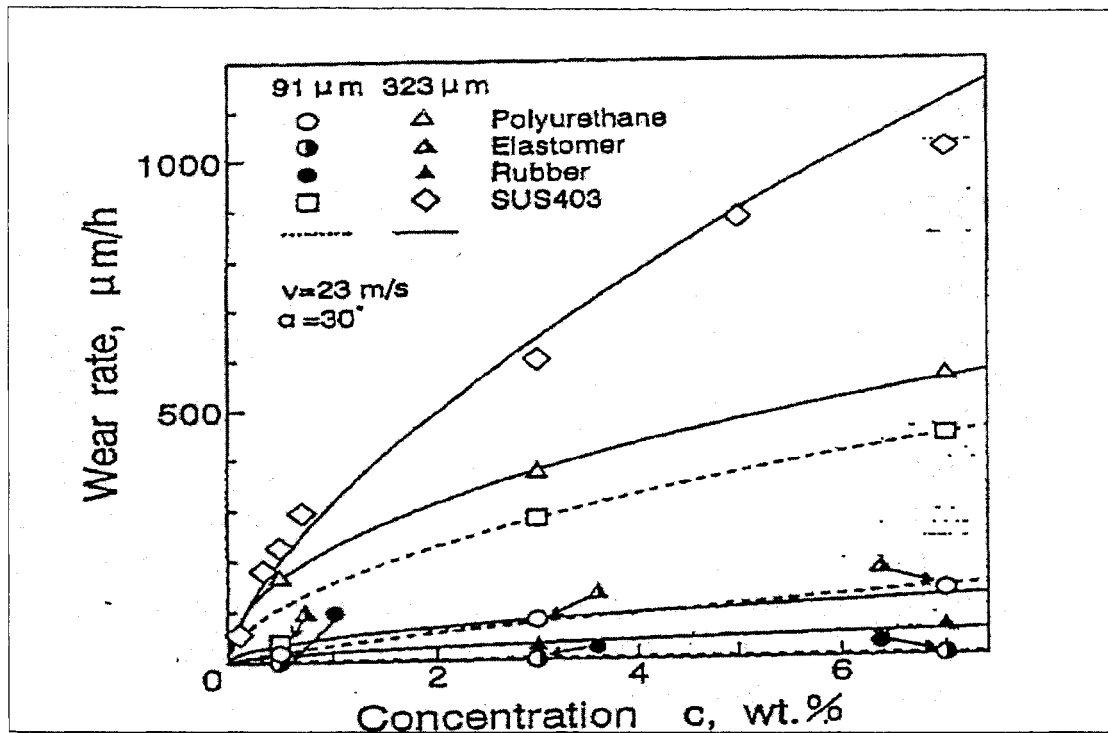
**Figure 2.15: Relationship between wear rate and silica sand concentration for polyurethane, elastomers SUS403 and rubber material [4].**

Iwai and Nambu tested three elastomeric materials using a slurry pump with a flow velocity 23 m/s at an angle of $30^0$ and found volumetric wear rates of those materials increased with increasing solid weight concentration (refer to Figure 2.15) [4]. However he could not determine any peak or critical value for solid concentration. Horn claimed that the solid concentration of slurry was a predictor for the location and wear rate in the slurry pipe [22]. He also established that at lower concentrations some wear was only visible on the base of the pipe line, whereas at higher concentrations wear was visible around the circumference of the pipe. These results seem quite acceptable since at higher concentration more particles have opportunity to come in contact on the pipe's internal surface. In another study, Xie *et al.* concluded that the solid concentration increased the particle to particle interactions which must be taken into account [13]. It generally makes the problem intractable for computational analysis.

**Slurry abrasiveness**

Slurry abrasiveness is determined by evaluating the partial derivative of the weight loss of a chromium steel block sliding over the slurry for a fixed cycle time. The weight loss of the chrome steel block is determined by the equation.

$$\text{Weight loss} = a(t)^b \tag{4.6}$$

where, a = constant, t = time and b = power of loss with time. Horn studied wear in polymer and ceramic slurry pipelines and found increasing wear rates for steel and polyethylene as slurry abrasiveness increased [22]. With elastomers, there was no rapid increase in wear as slurry abrasiveness increased. Table 2.2 presents, information on relative abrasiveness of solids.

Table 2.2: Relative abrasiveness of solids [32]

| Material (source) | Description or composition | Abrasivity (Miller no.) |
|---|---|---|
| Bauxite | Aluminium hydroxide mixture | 9, 33, 50, 134 |
| Irone ore | - | 28, 64, 122, 234 |
| Limonite | $FeO(OH).nH_2O$ | 113 |
| Magnetite | $(Fe,Mg)Fe_2O_4$ | 64, 71, 134 |
| Sand, silica | $SiO_2$ | 51, 68, 116, 246 |

### 2.2.3 Eroding material properties

The wear rate and wear mechanisms that occur in a wearing situation are clearly dependent upon the nature of the material being worn, denoted here as the eroding material. A number of properties of eroding materials are discussed below based on the available literature.

**Material degradation**

Material degradation may come about through a number of mechanisms. Chemical degradation of materials is highly likely in chemical slurry environments, particularly where elevated temperatures are maintained. In a wearing environment, the wear mechanisms and chemical degradation mechanisms may interact, accelerating or inhibiting the wear rates over those expect from each mechanism alone.
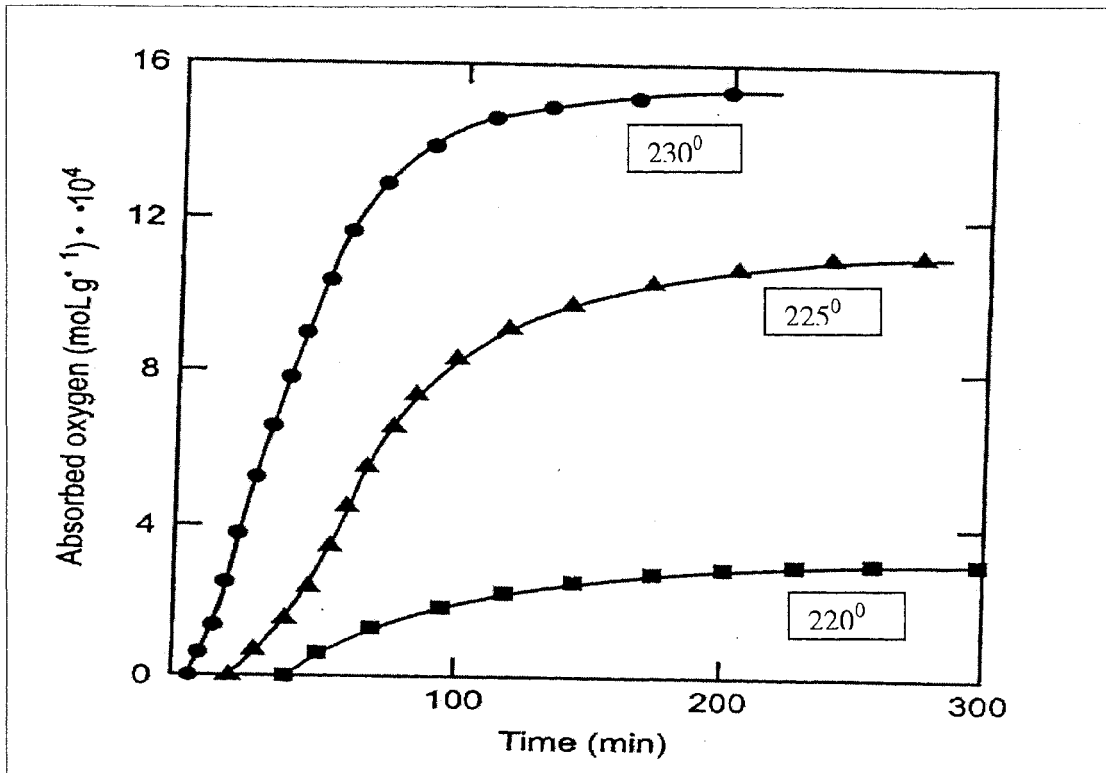
**Figure 2.16: Dependence of oxygen uptake on time for butyl rubber at $220^0$, $225^0$ and $230^0$C [23].**

Zaharescu measured the thermal degradation of butyl rubber using oxygen-absorption technique at temperature of 220, 225 and $230^0$ C and found higher oxygen uptake at highest temperature ($230^0$ C) [23]. He argued that at higher temperatures a greater quantity of thermal energy was absorbed by the sample which was large enough to accelerate the rubber decomposition (refer to Figure 2.16).

**Materials hardness**

It is generally understood that alloys demonstrate higher wear resistance with increased hardness. Thus, conventional design of wear resistant coatings generally follows the premise that "harder the better" [1]. But this adage does not hold true with elastomers (refer to Figure 2.17), which can show wear rates many times lower than much harder metals in the same circumstances [12]. Furthermore, as elastomers become stiffer, they often become more brittle and may show increased wear rates.
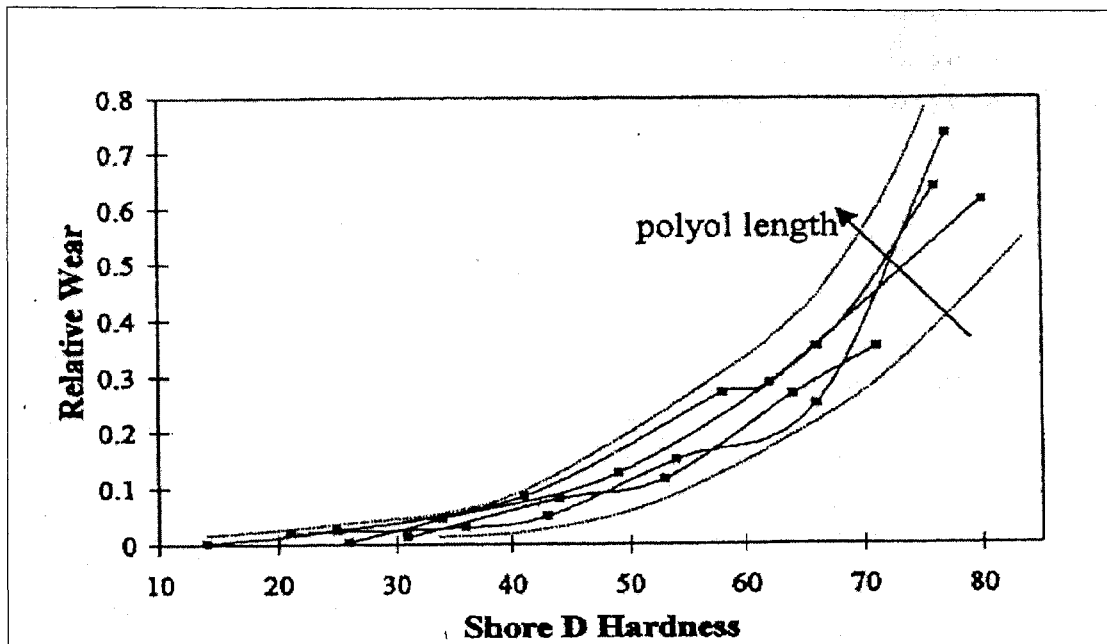
**Figure 2.17: Variation in wear rate for polyurethanes as a function of Shore D hardness [12].**

Hill *et al.* assessed polyurethane over a range of hardness using dry rubber sand wheel (DRSW) method and found wear rate increased with increasing hardness [24]. Polyurethane is comparatively a harder material than other elastomers and it may be a suitable option as coating for dry wear environment specifically with shore hardness under 95A.

## Material properties

Most researchers in erosion have focused their studies on the wear mechanisms and the mechanics of particle-fluid interaction. Few have identified the potential reasons for failure due to inadequate properties of materials.

Sare *et al.*, attributed several cases of premature elastomer failure in Australian mining industries to a lack of understanding of the nature of the physical properties of elastomers [12]. He also indicated the narrow operating window of elastomers where they could perform optimally. Table 2.3 lists the operating ranges for some elastomers.

**Table 2.3: Temperature window for various elastomers [12].**

| Elastomer | Operating temperature | Glass transition temperature $T_g$ ($^0$ C) |
|---|---|---|
| Polyurethane (PUR) | Up to 75 | -40 to -20 and 50 to 80 |
| Polysiloxanes | -100 to 300 | <-50 |
| Polybutadienes | Up to 80 | -70 to -50 |
| Natural rubber (NR) | -50 to 105 | -52 |
| Nitrile butadiene rubber (NBR) | -50 to 120 | -55 to -20 |
| Chlroprene (CR) | -45 to 120 | -45 |
| Ethylene propylene diene (EPDM) | -50 to 125 | -50 to -40 |
| Synthetic polyisoprene | Up to 110 | -60 |
| Styrene butadiene rubber (SBR) | Up to 110 | -60 to -50 |
| Fluorocarbon | -30 to 205 | Varies |
| Butyl rubber (IIR) | -50 to 115 | -63 |

**Material composition**

The importance of material composition on erosion behaviour is not yet fully understood. Horn stated that elastomers have quite different characteristics from steel in terms of wear sensitivity with solid particle velocity [22]. Fukahori and Yamazaki determined that the rate of abrasion loss greatly increased with increasing carbon black content until stable abrasion was reached [25]. They also discovered that the crack rate growth was not improved by carbon black at small strain amplitudes. Rather, faster growth was observed with more carbon black. No such information was found by researchers in slurry erosion except for Clark and Wong in specific energy of materials [11].

**Specific energy**

Several researchers have discussed the effects of specific energy on material removal. Finnie *et al.* proposed that the erosion rate of material was related to the specific energy for material removal which was in turn related to the rate of dissipation of kinetic energy (refer to Figure 2.18) according to the following equation

$$\text{Specific energy} \cong \frac{(MV^2)/2}{Q_{max}}$$

(4.7)

where, M = mass of solid particles, V = particle velocity and $Q_{max}$ = volume of materials removed by particles [16]. Bitter incorporated the term specific energy for both deformation and cutting wear in his model; however he could not provide any quantitative information on these two specific energy factors for different materials [26]. Clark and Wong empirically determined specific energy of material-removal separately for both deformation and cutting wear [11]. According to their study, the value of these two factors differed significantly for metallic materials and little difference was obtained for polymeric materials except for phenolic.
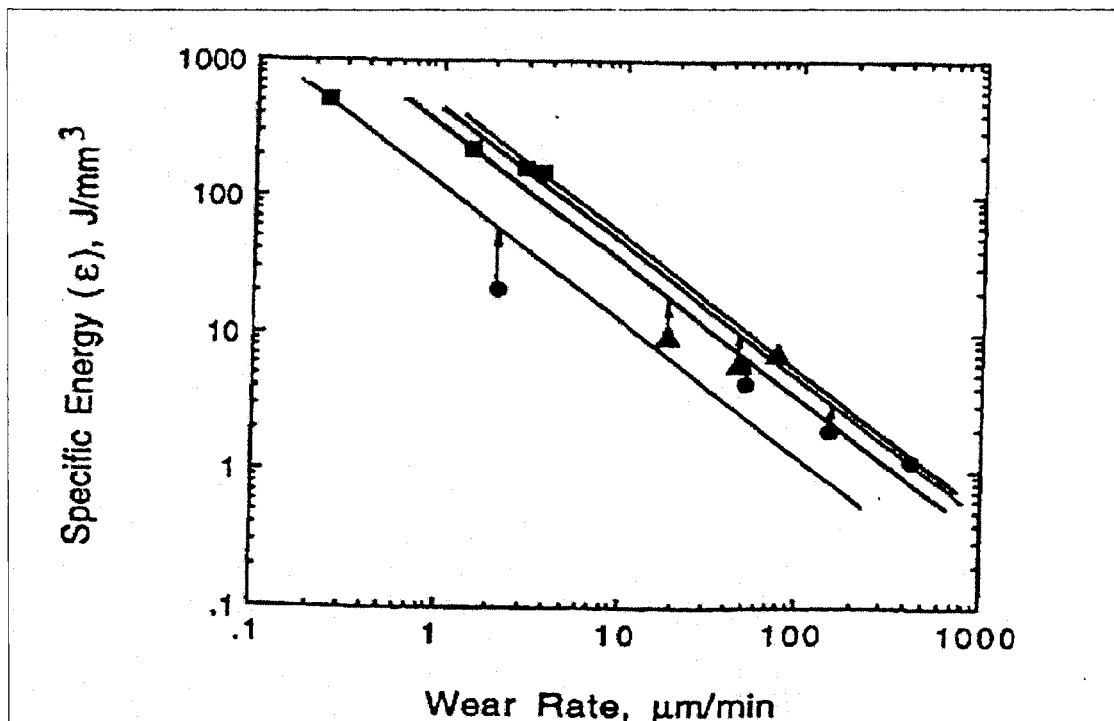


Figure 2.18 Specific energy for deformation wear as a function of deformation wear rate for steel, alumina and pyrex glass [11].

### Surface preparation and rubber vulcanization

Sere *et al.* investigated the effect of surface condition on adhesion and corrosion resistance of carbon steel/chlorinated rubber/artificial sea water systems. They concluded that the performance of high grade dry adhesion was not always satisfactory. They also claimed that the substrate structure and roughness changes did not produce significant changes in adhesion strength and corrosion resistance [27]. Lalit *et al.*, suggested aqueous-based adhesives (instead of flammable solvent-based adhesives) for metal

rubber bonding, in order to reduce the level of volatile organic compound, to increase a level of safety which was not much known in the rubber lining industry [28].

## 2.3 References

1. ASTM Standards, 1998, "Metal test methods and analytical procedure", volume 03.02, Wear and Erosion, pp. 211-359.
2. Ekberg et al (1997), 'Wear – Some Notes', Department of solid Mechanics, Chalmers university of Technology.
3. Hutchings, I.M., "Tribology: Friction and Wear of Engineering Materials," Edward Arnold, pp. 132-171.
4. Iwai, Yoshiri and Nambu, Kazuyuki 1997, "Slurry wear properties of pump lining materials," Wear, Vol. 210, pp. 211-219.
5. Clark, H. McI. and Wong, K.K., 1993, " A model of particle velocities and trajectories in a slurry pot erosion tester," Wear, Vol. 160, pp. 95-104.
6. Arnold, J.C. and Hutchings, I. M., 1992, "A model for the erosive wear of rubber at oblique impact angles," Journal of Physics, Vol. 25, pp. A222-229.
7. Bell, J.F. and Rogers, P. S., "Laboratory scale erosion testing of wear resistant glass-ceramic", Materials Science and Technology
8. Kaya, E.; Hogg, R.; Kumar, S.R., 2002 "Particle shape modification in communication", KONA, No. 20, pp. 188-195.
9. Roy, M. ; Pauschitz, A.; Wernisch, J. ; Franek, F., 2004, The influence of temperature on the wear of $Cr_3C_2$- 25(Ni20Cr)coating – comparison between nanocrystalline grains and conventional grains", Wear Vol. 257, pp. 799-811.
10. Ahn, Y, ; Yoon, J. ; Baek, C. ; Kim, Y., 2004, "Chemical mechanical polishing by collidial silica-based slurry for micro-scratch reduction", Wear, Vol. 257, pp. 785-789.
11. Clark, H. McI. and Wong, K.K., 1995, " Impact angle, particle energy and mass loss in erosion by dilute slurries," Wear, Vol. 186-187, pp. 95-104.
12. Sare, I.R., Mardel, J.I. and Hill, A.J., 2001, "Wear –resistant metallic and elastomeric materials in the mining and mineral processing industries – an overview," Wear, Vol. 250, pp. 1-10.
13. Xie, Y., Clark, H. McI and Hawthorne, H.M., 1999, "Modeling slurry particle dynamics in the Coriolis erosion tester", Wear, Vol. 225-229, pp. 405-416.
14. Hu, X. G. ; Momber, A. W. ; Yin Y. ; Wang, H. ; Cui, D.M., 2004 "High-speed hydrodynamic wear of steel-fibre reinforced hydraulic concrete" Wear, Vol. 257, pp. 441-450.
15. Mbabazi, J. G. ; Shear, T. J. ; Shandu, R., 2004, "A model to predict erosion on mild steel surfaces impacted by boiler ash particles", Wear, Vol. 257, pp. 612-624.
16. Finnie, I., 1995, "Some reflections on the past and future of erosion," Wear, Vol. 186-187, pp. 1-10.
17. Klemm, Robert E., 1999, "Abrasion resistant steel piping systems for slurry transport in mining applications", UltrTech, Port Washington, WI 53074-308 USA

18. Mesa, D. H., Toro, A., Sinatora, A., and Tschiptschin, A. P., 2003, "The effect of testing temperature on corrosion-erosion resistance of martensitic stainless steels," Wear, Vol. 255, pp. 139-145.

19. Clark, H. McI., 1993, "Test methods and applications for slurry erosion – A review," American Society for Testing and Materials, Philadelphia, USA, pp. 113-132.

20. Clark, H. McI. and Burmeister, L.C., 1992, "The influence of the squeeze film on particle impact velocities in erosion," Int. J. Impact Engg. Vol. 12, No. 3, pp. 415-426.

21. Pourahmadi, F. and Humphery, J. A. C., 1983, "Modelling solid-fluid turbulent flows with application to predicting erosive wear," PCH Physico-Chemical Hydrodynamics, Vol.4, No. 3, pp. 191-219.

22. Horn, A.1992, 'Case studies of wear in polymer and ceramic slurry pipelines," International Conference on Bulk Materials Handling and Transportation, Wollongong, Australia, 6-8 July 1992.

23. Zaharescu, T. and Podina, C., 1997, "Thermal degradation of butyl rubber", Journal of Materials Science Letters, Vol. 16, pp.761-762.

24. Hill, D.J.T., Killen, M.I. and Whittaker, A.K., 1997, "Laboratory wear testing of polyurethane elastomers," Wear, Vol. 208, pp. 155-160.

25. Fukahori, Yoshidie and Yamazaki, Hirotaka, 1995, "Mechanism of rubber abrasion, Part 3: how is friction linked to fracture in rubber abrasion?," Wear, Vol. 188, pp. 19-26.

26. Bitter, J.G.A., 1963, "A study of erosion phenomena," Part 2, Wear, Vol. 6 pp. 169-190.

27. Sere, P.R. ; Armas, A.R. ; Elsner, C.I. and DI Sarli, A.R.,1996, "The surface condition effect on adhesion and corrosion resistance of carbon steel/chlorinated rubber/artificial sea water systems", Pergamon, Corrosion Science, Vol. 38, No. 6, pp. 853-866.

28. Mehra, lalit, Polski, Eugene L. and Mauri, A., 1996, "Rubber linings overview and new technology," Journal of Coatings & Linings, pp.33-39.

29. Shook, C.A. and Roco, M.C., 1991, "Slurry flow: principle and practice", Butterworth-Heinmann, Boston, pp. 157.

30. Schnabel, W. "Polymer Degradation – principles and practical applications", Hanser International.

31. Baha E. Abulnaga, P.E.,2002, "Slurry systems handbook," Mcgraw-Hill, pp.A1-A12.

32. Baha E. Abulnaga, P.E.,2002, "Slurry systems handbook," Mcgraw-Hill, p.10.21.

Chapter 3

# Failure Analysis

Failure analysis is a key process in the search for solutions to problems of materials failure [1]. A good failure analysis will provide necessary information which can form a roadmap for the solution of the problem. In this project, a failure analysis has been performed to solve the problem of premature failure of agitator blades in the AMC process. Failed rubber samples and magnesite ore were collected for the investigation. Information about the AMC leaching process and photographs of the failed rubber were also obtained from the plant site. In order to investigate the wear mechanisms, the failed rubber samples were analysed using Scanning Electron Microscopy (SEM). Magnesite ore particles were screened to determine particle size distribution. The technique of X-ray Diffraction (XRD) analysis was used to investigate the impurity concentration of the magnesite ore. The influence of slurry parameters in the failure of agitator blades was also discussed.

A brief discussion has been made on failure criteria and mode in the following sections.

## 3.1 Failure criteria

The inability of a component to perform the function it was designed to perform is regarded as a failure of the device [1]. Despite the efforts of design engineers to ensure that the device functions for the prescribed design life time, the failure of materials still remains an ongoing phenomenon. The following reasons have been advanced as major contributing factors for materials failure.

- *Poor materials selection.*
- *Improper materials processing.*
- *Inadequate design of components.*
- *Lack of proper understanding of functioning environments.*

Success in designing equipment and components can be achieved by recognizing and evaluating the potential modes of failures. To recognize these modes, a designer must

be acquainted with the array of failure modes observed in practice and with the conditions leading to failure [1].

## 3.2 Failure modes

A failure mode may be defined as the physical process or processes that take place or that combine their effects to produce a failure [8]. The current trend in performance, reliability and safety of machine and machine components have resulted in the need for better materials and an improved understanding of their behaviour under extreme conditions. Since the operating conditions are becoming more severe, it is very important to understand the different failure modes for the available materials under service conditions [8].

The following list includes most of the commonly observed modes of mechanical failure.

- Fatigue
- Corrosion
- Wear
- Fracture
- Creep
- Stress corrosion
- Corrosion wear
- Corrosion fatigue

These failure modes only produce failure when they generate a set of circumstances that interferes with the proper functioning of a machine or device.

## 3.3 Sample collection

Representative samples such as failed rubber parts and crushed magnesite ore were collected from the demonstration plant of AMC at Gladstone. Rubber parts were cleaned with detergent solution and then were marked with the date that the failure occurred and the direction of rotation in the magnesite slurry. Magnesite ore of size -3.5mm and -5.5mm respectively, were used in the AMC demonstration process. Initially -5.5mm size magnesium ore was used by AMC but late in the process they decided to use -3.5mm size in order to reduce the failure of the agitator blades.

**Figure 3.1: Failed bromobutyl rubber found in the slurry mixing tank of AMC.**

Information about failure issues was obtained through discussions with AMC staff (process supervisors, engineers and managers). AMC also provided a report on failure issues and photographs of failed components (as shown in Figure 3.1). This information formed the basis of the investigation described in this thesis. Some of the photographs of failed samples can be seen in Figure 3.1 and Figure 3.3.

## 3.4 Process description

A brief discussion of the leaching circuit of the AMC process was presented in chapter one, however, a more detailed discussion of the leaching circuit is necessary to gain a better understanding of the causes of failure.

The leaching circuit consisted of a number of stages such as mixing, purification and filtration stage (refer to Figure 3.2). The temperature thorough out the process was maintained at $70^0C$. Each stage consists of a number of tanks. The premature and repeated failure of the agitator blades was occurring in the mixing tank at intervals of three to eight months. In contrast, agitator blades in the purification tank lasted two and a half years. The demonstration plant was only operational periodically and the maximum duration of continuous operation was a period of four weeks.

```
┌─────────┐        ┌─────────┐        ┌─────────┐
│         │───────▶│         │───────▶│         │
│         │        │         │        │         │
└─────────┘        └─────────┘        └─────────┘
  Mixing         Purification stage     Filtration stage
```
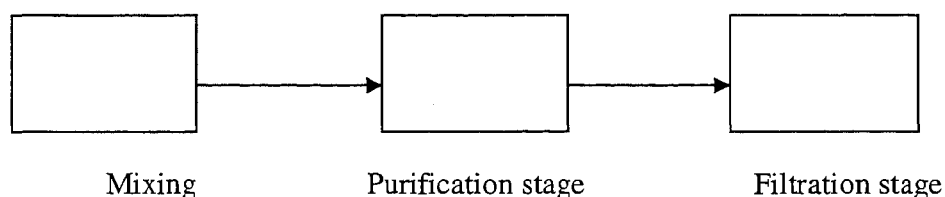
**Figure 3.2: Stages of the leaching circuit in the AMC demonstration plant.**

### 3.4.1 Mixing stage

Magnesite particles of size -3.5 mm were mixed with hydrochloric acid (33% concentration) in the mixing tank. The hydrochloric acid was added into the tank through a submerged nozzle at the bottom. The magnesite particles were added into the mixing tank by a rotating conveyor belt. The mixture was digested by the mechanical action of the agitator blades. One set of hydrofoil type impeller (with three blades) was used for the agitation. The blade-tip velocity was approximately 6 m/s. The duration of leaching for each batch was approximately one hour.

### 3.4.2 Purification stage

The partially digested magnesium slurry was discharged to this stage for further digestion and clarification. The purification stage consisted of a number of purification tanks. The tanks in this stage were smaller in size compared to the tanks of the previous stage. Two sets of agitator blades, similar in size to those used in the mixing tank, were used in each of the purification tanks. The blade-tip velocity was maintained at nearly double the blade-tip velocity of the mixing tank. The liquor with impurities was discharged to the filtered feed-tank.

### 3.4.3 Filtration stage

This stage consisted of a number of filtered-feed and polished-liquor tanks and a series of filter circuits. The filtered feed tank contained the liquor received from the purification tank which was then passed through the filter circuits. The filtrated liquor reached the polished-liquor tank and was then transported to the dehydration circuit.

## 3.5 Visual inspection

The failed rubber surfaces were visually examined as part of the failure investigation. Numerous scratches and a few small holes with a variety of shapes and sizes were observed on the failed rubber surfaces near the blade tips. The density of these scratches was greatest near the blade-tip area and few such defects were found in the rubber surface near the agitator shaft. The rubber surface at the middle section of the agitator blades was found to have little damage.

A reason for such damage could be the cutting, plowing and sliding action of magnesite particles on the rubber surface. The particles are suspended within the liquid

and hence an understanding of the relative movement of the liquid, the rubber and the particles may give greater insight into the causes of failure of the rubber. The failure of the agitator blades (refer to Figure 3.3) was observed at blade-tips on every occasion. The failure was initiated on rubber surface at the edge of the agitator blades facing towards the direction of rotation.

The following defects were identified:

- Initiation and development of the small holes on the rubber surface.
- Scratches near the blade-tips.

The formation of the small holes could be due to repeated indentation of a number of particles on the intersections already formed by the numerous scratches. The scratches were more likely to have formed as a result of impact of the particles on rubber surface at low impingement angle. At low impingement angle, the normal component of the stress is low and the horizontal component is high. The above observations indicate that the impact of particles as a result of the mechanical action of the agitator blades could be a potential cause for the failure of agitator blades. However, further investigations were necessary to confirm this and to this end, a characterization of the failed rubber and the nature of the particles were necessary.
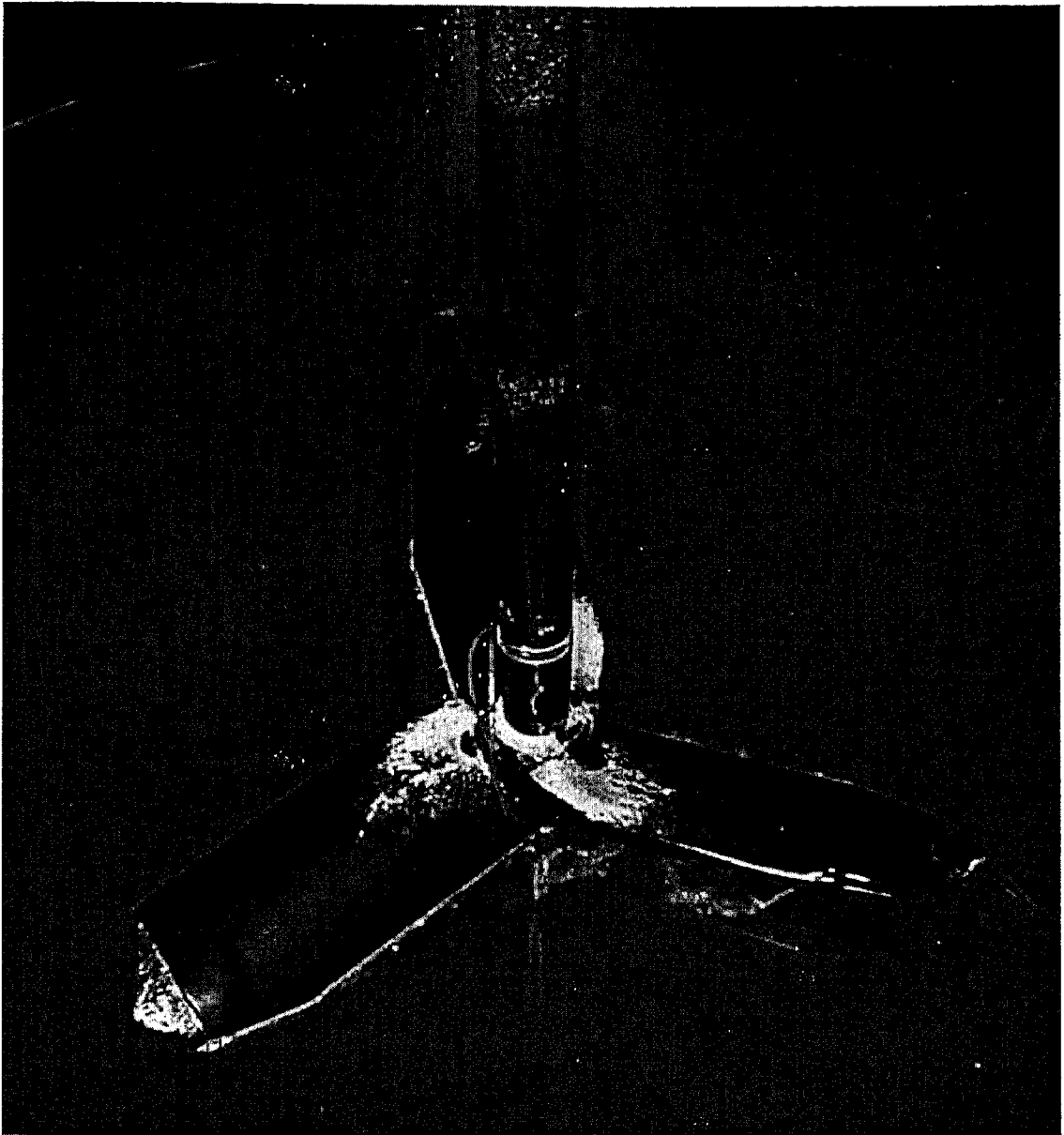
Figure 3.3: A failed agitator blade in the slurry mixing tank of the AMC demonstration plant.

## 3.5.1 Summary of the visual inspection

Damage to the rubber surface appeared to the naked eye as a few scratches, cracks and small holes. This suggested that any single defect or a combination of the defects mentioned above could be involved in the failure of the agitator blades. It was decided to use scanning electron microscopy (SEM) to gain additional information about the failure process.

## 3.6 Particle analysis

As received magnesite ore from the demonstration plant was screened to analyse the particle size distribution in accordance with ASTM 1921.

### 3.6.1 Particle screening

The magnesite ore was conditioned and stored at room temperature (approximately $25^0$C). It was assumed that the temperature & moisture in normal atmosphere would not significantly affect the test results. The ore was then screened using sieves ranging from 75 to 3500 microns. The sieves chosen for the test were arranged in a stack with the coarsest sieve on the top and the finest at the bottom. A pan was placed under the bottom sieve to receive the final undersize. A known quantity of ore was put in the uppermost sieve for each run. The sieve-stack was placed in a sieve shaker which vibrated the materials in a vertical plane. A standard period of ten minutes was maintained for every run.

### 3.6.2 Results and analysis

The magnesite ore retained in each sieve was measured using a top-loading balance (capable of measuring accurately to two decimal places). The results obtained in the particle screening procedure are summarised in Table 3.1.

Table 3.1: Particles size distribution of magnesite ore which was used by the AMC demonstration plant.

| Nominal Screen (Particle) Size (microns) | Weight Fractions (percentage) | Cumulative Passing (percentage) | Cumulative Retained (percentage) |
|---|---|---|---|
| 3500 | 6.14 | 93.86 | 6.14 |
| 3350 | 2.84 | 91.02 | 8.98 |
| 2360 | 18.69 | 72.33 | 27.67 |
| 1400 | 7.53 | 64.80 | 35.20 |
| 1180 | 9.59 | 55.22 | 44.78 |
| 1000 | 14.16 | 41.06 | 58.94 |
| 710 | 5.71 | 35.35 | 64.65 |
| 600 | 15.17 | 20.18 | 79.82 |
| 355 | 11.43 | 8.75 | 91.25 |
| 212 | 7.25 | 1.50 | 98.50 |
| 125 | 1.18 | 0.32 | 99.68 |
| 75 | 0.32 | 0.00 | 100.00 |

Screen sizes ranging from 75 to 3350 microns were used to analysis the magnesite particles. The percentage amount of magnesite particles in weight fraction, cumulative under size and cumulative over size were described in the Table 3.1.
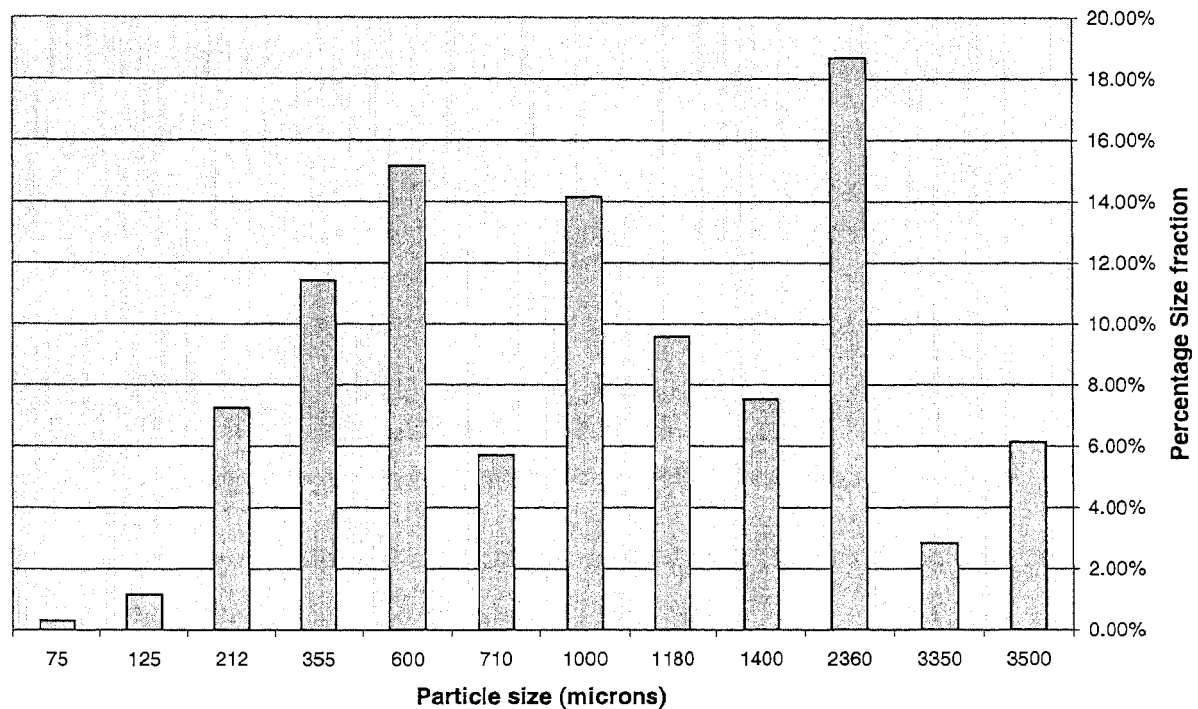


**Figure 3.4: The size fractions of magnesite ore used in the AMC process.**

Figure 3.4 shows the variation of percentage size fraction of magnesite particle against nominal particle size. The highest and the lowest size fractions were obtained for particles size 2360 and 75 microns respectively. Figure 3.4 also indicates that the size fraction with a mid-range of 6675 microns is approximately 6% of the weight of the particles. AMC used -3500 microns magnesite particles in their process. The results indicate that a significant quantity of magnesite particles over -3500 microns were present in the slurry. Larger particles possess higher kinetic energy than smaller particles if travelling at the same velocity. It may be that the higher kinetic energy of the larger particles is causing most of the damage to the rubber and this was investigated further.
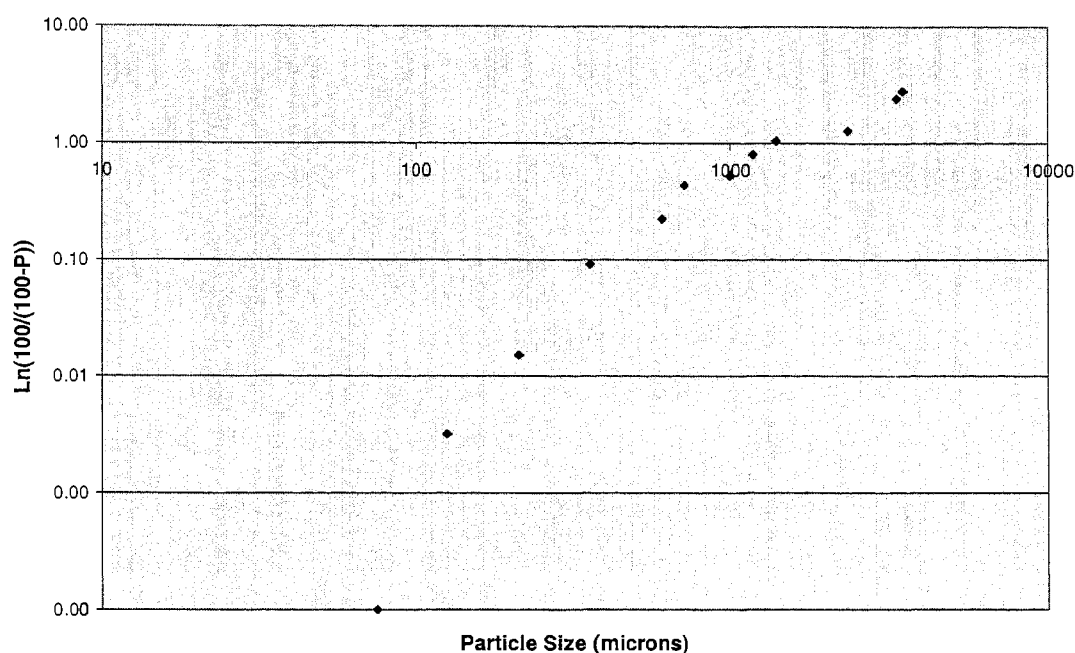
**Figure 3.5: The screen analysis graph of cumulative undersize weight fraction against mean particle size.**

The results of the particle screening were plotted (refer to Figure 3.5) in order to assess the full significance of magnesite particles in the size distribution. The logarithmic value of cumulative passing (weight %) was plotted in the vertical axis and the particle size (nominal screen size) was plotted in the horizontal axis. According to the plot (as shown in Figure 3.5) a significant quantity of magnesite particles were found larger than 1000 micron.

## 3.6.3 XRD analysis

The XRD analysis was carried out to determine how the impurities particularly silica, was distributed in the particle size fractions. A Siemens D500 X-Ray diffractometer, operated by a quantitative XRD software Siroquant version 2.5, was used to determine impurity concentration of the magnesite ore. The diffraction angle ($2\theta$) ranged from 20 to $90^{0}$. The goniometer speed was maintained at $0.5^{0}$/minute. The voltage and current for the power supply to the X-Ray generator were 35.5 kV and 28.5 mA respectively.

Magnesite particles as tabulated in Table 3.2 were collected to prepare specimens for XRD analysis. The particles were then ground with a mortar and pestle. The powder specimen was then placed in the circular groove of the specimen holder and pressed

gently for compaction to avoid misalignment to the crystal orientation of the powder. The sample holder was then placed into the diffractometer.

The XRD analysis indicates that a number of impurity compounds such as silica, dolomite, calcium carbonate, iron and manganese oxides were present in the magnesite ore. Silica and dolomite were found as major impurity compounds. The effect of dolomite particles on wear is likely to be insignificant because it tends to dissolve readily in the hydrochloric acid. However, silica generally does not take part in chemical reaction and it remained as a solid compound in the magnesite slurry. The concentration of other impurity compounds was considered to be insignificant in the magnesite ore.

Table 3.2: Impurity contents (quartz and dolomite) in magnesite ore used by AMC.

| Particle size (microns) | Quartz (%mass) | Dolomite (%mass) | Magnesite (% mass) |
|---|---|---|---|
| 125 | 3.25 | 2.75 | 94.05 |
| 212 | 5.15 | 2.10 | 92.75 |
| 355 | 3.90 | 2.45 | 93.70 |
| 600 | 0.30 | 1.65 | 98.05 |
| 710 | 0.35 | 0.80 | 98.80 |
| 1000 | 0.15 | 1.60 | 98.25 |
| 1180 | 0.35 | 0.75 | 98.90 |
| 1400 | 0.50 | 1.20 | 98.20 |
| 2360 | 0.70 | 0.95 | 98.35 |
| 3350 | 0.40 | 0.85 | 98.80 |

The Moh hardness of silica and magnesite was found to be 7.0 and 3.5 respectively (see Table 2.1). The hardness and the asperity of solid particles play a great role in wear. Therefore, there was a question as to whether or not the silica will have an influence on the wear of the rubber.
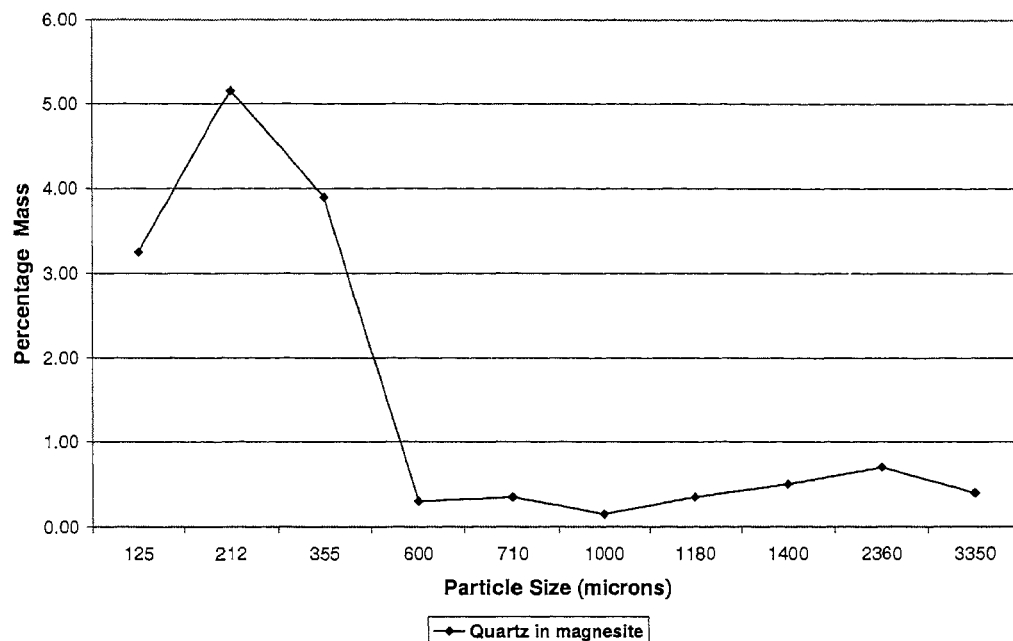
**Figure 3.6: Percentage mass of quartz present in magnesite in a wide range of particle size.**

The results of the XRD analysis (as shown in Figure 3.6) showed that the silica (quartz) was concentrated in the smaller particles. Particle with sizes over 478 microns contained little silica and the silica was concentrated in those particles under 600 microns. Approximately 20% of the magnesite ore (refer to Figure 3.4) was found less than 600 microns. It is questionable as to whether the fine silica particles could have had a major influence on the wear of the rubber.

## 3.6.4 Summary of the particle analysis

Six percent of the magnesite particles were found to be larger than the normal particle size (-3.5 mm) used by the AMC process. This tells us that excess kinetic energy was supplied to the rubber surface due to these over size particles. This may have influenced the failure process of the agitator blades.

Silica was suspected to be influencing the failure process because of its extreme chemical resistance properties. With large particles, the silica was expected to be in high concentration. However, the results suggested that the concentration of silica in particles over 600 microns size was insignificant. Hence it was verified that silica in the magnesite ore used in the AMC process became insignificant to accelerate wear process.

## 3.7 SEM analysis

The failed rubber samples collected from the AMC plant were examined using a JEOL 6360 JSM scanning electron microscope (SEM). Samples were examined uncoated using backscattered electrons in low vacuum mode.
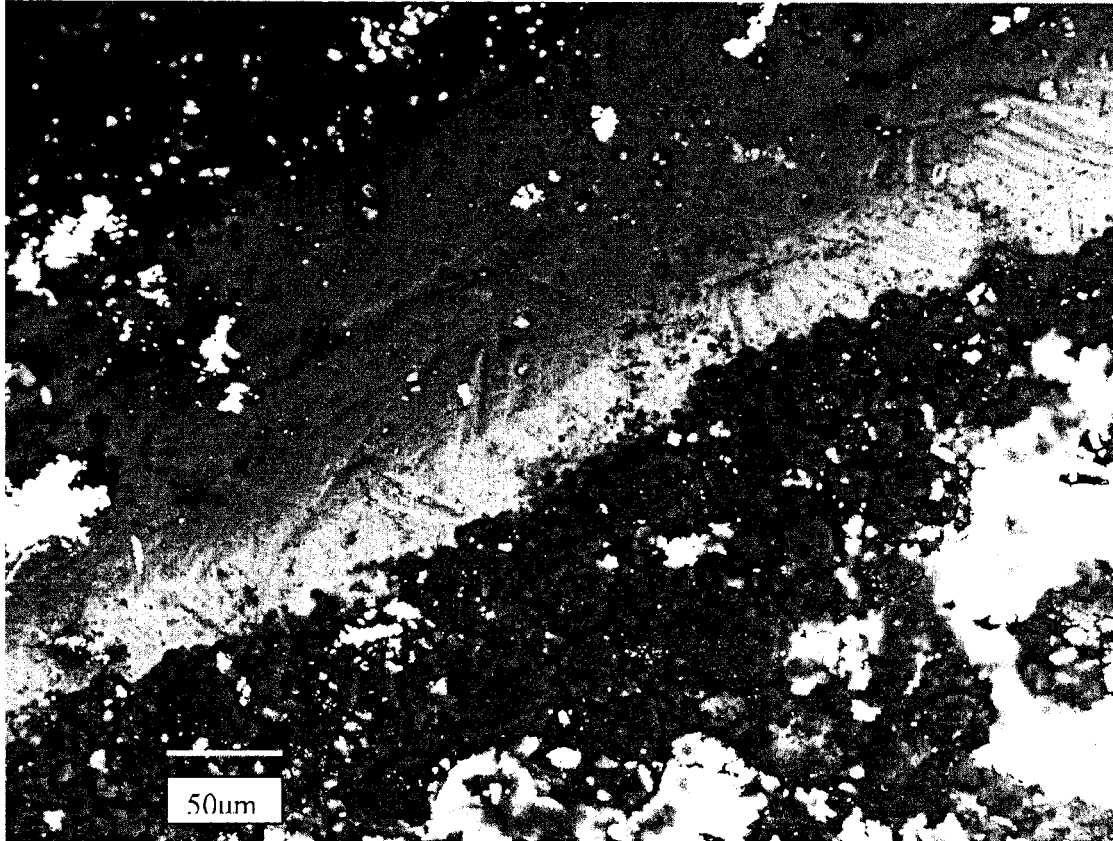


**Figure 3.7: Back scattered SEM image of bromobutyl rubber at the blade-tip after approximately five months in the service.**

Figure 3.7 is a micrograph of a bromobutyl rubber. The rubber stripe was taken from a failed agitator blade. The SEM investigation was carried out in order to investigate the surface morphology of the rubber specimen. The diagonal stripe appearing in the image was the joint of upper and lower layers of the coating rubber. This particular stripe was located on the front edge of the agitator blades.

A number of grooves with multiple orientations appear on the diagonal stripe as shown in Figure 3.7. Pitting spots and holes also appeared in the image. Below the diagonal stripe, a network of micro-cracks was observed which divided the rubber surface into many segments of various sizes. The network appeared like as grain

boundaries of metallic alloys. The cracks around some of the smaller segments (at left bottom in Figure 3.3) were wider than the cracks around the bigger segments.
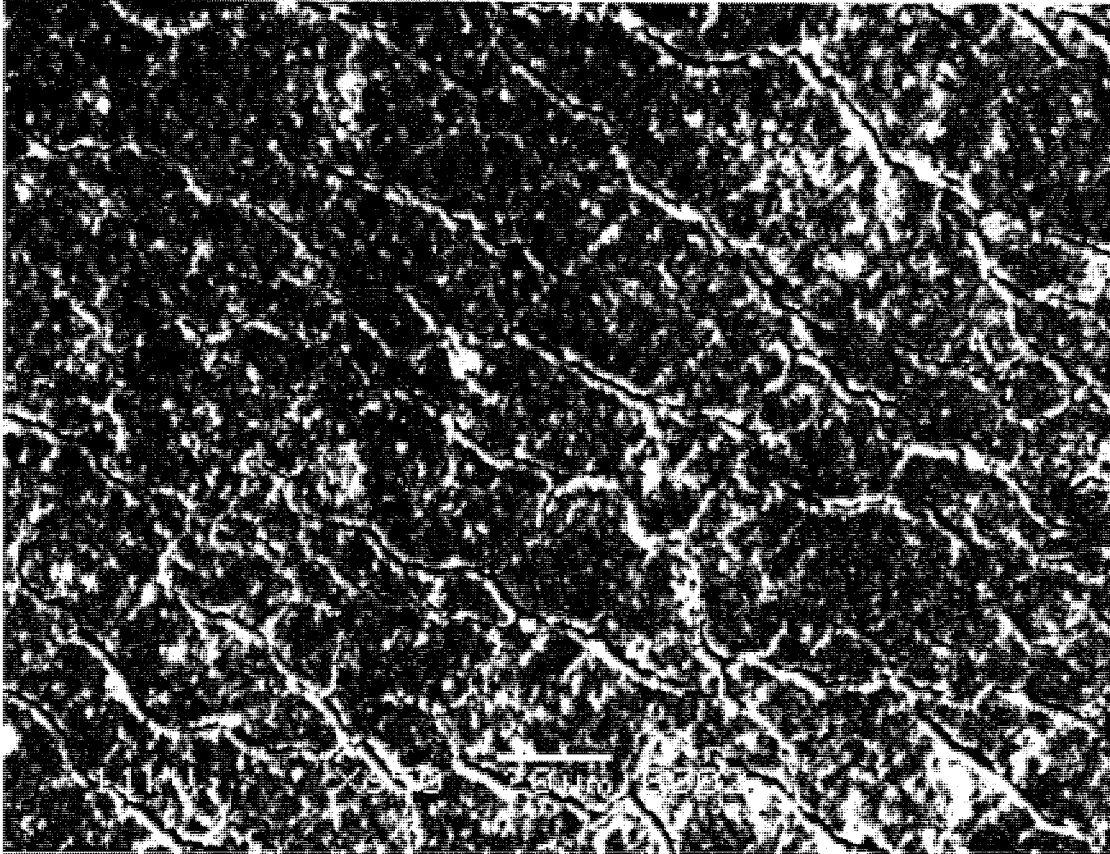


**Figure 3.8 Backscattered electron micrograph of bromobutyl rubber used on the upper side of an agitator blade near the blade-tip after six months in service.**

A networks of micro-cracks also appeared (Figure 3.8) on the failed rubber surface. The cracks were wider than those in the previous image (Figure 3.7). This effect may be an indicator of the growth rate of micro-cracks. At some point, the cracks could be stretching to form elliptical or round holes. A number of pitting spots are also visible despite the poor quality of the image. The white spots appear on the image could have resulted from excessive deposition of electron charges at various points on the specimen.
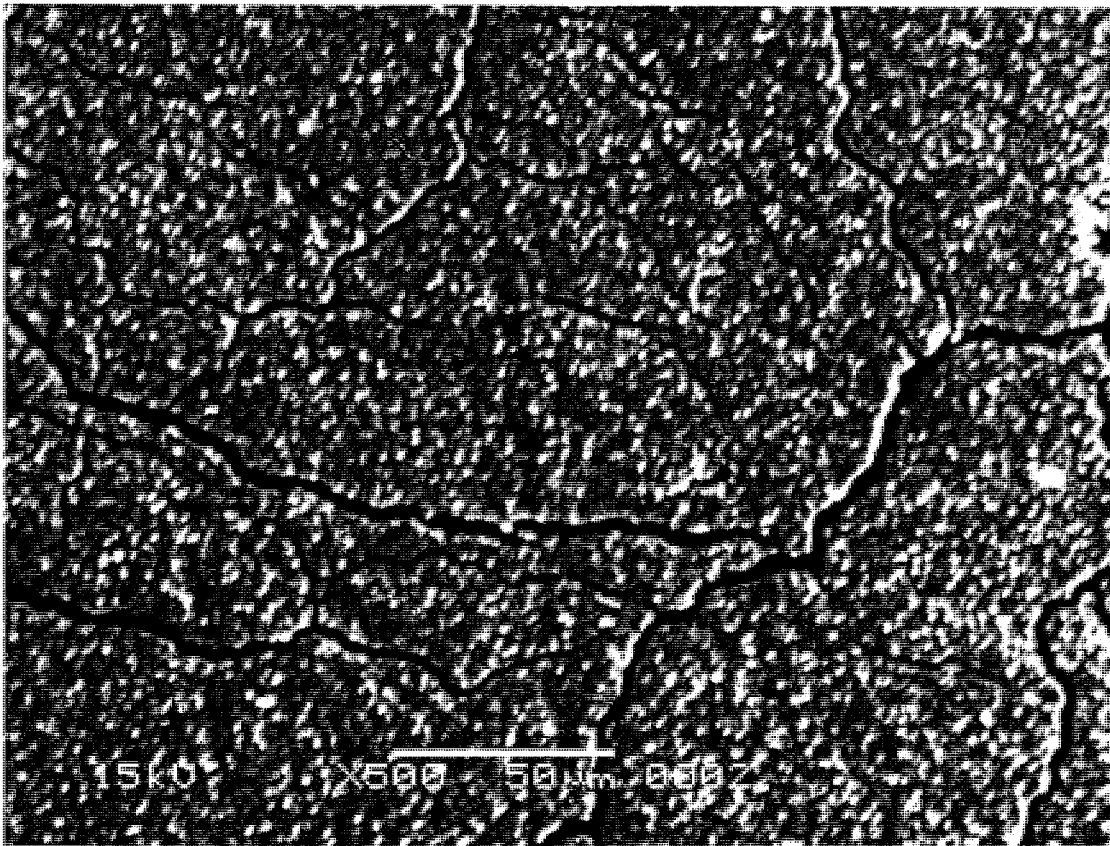
**Figure 3.9: Back scattered electron micrograph of bromobutyl rubber on agitator blades which failed after eight months in service.**

Figure 3.9 is a micrograph of coating bromobutyl rubber on agitator blades which failed after eight months. A network of cracks also appeared in Figure 3.9 as in the previous figures. The cracks were found to be wider than the cracks in Figure 3.7 and in Figure 3.8. New cracks being initiated and developed remained as part of the network.

## 3.7.1 Summary of the SEM analysis

The stresses, due to impact of the particles, on the rubber surface contribute to losing the elasticity of the rubber material. In course of time, the rubber surface becomes plastic due to repeated impact of the particles. This is likely to be a result of changes in molecular rearrangement in the structure are likely to cause it. At this stage, the tensile stresses produced by micro-plowing of the particles can cause micro-cracks on the rubber surface. Due to the cyclic load of the particles, these micro-cracks can grow in size and in number. The lateral growth of the fatigue cracks appear as grain boundary which, in turn can accelerate erosion. It seemed that the failure did not occur only for erosion of the

bromobutyl rubber. A prolonged period of time might be required to erode rubber layers to reach the blade material. As the failures occurred in a period of three to eight months, erosion only was not responsible for the failures.

The vertical growth of the fatigue cracks can reach the blade material in relatively short period of time depending on the stresses on the rubber surface. The penetration of rubber surface due to the fatigue cracks growth can expose the mild steel blade material to the acidic slurry medium. The blade material as a result can be corroded rapidly and fail in service.

## 3.8 Slurry chemical analysis

Slurry parameters, which vary from one process to another, may have an important role in failure of the agitator blades. Table 3.3 provides information about slurry parameters of various stages in the leaching circuit.

### 3.8.1 Acid concentration and pH

The weight concentration of hydrochloric acid in the mixing and purification tank was 2.09 and 0.09% respectively. No concentration of hydrochloric acid was given for the filtration stage, which consisted of filtered feed and polish liquor tanks. The pH in the mixing, purification, filtered feed and polish liquor tank was measured as 1-1.5, 1.5, 5.2 and 4.5-6.9 respectively. According to the information (in Table 3.3) the highest acidity was observed in the slurry mixing tank.

A chemical degradation test of bromobutyl rubber was conducted by an external laboratory for AMC. The tests were carried out using rubber samples which were submerged for a period of two weeks in the slurry mixing tank during operation. The outcomes revealed that the chemical degradation of bromobutyl rubber in such slurry was insignificant. However, there are a number of flaws in this test. First, the samples were kept in the service for a short period such as two weeks. Second, the bromobutyl rubber has reasonably good acid resistance and it performs well up to a temperature of $150^0C$.

Table 3.3: Slurry parameters in the leaching circuit of AMC [9].

| Ser ial. | Tank | pH | Acid (weight %) | Solids (weight.%) | Cl$_2$ (ppm) | Temp ($^\circ$C) |
|---|---|---|---|---|---|---|
| 1 | Leach tank 1 | 1.0-1.5 | 2.09 | 3.54 | - | 70 |
| 2 | Purification tank 1 | 1.5 | 0.09 | 1.60 | - | 70 |
| 3 | Filtered feed tank | 5.2 | - | 1.49 | 10 | 70 |
| 4 | Polished liquor | 4.5-6.9 | - | - | 10 | 70 |

Researchers including Ahn et al.[5] have studied the effects of pH on wear in chemical processes. They also examined the effect of pH on the wear of metallic materials in chemical slurries. Although no chemical degradation was observed in the tests carried out for AMC, it may be that the failures were caused by the combined effects of temperature, chemical environment and mechanical wear.

## 3.8.2 Solid concentration

The percentage weight concentration of solids in the mixing, purification and filtered-feed tank was found to be 3.54, 1.60 and 1.49 respectively. There were no solids present in the polished-liquor tank.

As mentioned earlier, the failures were predominantly in the mixing tank and no failures were observed in the purification tank. One set of hydrofoil type agitator blades was used in the mixing tank. Two sets of similar agitator blades were used in the purification tank, which was about 60% of the volume of the mixing tank. No agitation was required for the filtered-feed and the polished-liquor tank and therefore no agitator blades were used in those tanks.

The solid concentrations in Table 3.3 refer to the concentrations at the end of each process. Hence the solid concentrations during the process can be assumed to be higher. In the mixing tank, the solid concentration of the outflow was 3.54% which was more than double of the solid concentration of the outflow of the purification tank (1.60%) (see Table 3.3). This indicates that weight of particles striking the rubber will be higher in the mixing tank than in the purification tanks. Furthermore, it is expected that the size of individual particles in purification tank would be considerably smaller on average than those in the mixing tank. Hence, the kinetic energy of individual particles available to transfer on rubber surface in the mixing tank would be much higher than for the

purification tank. It can be expected that the bromobutyl rubber coating in the mixing tank will experience more severe conditions than the coatings in the purification tanks.

### 3.8.3 Slurry temperature

The slurry temperature was maintained $70^0C$ throughout the leaching circuit of the AMC. Researchers in slurry erosion have emphasized the importance of temperature in wear on many occasions. Wu *et al.* [6] found erosion-corrosion of carbon steel increased with increasing temperature. A similar result was reported by Mesa *et al.* [7] who also worked on metallic materials. No data on the effects of temperature on the wear behavior of bromobutyl rubber are currently available.

### 3.8.4 Summary of the slurry chemical analysis

The solid concentration was found significantly higher in the slurry mixing stage than the purification stage. This suggests that the kinetic energy transferred to the rubber surface was much higher in the mixing stage than the purification stage. The acid concentration of liquor in the slurry mixing (leach) stage was also found significantly higher than the purification stage. As the rubber experienced contact with the concentrated hydrochloric acid together with the mechanical action of the agitator in an ambient temperature $70^0C$, a synergy of combined action such as thermal, chemical and mechanical effect could have occurred. Although the process temperature $(70^0C)$ lies within the range of the temperature $(-50$ to$115^0C)$ in which bromobutyl rubber can perform well, the effect of temperature is insignificant. It may be concluded that the solid and the acid concentration were most likely contributors to the failure of the agitator blades.

## 3.9 References

1. Megud, S. A.,1989, "Engineering fracture mechanics," Elsevier Science Publishers Ltd., England, U.K., pp. 59-92.
2. Iwai, Yoshiri and Nambu, Kazuyuki 1997, "Slurry wear properties of pump lining materials," Wear, Vol. 210, pp. 211-219.
3. Clark, H. McI. and Wong, K.K., 1993, " A model of particle velocities and trajectories in a slurry pot erosion tester," Wear, Vol. 160, pp. 95-104.
4. Arnold, J.C. and Hutchings, I. M., 1992, "A model for the erosive wear of rubber at oblique impact angles," Journal of Physics, Vol. 25, pp. A222-229..
5. Ahn, Yoomin ; Yoon, Joon-Yong ; Baek, Chang-Wook ;Kim, Yong-Kweon, 2004, "Chemical mechanical polishing by colloidal silica-based slurry for micro-scratch reduction, Wear, Vol. 257, pp. 785-789.

6. Wu, Xinqiang ; Jing, Heming ; Zheng, Yugui ; Yao, Zhiming ; Ke, Wei, 2004, "Erosion-corrosion of various oil-refining materials in naphthenic acid", Wear, Vol. 256, pp. 133-144.

7. Mesa, D. H., Toro, A., Sinatora, A., and Tschiptschin, A. P., 2003, "The effect of testing temperature on corrosion-erosion resistance of martensitic stainless steels," Wear, Vol. 255, pp. 139-145.

8. Gates, J.F.,2003, "Material selection for wear," A seminar handout on Materials Selection at Gladstone, Australia, pp.1-11.

9. Peg, I., 2003, "Assessment of rubber lining for steel process tanks- Stanwell magnesium project, area 20, pp. 2-16.

Chapter 4

# Chemical Degradation of Rubber

Degradation of materials in natural and artificial systems is a common phenomenon. The rate of degradation depends on several factors including the chemical, thermal and mechanical environment. Materials may exhibit a number of degradation mechanisms depending on their environment. Bromobutyl rubber is a synthetic polymeric material and degradation modes and mechanisms of polymeric materials can be applied to it [1].

Synthetic rubber such as bromobutyl rubber is widely used in chemical and mineral processing industries due to its wear and acid resistance. Natural rubber contains raw gum elastomer with various ingredients. The chemical nature of natural rubber can make it vulnerable to attack in environments containing concentrated hydrochloric acid is leached at ambient temperature of $70^0$C. Whether or not this attack occurs is dependent on the nature of the rubber and the bromobutyl rubber studied here was expected to be resistant to attack. Nonetheless in this chapter, a study will be carried out to measure degradation in the rubber on the basis of hardness tests and SEM examination. This is done in order to determine whether or not chemical degradation is likely to be a major contributing factor in the breakdown of the rubber samples.

## 4.1 Modes of degradation

Degradation of synthetic rubber is mainly caused by chemical chain scission reactions in macromolecules [2]. The level of degradation considerably influences the length of the material's service life. Energy transfer to rubber yields the structural changes, which influence modifications in the chemical behaviour of the material [4]. Depending on the situation, the following modes of degradation may occur.

- Thermal degradation
- Mechanical degradation
- Chemical degradation
- Petrochemical degradation
- Radiation chemical degradation

- Biological and chemical degradation

Since bromobutyl rubber is considered capable of performing well in acidic environment at temperature up to $115^0C$, it was not expected to have suffered chemical and thermal degradation. However, the operating conditions in AMC refinery were unique and so an investigation was carried out in order to determine chemical degradation of bromobutyl rubber. Studies were also made to identify any possibility of thermal degradation for bromobutyl rubber.

## 4.2 Bromobutyl rubber

Butyl rubber is a copolymer of isobutylene with 1 to 2.5 mole % of cure site monomer isoprene. Bromobutyl rubber is a halogenated butyl rubber with approximately 2 mole% of bromine [8].

$$[C(CH_3)_2=CH_2]_n+[CH_2=C(CH_3)-CH=CH_2]_n \Rightarrow [-C(CH_3)_2-CH_2-CH_2-C(CH_3)=CH-CH_2-]_n \quad (4.1)$$

**Isobutylene**         **Isoprene**                                      **Butyl Rubber**

$$[-C(CH_3)_2-CH_2-CH_2-C(CH_3)=CH-CH_2]_n-+[Br_2]_{n/2} \Rightarrow [-C(CH_3)_2-CH_2-CH_2-C(=CH_2)-CH(Br)-CH_2-]_n$$
(4.2)
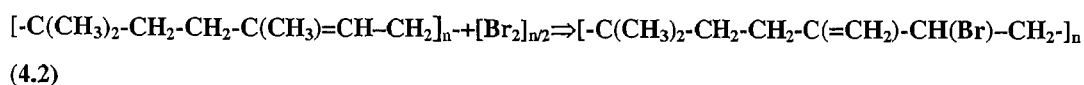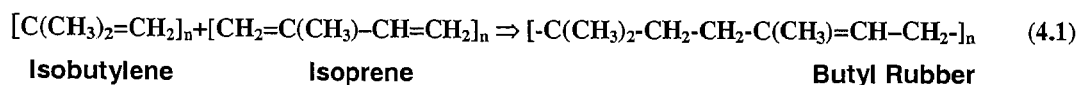
**Butyl Rubber**                                         **Bromobutyl Rubber**

Raw gum elastomer is a key ingredient of any synthetic rubber and it can be cross-linked into the polymer to improve the rubber properties. To manufacture rubber compounds, a number of additives need to be added to develop the required properties of rubber. A typical rubber compound may contain a number of ingredients including zinc oxide, stearic acid, accelerators, antioxidants, carbon black and plasticiser.

## 4.2.1 Chemical degradation

Chemical degradation refers exclusively to processes which are induced under the influence of chemicals into contact with polymers. In practice, all synthetic rubbers contain a small amount of low molecular weight compounds. These compounds could undergo chemical reactions with the macromolecules particularly as temperature is increased. Furthermore, rubbers contain unsaturated carbon-carbon bonds which are susceptible to metathesis reactions. Reactions of rubbers with molecular oxygen may be quite common as oxygen is ubiquitous. In some cases, significant conversion of rubber can be observed only at elevated temperature in the presence of molecular oxygen as a

result of high activation energy [2]. A few common forms of chemical degradation of rubber are solvolysis, reactions of olefinic double bonds, oxidative degradation, ionic degradation and selective degradation. Of them solvolysis, oxidative and ionic chemical degradation may be involved in the AMC process.
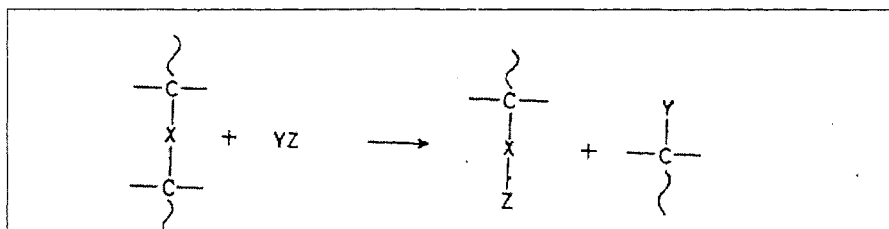


**Figure 4.1: Typical solovolysis reaction process [2].**

*Solovolysis* reactions generally break C-X bonds, where X represents hetero atoms like O, N, P Cl, Br and S. Solvolysis implies main-chain rupture as indicated in Figure 4.1 and common solvolysis agents are water, alcohols, ammonia and hydrazine. Water insoluble rubbers are attacked very slowly and the occurrence of the reaction is restricted to the surface of the rubber. Bromobutyl rubber is a water insoluble polymer. Water was produced during the reaction of magnesite with hydrochloric acid (refer to Figure 4.1). The molecular weight of water is significant compared to other compounds in the magnesite slurry. So, the degradation of bromobutyl rubber due to solvolysis reactions may be possible in long periods of time in an ambient temperature $70^{0}C$.

*Reactions of olefinic double bonds* are applicable to a number of rubbers which may contain carbon double bonds either as a chemical impurity or as a part of molecular structure.
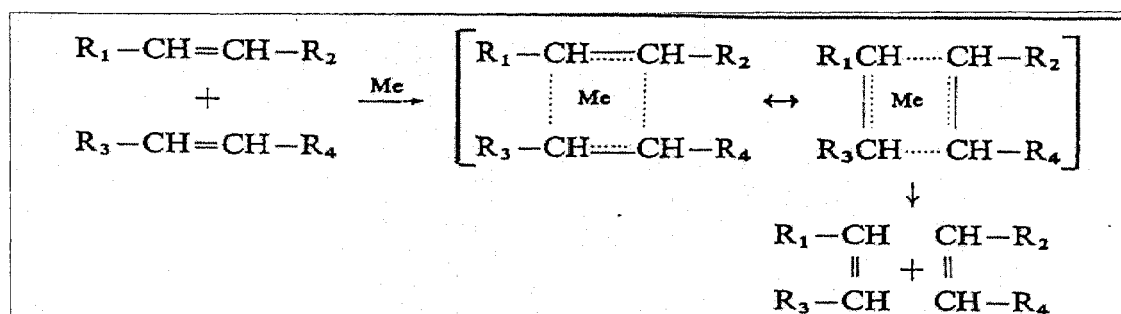


Figure 4.2: The figure represents an equation of general scheme of metathesis. Me denote a catalyst system consisting of catalyst/co-catalyst pair [2].

It is well known that C-C double bonds are reactive towards various chemicals. Metathesis and ozonization are two chemical reactions of olefinic double bonds leading to the scission of the C-C double bonds (see Figure 4.2). Although C-C double bonds exist in bromobutyl rubber, for metathesis reactions to occur, a catalyst system consisting of a catalyst/co-catalyst pair is necessary. Although no testing was carried out to determine whether such reagents are present in the AMC process, if such catalysts were present, reactions of olefinic double bonds for bromobutyl rubber may occur.
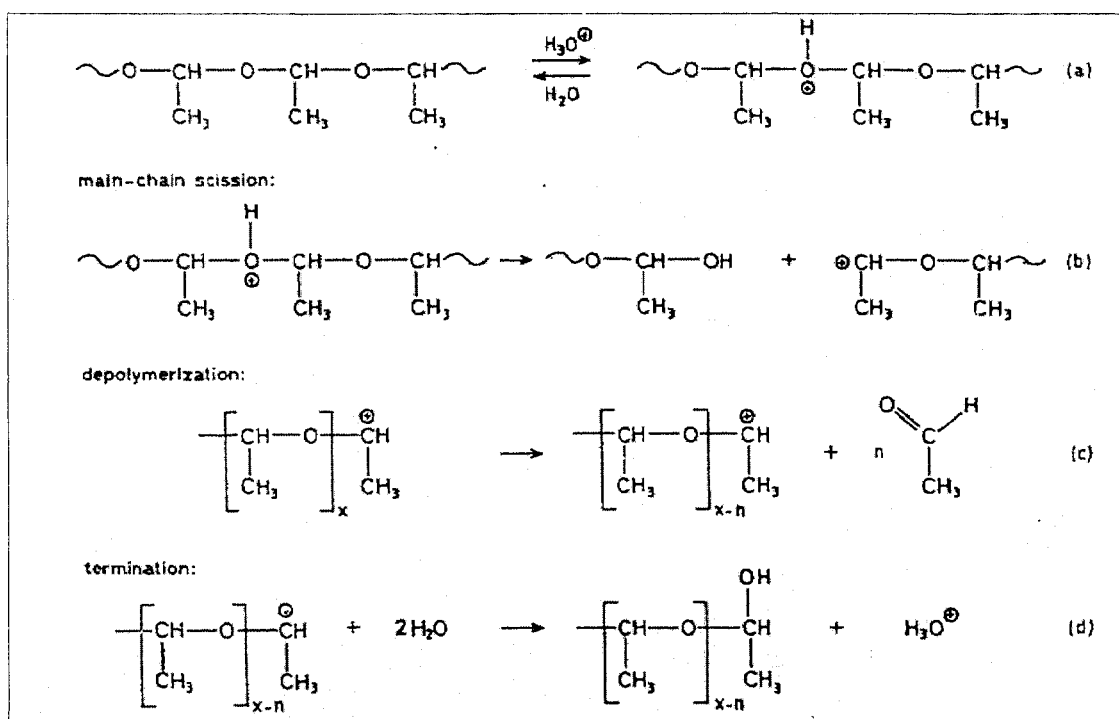


Figure 4.3: Figure represents an equation of acidic degradation of poly-acetaldehyde where main-chain scission and de-polymerization occurs before termination [2].

*Ionic degradation* plays a significant role in chemical degradation. In the acidic degradation of poly-aldehydes, the initial and final step is main-chain scission and depolymerisation respectively. A typical polymer exhibiting this behaviour is poly-acetaldehyde and the mechanism is illustrated in Figure 4.3.

## 4.2.2 Thermal degradation

Thermal degradation refers to the case where the polymer, at elevated temperature, starts to undergo chemical changes without the simultaneous involvement of another compound [2]. Judging by this definition, thermal degradation was less likely to be involved in the failure of bromobutyl rubber coating on agitator blades. In the AMC process, coating

rubber remained in contact with a number compounds such as magnesite, hydrochloric acid, magnesium chloride and water. However, chemical degradation of bromobutyl rubber may be influenced by the thermal effect.

Oxygen uptake of butyl rubber, under various temperatures, has been investigated by Zaharescu and Podina which indicated (refer to Figure 4.4) quick thermal degradation of butyl rubber occurred at $220^{0}C$. The oxidation rate at $230^{0}C$ was about 3-5 times than the rate at $220^{0}C$ [4].
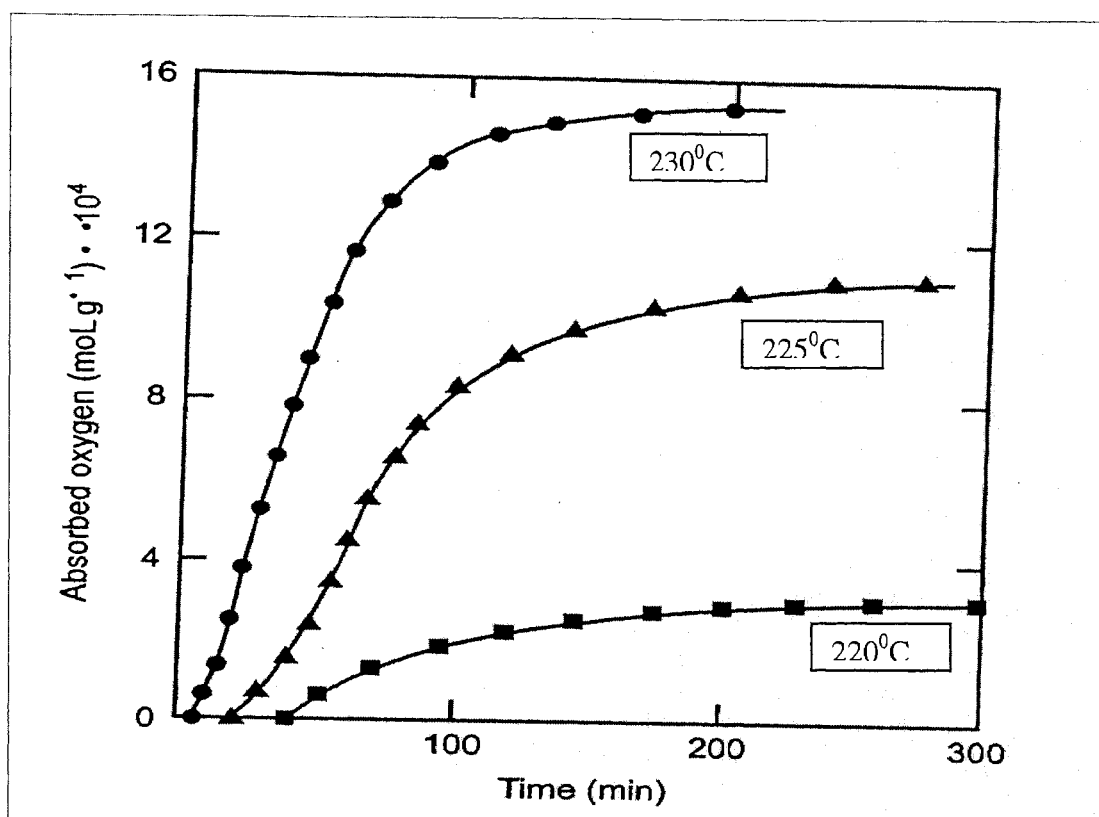


Figure 4.4: Dependence of oxygen intake on time for butyl rubber under 220, 225 and 230°C [4].

It is often difficult to distinguish between thermal and thermo-chemical degradation due to impurities in the polymeric materials. Impurities present may react with the rubber matrix if the temperature is high enough. At such a moderate temperature as $70^{0}C$, it is unlikely that thermal degradation will be the principal mechanism of degradation. However, the synergy between the chemical environment and elevated temperature may increase the likelihood of degradation. At the commencement of this study, it was not known whether the synergy of these factors would affect the degradation

behaviour, and hence a limited experimental study was initiated in order to determine the effects of long-term immersion on the mechanical behaviour of bromobutyl rubber.

### 4.2.3 ASTM standard test methods for rubber

ASTM international has designed and developed a number of experimental methods to determine the properties of rubber under various conditions. The following ASTM standard test methods may be applied in order to investigate the degradation of bromobutyl rubber. However, they were not particularly designed to measure chemical degradation of rubber.

- Test methods for rubber deterioration by heat and oxygen D 572.

- Standard test methods for rubber deterioration by heat and air pressure D454-04.

- Test methods for rubber deterioration by heat and ultraviolet light D1148-95 (2001).

- Standard test methods for rubber –evaluation of BIIR and CIIR D3958-00 [3].

There is little information available on the interactions between wear and degradation and no ASTM Standards directly addresses this issue. Furthermore, the ASTM standard test methods do not simulate the conditions existing in the AMC process. This is why an experimental method was established to determine changing rubber properties under the influence of thermo-chemical processes. The test method D 2240-04 was used to examine the change of rubber hardness (shore A) at intervals during testing.

The test does not propose to examine the interactions between wear and degradation. It is limited in scope to examining the changes in mechanical behaviour of the rubber during immersion.

### 4.2.4 Description of the equipment

A round bottom flask was mounted on an electric heater fitted with magnetic stirrer. A reflux condenser, with submersible electric pump, was attached to the flask in order to circulate water to condense the vapour. A mercury thermometer was incorporated into the apparatus to monitor the solution temperature. A circular plate rig made of Teflon was mounted in the flask in order to place the samples on it. Holes were drilled on the plate rig to ensure adequate circulation of magnesium chloride solution while it was being heated. The experimental set up is illustrated in Figure 4.5.
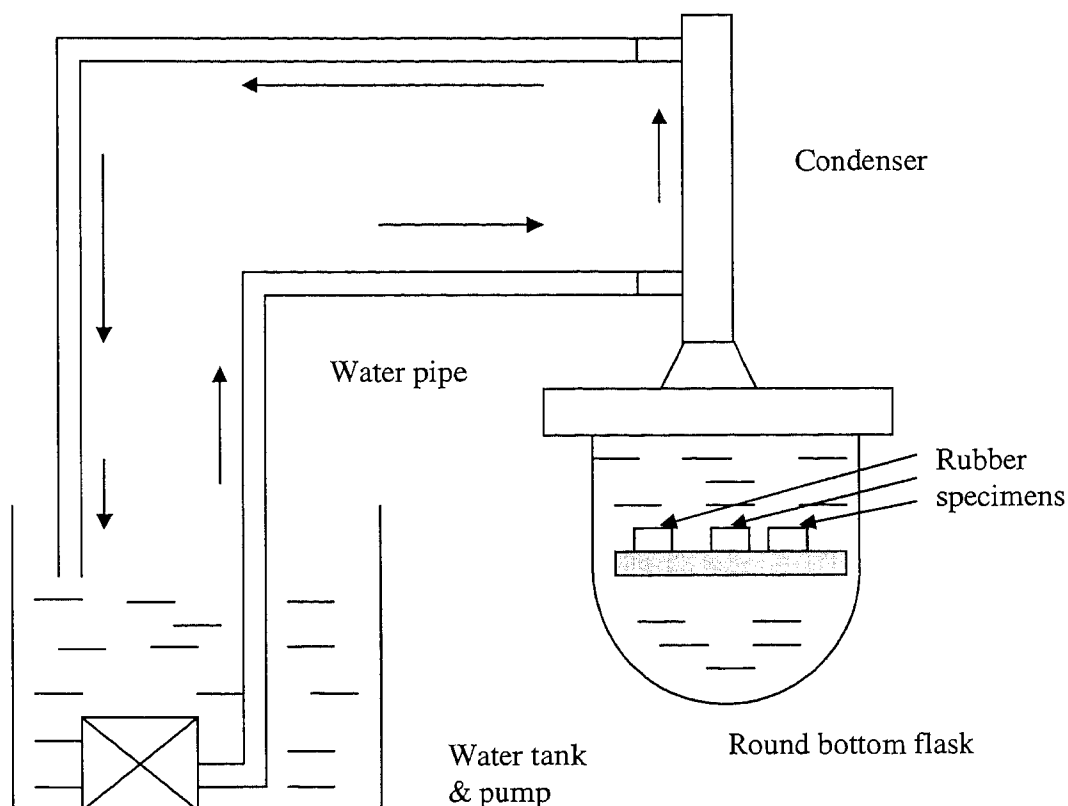
Figure 4.5: A schematic diagram of rubber degradation test method.

## 4.3 Experimental Design & Procedure

### 4.3.1 Sample and solution preparation

Samples were cut to size (50 mm X 10 mm X 6 mm) using a sharp knife and each sample was marked to distinguish it from the others. A total of six samples were used for each test. Natural and bromobutyl rubber only were used in this procedure.

A volume of 700 mL of magnesium chloride containing 5% excess hydrochloric acid was used for this experiment. Magnesite ore (291.7 gram) was mixed with 845 gram of 35% concentrated hydrochloric acid to produce magnesium chloride solution containing 5% excess hydrochloric acid. The liquor left the slurry mixing tank with 1-2 % excess hydrochloric acid.

### 4.3.2 Test materials & scheduling

The following materials were selected for the experiments.

- Natural rubber

55

- Bromobutyl rubber

Six specimens were tested for each rubber. In order to avoid contamination between rubbers, tests were carried out separately. The specimens were made as blocks of 50 mm x 10 mm x 6 mm in dimension.

**Table 4.1: Physical properties of natural and bromobutyl rubber [6].**

|  | Hardness (Shore-A) | Abrasive Resistance | Resilience | Tensile strength | Acid Resistance |
|---|---|---|---|---|---|
| Bromobutyl rubber | 30-90 | Good | Poor-Fair | 2500 MPa | Good-Excellent |
| Natural rubber | 30-100 | Excellent | Excellent | 4000 MPa | Fair-Good |

A number of tests were scheduled for natural and bromobutyl rubber over periods up to 10 weeks. The hardness (shore A) of virgin bromobutyl rubber was measured using a pocket durometer prior the chemical test. At periodic intervals, the samples were removed from the flask and cooled to room temperature prior to testing. Samples used for SEM investigation and EDS analysis were cleaned using detergent solution. Measurements were taken at $1^{st}$, $2^{nd}$, $4^{th}$, $6^{th}$ and $10^{th}$ weeks during the experimental period. Table 4.2 summarizes the detailed test schedule.

**Table 4.2: Rubber degradation test schedule.**

| Time ( in week) | Temperature( in °C) |
|---|---|
| 0 | 70 |
| 1 | 70 |
| 2 | 70 |
| 4 | 70 |
| 6 | 70 |
| 10 | 70 |

## 4.4 Experimental results

The hardness (shore A) was measured in accordance with ASTM D 2240 [3]. A pocket durometer hardness tester was used to measure the hardness of rubber samples. Scanning electron microscope was used to obtain surface topography data of the bromobutyl rubber before and after the test. An elemental analysis was also performed in order to investigate

any inclusions in the rubber that may have been caused by the immersion in the chemical solution.

Figure 4.6 compares the variation of hardness for natural and bromobutyl rubber in magnesium chloride solution at an ambient temperature of $70^0C$. Apparently both natural and bromobutyl rubbers demonstrate similar tendency. For a better understanding the plot (see Figure 4.6) can be divided into three distinct zones in terms of time. The initial zone represents the period of 0 to 1-week. The middle and final zones represent the period of 1 to 4 and 4 to 10weeks respectively.
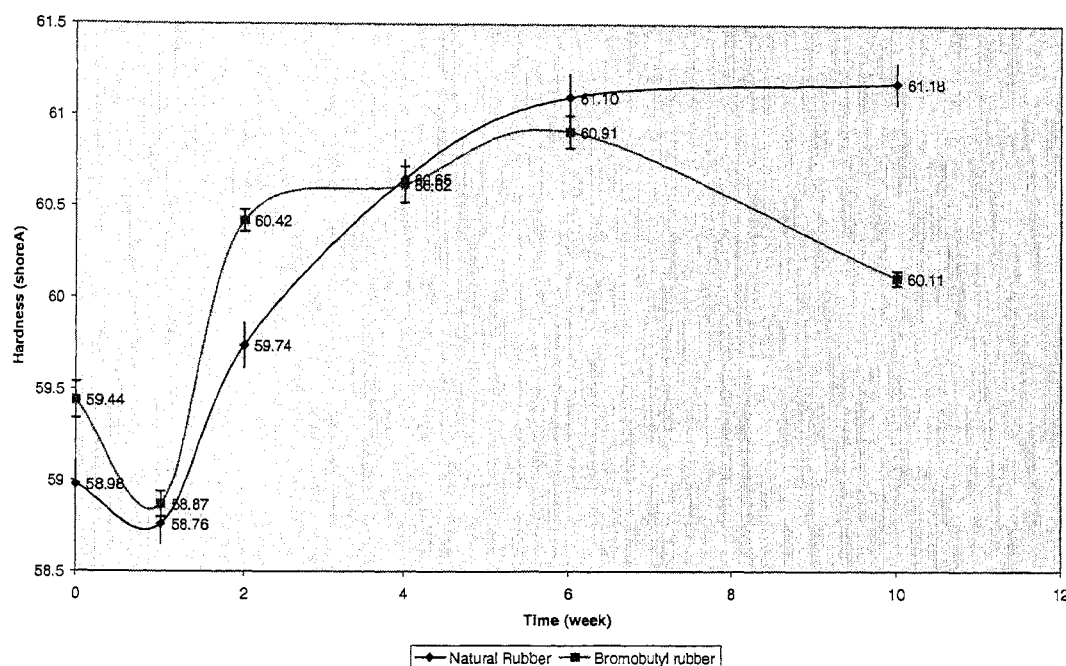


Figure 4.6: A comparison of hardness (shore A) between natural and bromobutyl rubber in magnesium chloride liquor (with 5% excess hydrochloric acid) over a period of 10-week.

In the initial zone, the hardness of natural and bromobutyl rubber decreased to about 58.76 and 58.87 respectively. In the middle zone, the hardness increased for both rubbers until week-4. In the final zone, the hardness of natural rubber continued to increase with a slower rate but the hardness of bromobutyl rubber continued to decrease until week-10. The slopes of both curves tended to be steeper in the middle zone. The average rise (hardness) in this zone for natural and bromobutyl rubber was found 3.50 and 3.02%. In the final zone, the hardness of natural rubber continued to increase until week-10 whereas the hardness for bromobutyl rubber initially increased and then

decreased until week-10. The overall rise in hardness for natural and bromobutyl rubber was found 3.73% and 1.13% respectively.
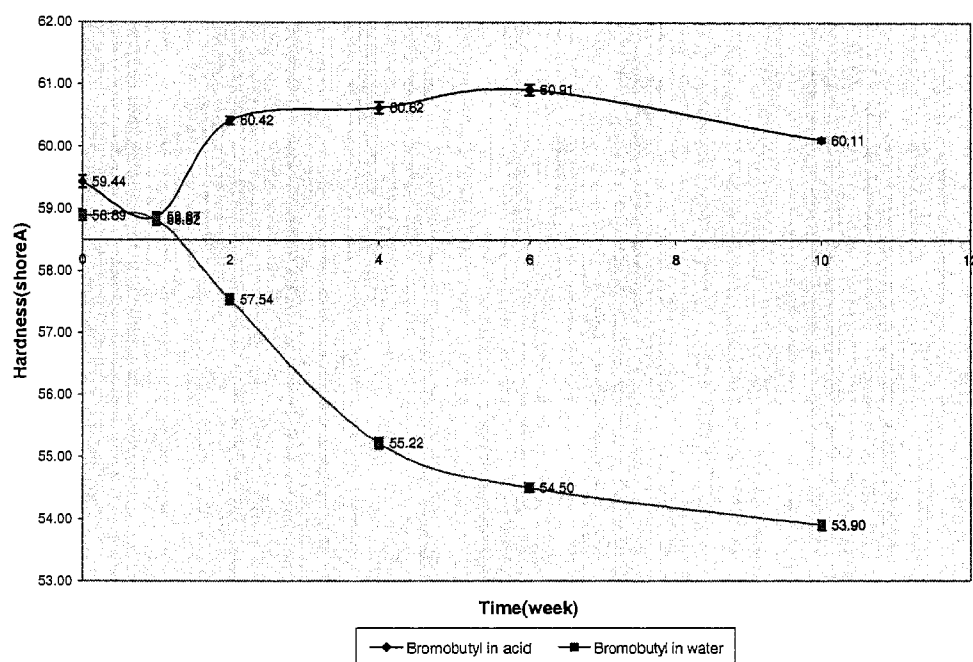


Figure 4.7: A comparison of hardness (shore A) between bromobutyl rubber in water and in magnesium chloride liquor (with 5 % excess hydrochloric acid) over a period of 10-week.

Figure 4.6 compares the variation of hardness of bromobutyl rubber in water and in magnesium chloride at an ambient temperature $70^0C$. At the end of week-1, the hardness of bromobutyl rubber decreased slightly under both conditions. The hardness decreased until the end of week-10 in water. It continued to increase up to a period of week-6 which then decreased in acidic magnesium chloride solution until week-10. A trend of increasing and decreasing hardness of bromobutyl rubber respectively appears in acidic and water medium (refer to Figure 4.7). The overall rise and fall in hardness of bromobutyl rubber in acidic and water medium was observed about 1.13 and 8.47 % respectively. One discrepancy that arises here (see Figure 4.6) is the difference in shore A hardness of bromobutyl rubber at 0 week. Measurements were taken in three months gap and the accuracy of the measurement of pocket durometer was relied on the proper operation. The discrepancy might have resulted in either way.

.SEM images (surface topography) of virgin and tested bromobutyl rubber are shown in Figure 4.8 (a) and in Figure 4.8 (b). The surface topography of virgin

bromobutyl rubber in Figure 4.8 (a) appears relatively even and smooth except for a few small lumps. During visual inspection, no such lumps were observed.


(a)


(b)
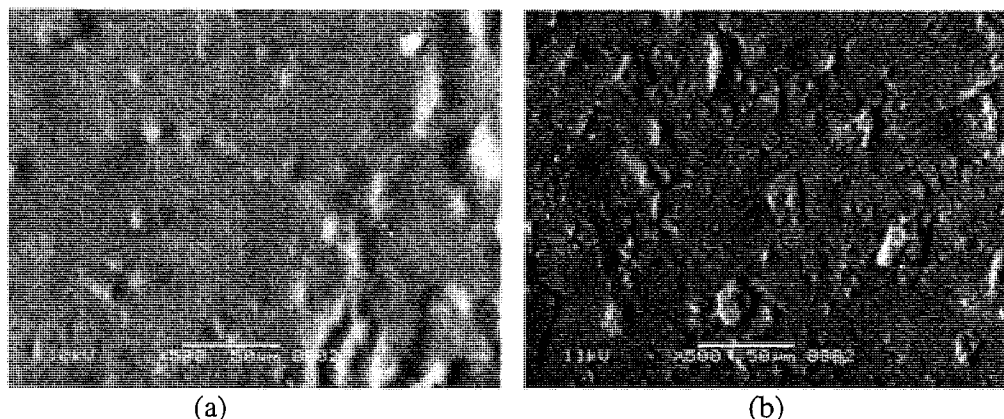
**Figure 4.8: Surface topography of bromobutyl rubber (a) virgin rubber (b) tested rubber.**

The surface topography of tested rubber is shown in Figure 4.8 (b) with various sized lumps and a few small black holes. The surface topography of a virgin rubber is shown in Figure 4.8 (a). No black holes but some lumps were visible. These lumps may


(a)


(b)
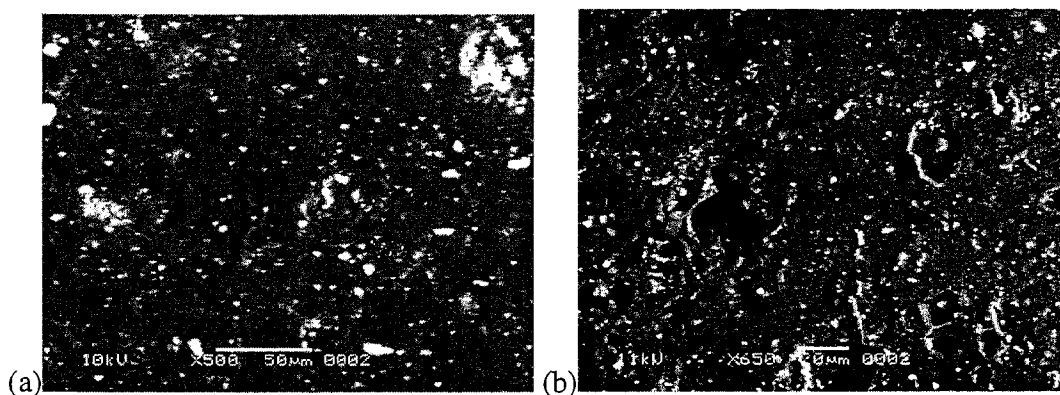
**Figure 4.9: Surface morphology of bromobutyl rubber (a) virgin rubber (b) tested rubber.**

have been caused due to handling damage.

The SEM image of virgin bromobutyl rubber in Figure 4.9(a) appears reasonably flat and smooth except for a few pores and a number of white spots. In Figure 4.9(b), damage appears including a number of larger pores and lumps.
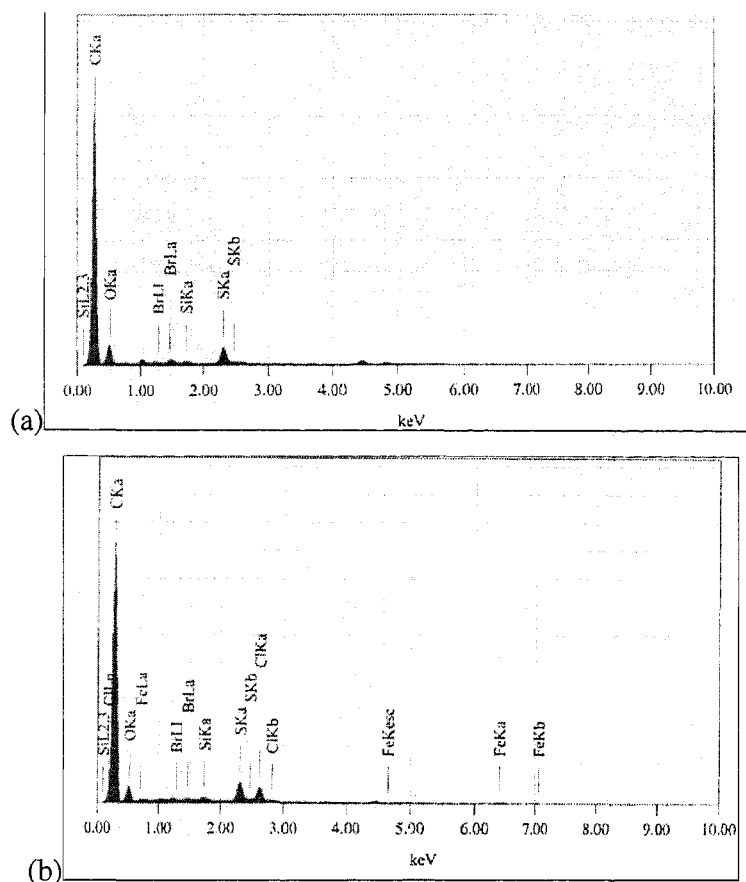
Figure 4.10: EDS analysis of bromobutyl rubber (a) virgin rubber stored in room temperature (b) tested rubber in magnesium chloride having 5% excess HCl at an ambient temperature $70^0$C for a period of 3-month.

The EDS analysis revealed the elements such as C, Si, Br, S and O were present in the virgin rubber (refer to Figure 4.10b). Hydrogen (H) element was not shown as EDS detector was unable to detect light hydrogen atoms. The same elements as virgin rubber were found in the EDS analysis of tested bromobutyl although some Fe and Cl were present.

## 4.5 Discussion

Degradation of rubber material may influence a number of properties such as hardness, tensile strength, compression set and tears resistance of the material. Hardness is the main property of interest because the wear resistance of a material is mainly evaluated according its hardness. In many materials, wear resistance is often found to increase with increasing hardness up to a certain limit, particularly in the case of metallic materials. However, for rubber materials the opposite is often observed [7].

In the tests carried out, the hardness of bromobutyl rubber displayed different behaviour in acidic magnesium chloride than in water. In water, the hardness decreased

over time, possibly suggesting a hydrolysis of the rubber. Even though the rubber is not expected to absorb significant amounts of water, there may have been some swelling of the rubber due to water penetration. No volume changes in the rubber were measured during these tests. The uptake of water is a likely reason for the decrease in hardness.

An opposite result was observed when the specimens were immersed in the HCl/MgCl$_2$ solution. It seems likely that a reaction was taking place between the rubber and the solution, possibly involving chlorination of the rubber. Significant quantities of chlorine were found in the EDS analysis suggesting that the rubber may have absorbed some of the chlorine from the solution. Partial chlorination may have led to an increase in cross linking of the rubber and this may have led to the observed increase in hardness.

After week 1, the hardness of the rubber in water alone and HCl/MgCl$_2$ solution was about the same. This may be due to the water uptake was similar in both cases and the hardening due to chlorination may take some time to begin. If this is the case, it suggests that a similar softening process due to the uptake of water may be occurring in the samples immersed in HCl/MgCl$_2$ solution, but that the hardening due to the chlorination is more than offsetting the softening of the rubber.

The SEM images of the virgin rubber showed a smooth surface with little evidence of damage. After immersion, the surfaces start to show some signs of damage in the form of pores and lumps. Significant difference in damage on rubber surfaces immersed in water and acid was observed. This may be due to some chemical reaction of rubber with the acidic solution.

One important fact not yet mentioned was that the same rubber samples were examined at times with a pocket durometer hardness tester. The indentation marks and the pressure applied on rubber surface by the hardness tester while measuring could appear as pore and lumps in the SEM images.

The results obtained in the EDS analysis indicated that there was some uptake by the rubber of elements such as Fe and Cl. As it was mentioned earlier that bromobutyl rubber is a brominated butyl rubber. There may be some further uptake of chlorine if there are some unsaturated bonds in the structure or there may possibly have been some substitution of chlorine for bromine. In the XRD examination of the magnesite ore, iron

oxide was found as one of the impurities in the magnesite ore and this is the likely source of Fe in the rubber. However, the way of its addition has not yet determined.

The study reported in this chapter shows that the immersion of bromobutyl rubber in the $HCl/MgCl_2$ solution caused an increase in the hardness of the rubber and that this hardening effect more than compensated for any softening caused by the uptake of water into the rubber. Hardening of the rubber will tend to make it more brittle and will reduce the ability of the rubber to absorb energy. Although the effect observed here was slight, it may have a minor influence on the rate of degradation of the impellor blade coatings.

The aim of this work was to see if the environment alone could affect the mechanical properties and surface topography of the rubber. It has been shown that there is a minor hardening effect from the immersion of the rubber in the $HCl/MgCl_2$ solution. This project/study does not propose to address the issue of the causes of the degradation of the rubber nor the chemical nature of the degradation and this is left to further work.

# 4.6 References

1. Wypych, George, "Handbook of Material Weathering" 2$^{nd}$ edition, chapter 14, pp. 391-396.
2. Schnabel, W. "Polymer Degradation – Principles and practical applications", Hanser International, pp. 25-205.
3. ASTM International online – Standard test methods for rubber material, www.astm.org
4. Zaharescu, T. and Podina, C. "Thermal degradation of butyl rubber", Journal of Materials Science Letters, 1997, Vol. 16, pp. 761-762.
5. Hofmann, Werner, "Rubber technology handbook", Hanser Publishers, chapter 3, pp. 85-95.
6. Long, Harry, "Engineering properties of elastomers," Source Internet, Author: Harry Long, Technical Manager, Goodal Rubber Co., Trenton, NJ, USA.
7. Gates, J.F., 2003, "Material selection for wear," A seminar handout on Materials Selection at Gladstone, Australia, pp.1-11.
8. Hofman, Werner, 1989, "Rubber technology handbook", Hanser Publishers, Oxford University Press, Canada, pp.90-92.

Chapter 5
# Erosion Modelling

Finnie defined erosion as "wear which occurs when solid particles entrained in a fluid stream strike a surface" [1]. Clearly in the situation discussed here, erosion is a potential cause of failure, with the solid magnesite particles in the slurry likely to cause erosion of the bromobutyl rubber coating.

Despite the large number of empirical tests carried out in order to obtain better understanding of the slurry erosion, there is still not a consensus regarding the theoretical underpinning of erosive wear. However without a sound theoretical understanding of erosion, there is little predictive power in the work and at best, the models currently available only provides a qualitative ability to predict erosive behaviour. The current state of knowledge of erosion wear is that much of the available information still relies on empirical studies and although some theoretical advances have been made, particularly in the area of numerical modelling, a truly unified theory of erosive wear is still a long way off.

Nonetheless, a number of semi-empirical qualitative models for erosive wear exist and can give some insight into the effects of experimental parameters. In this chapter, a number of these models are discussed and modelling is developed in order to provide some insight into the behaviour of the bromobutyl rubber in the wearing media.

## 5.1 Erosion Mechanism

Erosion occurs by a variety of mechanisms, such as cutting, plowing and deformation. These have been described in previous studies [1-6]. The following factors were also identified as being important in erosion:

- cutting mechanisms
- cutting and deformation mechanisms

The cutting mechanism was proposed by Finnie [1] and the cutting & deformation mechanisms were proposed by Bitter [5-6]. In real situations, a number of mechanisms may be involved in slurry erosion. Although their models were limited to specific erosion

situations, the models are still accepted as important by most of the researchers in slurry erosion.

## 5.1.1 Finnie's cutting model

Finnie presented his analysis on how eroding impacting particles cause erosive wear as they cut into ductile metal surfaces [1-3]. He estimated the volume of material removed by a certain mass of abrasive grains $Q$, by the following equation.
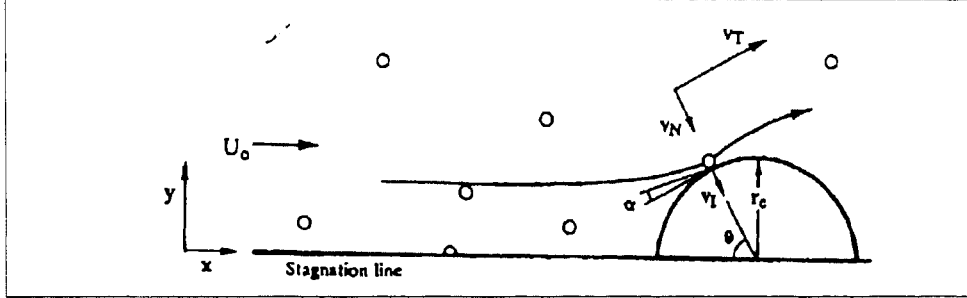


**Figure 5.1: Schematic diagram of particle impact on a cylinder [1].**

$$Q = C\frac{mv^2}{4}\frac{1}{p}f(\alpha)$$

(5.1)

where, p is the flow stress, C is particle fractions, m is mass of abrasives, $\alpha$ is the impacting angle and v is the velocity of abrasive particles. In a later study [4] Finnie altered his original cutting model to the following equation:

$$Q = C\frac{m^2v^n}{p}f(\alpha)$$

(5.2)

where, the exponent n is typically in the range 2.2-2.4.

Finnie's cutting model is mainly based on "the mechanism of metal cutting by a cutting tool" during machining process. As a result his model is limited to only one wear mechanism (cutting), whereas in complex slurry flow environment a number of wear mechanisms may be in existence. A schematic diagram of his model is as shown in Figure 5.1.

## 5.1.2 Bitter's cutting and deformation wear model

In 1963, Bitter proposed his erosion-model based on the assumption that impacting particles only cut and deform the surface of the material [5-6]. According to him, the total wear occurring in the unit time $W$, is given by

$$W = W_D + W_C \tag{5.3}$$

where, $W_D$ is deformation wear per unit time and $W_C$ is cutting wear per unit time. The expression developed by Bitter for deformation wear in equation (5.4).

$$W_D = \frac{M\left(V\sin(\alpha) - K\right)^2}{2\varepsilon} \tag{5.4}$$

where, M is the mass of the particles in unit time and $V$ ($V\sin\alpha = V_I$) is the velocity of the particles impinging at an angle $\alpha$ on a unit area. K is the normal component of particle impact velocity required for the initiation of erosion damage and $\varepsilon$ is the specific energy required for deformation wear per unit volume of material.

Bitter proposed his cutting wear model for two different cutting conditions when impacting particle velocity $V_p$ is parallel to body $V_p = 0$ and when the particle impinging the body at a particular angle i. e. $V_p \neq 0$. For $V_p \neq 0$, the cutting equation

$$W_C = 2M \frac{C\left(V\sin(\alpha) - K\right)^2}{\sqrt{V\sin(\alpha)}} \left[ V\cos(\alpha) - \frac{C\left(V\sin(\alpha) - K\right)^2}{\sqrt{V\sin(\alpha)}}\sigma \right] \tag{5.5}$$

where, C = $\frac{0.288}{y}\sqrt[4]{\frac{d}{y}}$ and $\sigma$ = the amount energy required to cut a unit volume of material from the surface.

For $V_p = 0$, the cutting equation is as below:

$$W_C = \frac{M\left[V^2\cos^2(\alpha) - K_1\left(V\sin(\alpha) - K\right)^{3/2}\right]}{2\sigma} \tag{5.6}$$

where, $K_1 = 0.82y^2\sqrt[4]{\frac{y}{d}}(\frac{1-q_1^2}{E_1} + \frac{1-q_2^2}{E_2})^2$, $q$ = Poisson's ratio and $E_1$ is Young's modulus of particle and $E_2$ is the Young's modulus of target material.

So, the total volume removed by the deformation and cutting wear is the addition of the contributions from deformation wear $W_D$ and cutting wear $W_C$.

Bitter's model is still widely accepted by many researchers despite some difficulties with material dependent constants. Although the model is based on erosion of metallic materials it may be less applicable in other situations particularly with elastomeric materials.

## 5.1.3 Arnold and Hutching's model

In 1992, Arnold and Hutching proposed a model for erosive wear at glancing impact following the model of Thomas, who determined the volume of material removed by fatigue crack growth per unit sliding distance, A [7]

$$A = hB \sin(\theta) \left( \frac{F}{h}(1 + \cos(\theta)) \right)^{\beta} \tag{5.7}$$

where h is the width of contact, F is the friction force, $\theta$ is the angle to the horizontal at which cracks grow and B & $\beta$ are constants, relating to crack growth.

Their model is complex with a number of constants and variables as shown in equation in equation 5.8.

$$\varepsilon = 2 \left( \frac{8}{3\pi} \right)^{(\beta-1)/2} B \sin(\theta)(1 + \cos(\theta))^{\beta} \rho_p^{(\beta-1)/2} u^{\beta+1} R^{\beta-1} \mu^{\beta} \rho_r \left( \frac{E}{1-v^2} \right)^{(\beta-1)/2} Q \tag{5.8}$$

where, $\varepsilon$ is the erosion rate, $v$ and E are the Poisson's ratio and Young's modulus of the rubber, R is the radius of the particle, u is the initial velocity of particle, $\rho_r$ is the density of rubber, and $\mu$ is the co-efficient of friction and $\rho_p$ is the density of the particle and Q is a function of the impact angle $\alpha$.

For $\mu \tan\alpha$ <0.5,

$$Q = \sin^{\beta}(\alpha)(\cos(\alpha) - \mu\sin(\alpha)) \tag{5.9}$$

For $\mu \tan\alpha$ >0.5,

$$Q = \frac{\pi^{(\beta-1)/2}}{2^{\beta}} \sin^{\beta}(\alpha) \left[ \cos\left( \alpha - \mu\sin(\alpha)\left( 1 - \frac{\sin(kt_c)}{kt_c} \right) \right) \right] kt_c \left( \frac{1 - \cos(kt_c)}{kt_c} \right) \tag{5.10}$$

Arnold and Hutchings simplified the equation, breaking it down into three terms referring to particle size, impact velocity and rubber properties. A good qualitative agreement was claimed between the predictions of the model and experimental measurements but the quantitative agreement was not so good and may be due to several assumptions.

In 1993, Arnold and Hutchings developed another model on erosive wear of rubber by solid particles at normal incidence [8]. They found that the erosion rate, $\varepsilon$, was:

$$\varepsilon = \frac{9\rho_\gamma B}{100R\rho_P}\left(\frac{16R\rho_P\left(a\mu\right)^2 u^2}{3\pi\left(1-v^2\right)}\right)^\beta$$

(5.11)

Empirical constants are still present in the equation which has made it more difficult for application.

A number of empirical constants are required to make these models represent practical cases. Considering these factors, a simplified model was established in order to predict a better understanding of erosion.

### 5.1.4 Proposed slurry erosion model

Prediction of slurry erosion still relies on experimental test methods. Due to the complexity of the process, these test methods have not yet provided adequate information. A numerical model has been proposed in order to describe the erosive wear of bromobutyl rubber in magnesite slurries. The model is developed based on the results of previous models. The assumptions for the proposed model are:

- Particles are spherical in shape.

- The motion of particles is sliding over the surface of specimen.

- Flow around the specimen is laminar.

- Reactions between particle and chemical can be neglected.

- The motion of particles is same as that of liquid.

Particles, along with liquid, move towards the bottom of the tank axially as the hydrofoil type agitator blades move around the agitator shaft at a constant speed. According to the flow stream close to the vicinity of the specimen holder, the particles impact on the specimen surface at an angle, between the axial velocity and its tangential velocity component. This angle is called the impact angle, which varies along the surface. To locate the point of impact on the surface, the location angle $\alpha$ is drawn between the stagnation line and the line of normal component of particle velocity (as shown in Figure 5.2). In reality, the flow of the fluid about the cylinder will mean that the true impact angles will be different from those shown here. However, without a comprehensive fluid dynamics analysis of the situation accounting for the relative densities and particle sizes, it is impossible to determine true impact angle and velocities of the particles. At this stage, however, the nominal angle of attack, $\alpha$, is used and as more information on the

fluid flow behaviour about the cylinder becomes available, the model will be modified appropriately.
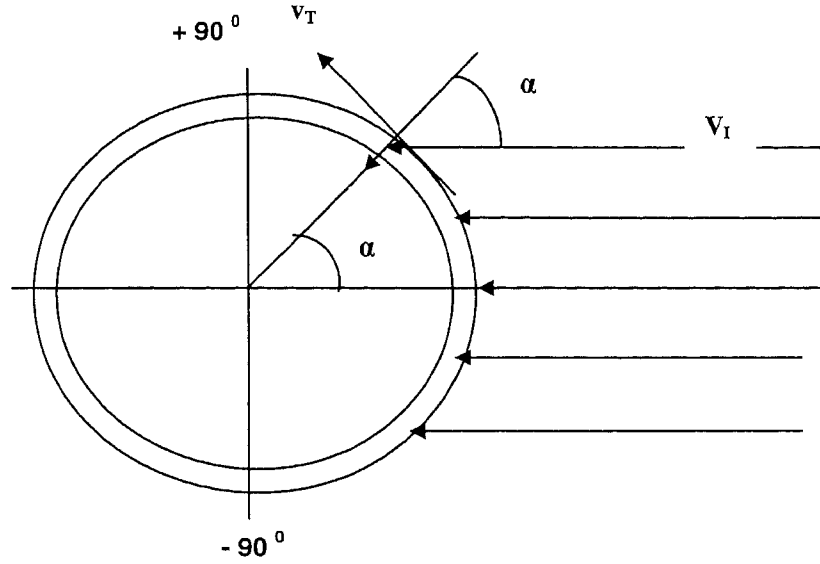


**Figure 5.2: Schematic diagram of particles impact around the rubber specimen.**

In this model, it is assumed that the normal component of the particle velocity principally causes deformation wear. The initial deformation of the material will be elastic, followed by plastic deformation. After wear has occurred, however, the elastic deformation is released and only plastic deformation is visible. Nonetheless, some of the impact energy is absorbed and released as elastic deformation. So deformation wear occurs due to normal velocity component of particle and can be expressed as:

$$W_D = \frac{(\frac{mv_1^2}{2} - \frac{mv_e^2}{2})}{\varepsilon} = \frac{mv_1^2}{2\varepsilon}(1-k_1^2)$$ (5.12)

where, $v_1$= velocity of slurry particle at the point of strike, $v_e$=($k_1 v_1$) = velocity required to produce elastic deformation, $\varepsilon$ = specific energy for deformation wear and $k_1$= fractional value for deformation wear.

Most particles slide over the surface of the specimen after they impact at a point on surface and then go back to the liquid medium. Assuming, there is no rolling of particles on surface and particles cause cutting wear along the direction of travel of the

particles. After the impact a particle travels a small distance ds over time dt. Therefore, the average velocity of a particle during cut can be expressed as

$$dv = \frac{ds}{dt} \qquad (5.13)$$

Particles that impact on near the edge of the specimen surface do not have an opportunity to slide over the surface and cause deformation and cutting wear simultaneously on the surface on edge towards the direction of travel.

The momentum of the particle is $mv_T$ and the particle starts to cut the surface with a velocity of $v_T$ (tangential component of impact velocity). If the particle leaves the surface with a velocity, $v_r$, then the cutting wear, due to tangential velocity of the particle, can be expressed as

$$W_C = \frac{(\mu m v_T \int_{v_T}^{v_r} dv)}{\phi} \qquad (5.14)$$

where, $\mu$ = cutting wear constant and $\phi$ = specific energy for cutting wear. The velocity of a particle at the end of the cut, $v_r$ must be less than the velocity of the same particle at the beginning of the cut, $v_T$. This is because the loss of energy of the particle and a relation can be expressed as $v_r = k_2 . v_T$, where $k_2$ is a fractional value for cutting wear velocity.

Solving equation (5.14) and substituting the value of $v_r$, the equation for cutting wear becomes

$$W_C = \frac{\mu m v_T^2 (1 - k_2)}{\phi} \qquad (5.15)$$

From the geometry of flow stream around the specimen, we get two relations for the components of particle impact velocity. For normal component, $v_I = v \cos \alpha$.
For tangential component, $v_T = v \sin \alpha$.

Adding the absolute value of cutting wear from equation (5.15) to the value of deformation wear from equation (5.12), gives an equation for total wear,

$$W = W_D + W_C = \frac{-\mu m v_T^2 (1 - k_2)}{\phi} + \frac{1}{2\varepsilon} m v_I^2 (1 - k_1^2) \qquad (5.16)$$

Solving equation (5.16) substituting the value of $v_l$ and $v_T$, we get the equation for wear

$$W = \frac{mv^2}{2\varepsilon}(2k_D sin^2\alpha + k_C \cos^2\alpha) \qquad 5.17$$

where, $\varepsilon = \phi$ can be considered for polymer and rubber materials [4].

Deformation wear co-efficient, $k_D = (1-k_1^2)$ and cutting wear constant, $k_C = (1-k_2)$. Differentiating equation (5.17) and setting the right hand side equal to zero, we get the value of $\alpha$ for maximum wear to occur.

$$\frac{dW}{d\alpha} = \frac{mv^2}{2\varepsilon}\sin 2\alpha(2k_D - k_C) \qquad (5.18)$$

Since, $(2k_D - k_C)(\frac{mv^2}{2\varepsilon}) \neq 0$, for maximum or minimum value of $\alpha$, $\sin 2\alpha$ must be zero. By solving, $\sin 2\alpha = 0$, we get the value of $\alpha$ is zero ($\alpha = 0$ or $180^0$). Differentiating equation (5.18) further with respect to impact angle $\alpha$, we get

$$\frac{d^2W}{d\alpha^2} = (2k_D - k_C)(\frac{mv^2}{2\varepsilon})\cos 2\alpha = 0 \qquad (5.19)$$

Since, $(k_C - 2k_D)(\frac{mv^2}{2\varepsilon}) \neq 0$

Therefore, for maximum or minimum value of $\alpha$, $\cos 2\alpha$ must be 0. Solving $\cos 2\alpha = 0$, we get $\alpha = 45^0$.

Two values of $\alpha$ suggest that the maximum wear can occur when the incident angle of particle is either $0^0$ or $45^0$. Deformation wear, for rubber materials having high resilience, can be ignored because deformation wear is less dominant for polymer materials [4].

Assuming zero deformation wear, we get the equation of maximum slurry erosive wear of rubber material

$$W_{max} = \frac{mk_W v^2}{2\varepsilon} = \frac{\pi \rho d^3 k_W v^2}{12\varepsilon} \qquad (5.20)$$

where, $\rho$ = particle density, d= average particle diameter and $k_w$ = wear constant and

mass of the particle $m = \dfrac{\rho \pi d^3}{6}$ .

The simplicity of this model is that there is only one wear related constant. Specific energy of target materials may be obtained from manufacturer. Hence, for known particle velocity, wear constant can easily be determined by experimental test method. Once the wear constant is known, maxim wear due to slurry erosion can be solved using the model (refer to Equation 5.20).

## 5.2 References

1. Finnie, I., 1995, "Some reflections on the past and future of erosion," Wear, Vol. 186-187, pp. 1-10.
2. Finnie, I.,Wolak, J. and Kabil, Y., 1967, "Erosion of metals by solid particles," Journal of Materials, Vol. 2, pp. 682-700.
3. Finnie, I., Stevick, G. R. and Ridgely, J. R., 1992, "The influence of impingement angle on the erosion of ductile metals by angular abrasive particles," Wear, Vol. 152, pp. 91-98
4. Finnie, I., and Mcfadden, D. H., 1978, "On the velocity dependence of the erosion of ductile metals by solid particles at low angle of incidence," Wear, Vol. 48, pp. 181-190.
5. Bitter, J.G.A., 1962, "A study of erosion phenomena," Part 1, Wear, Vol. 6 pp. 5-21.
6. Bitter, J.G.A., 1963, "A study of erosion phenomena," Part 2, Wear, Vol. 6 pp. 169-190.
7. Arnold, J.C. and Hutchings, I. M., 1992, "A model for the erosive wear of rubber at oblique impact angles," Journal of Physics, Vol. 25, pp. A222-229.
8. Arnold, J.C. and Hutchings, I. M., 1993, "Erosive wear of rubber by solid particles at normal incidence," Wear, Vol. 161, pp. 213-221.

Chapter 6

# 6 Experimental Procedures for Slurry Abrasion Testing

An experimental method established to quantify abrasion erosion of bromobutyl rubber in magnesite slurries has been described in this chapter. Prior to developing this test method, studies have been carried out to explore techniques and facilities available to the standard test methods. Description of these standard test methods with diagrams are placed in the following section. A detailed description of the slurry abrasion testing method including schematic diagram, design and materials selection and experimental procedures are described in this chapter.

## 6.1 Standard slurry abrasion test methods

The erosion of materials in slurry mixing facilities is relatively a slow process. Hence, it takes a reasonably long period of time to generate visible wear for the materials of interest. A number of test methods are available to determine slurry abrasion and erosion wear of materials. The following test methods are widely used by researchers, scientists and engineers.

- Wet Sand/Rubber Wheel Abrasion Tests
- Slurry Jet Test
- Slurry-pot Erosion Test
- Repeated Indentation Test

### 6.1.1 Wet sand/rubber wheel abrasion tests

This standard test method involves the abrading of a test piece with a slurry containing grit of controlled size and composition. In this technique, the abrasive is introduced between the test specimen and rotating wheel fitted with a neoprene rubber tyre. The test specimen is pressed against the rotating wheel at a specified force while the grit abrades the test surface (see Figure 6.1). The results are expressed in terms of mass or volume loss of the original test material [1].

FIG. 1 Schematic Diagram of the Wear Test Apparatus
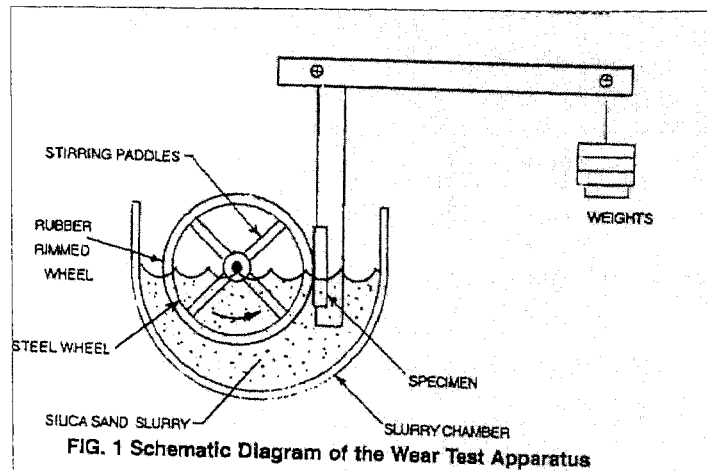
**Figure 6.1: Schematic diagram of the wet sand/rubber wheel abrasion test apparatus [1].**

## 6.1.2 Slurry jet test apparatus

The slurry jet test apparatus consists of several elements: a specimen holder, a nozzle to propel out the test liquid, a tank and stirrer to mix solid particles in a liquid (as shown in Figure 6.2). The test piece is a plate of length 20 mm, width 30 mm and thickness 5 mm. It is attached to the holder and is set 20 mm above the exit of the nozzle. The diameter of the nozzle is 3 mm and adjusting the valve varies the flow velocity. The slurry jet velocity is measured as follows: the sampling volume of the flow is collected from the nozzle into a graduated beaker. The volume is divided by the time of sampling and the area of the nozzle exit to obtain the velocity. The impingement angle of the jet relative to test surface is varied from 10 to $90^0$ [2].

73

| | |
|---|---|
| 1. Test piece | 6. Stirrer |
| 2. Nozzle (dia.3mm) | 7. Cooler |
| 3. Water bath | 8. Pump |
| 4. Test liquid | 9. Valve |
| 5. Tank | |
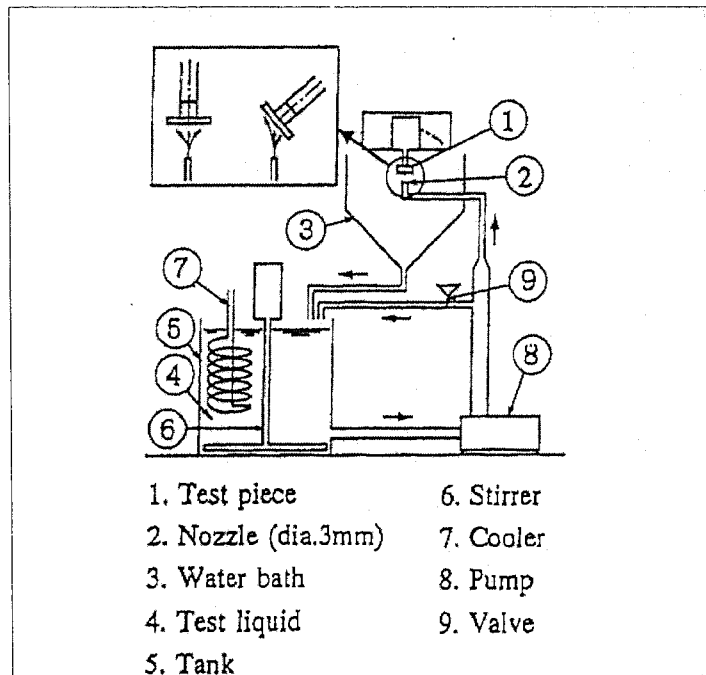
Figure 6.2: Schematic view of the slurry jet test apparatus [2].

## 6.1.3 Slurry pot erosion test rig

The apparatus consists of a water cooled vessel, stirrer, specimen-holder, over pressure valve and bottom valve (refer to Figure 6.3). The drain valve is used to discharge slurry after each test. Specimens are attached to the specimen holders. A minimum of four specimens can be tested simultaneously and this number can be increased by changing the design of slurry pot. Wear is measured as mass or volume over time. For this particular slurry erosion tester, specimen velocity is kept above 10 m/s. The test duration is between 4 to 24 hours [3].

Figure 6.3: Schematic diagram of the slurry-pot erosion test apparatus used by Clark and Wong [3].

## 6.1.4 Repeated indentation test

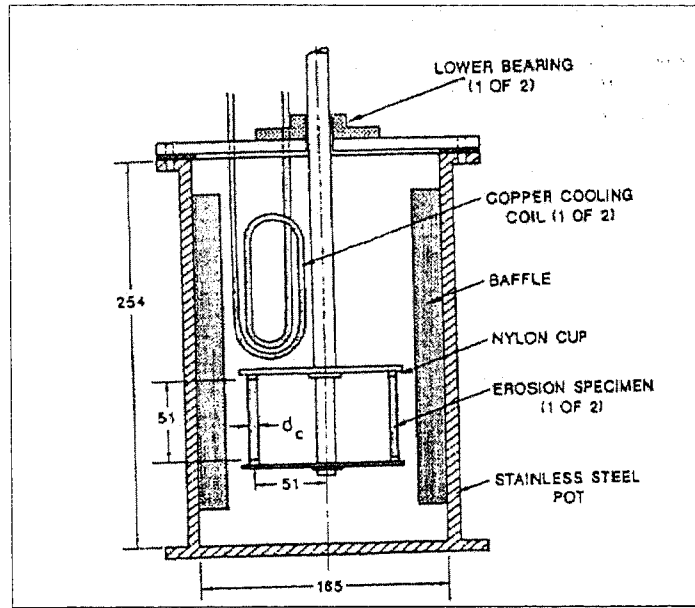This technique simulates the growth of fatigue cracks caused by multiple-particle impacts during erosion. A pivot arm raised by the solenoid carries loading weights to provide the indentation force as shown in Figure 6.4. The indenter, a spherically tipped steel shaft with a radius of 0.7 mm just touches the sample surface when in the raised state. The current through the solenoid is controlled electronically to release the loading indentation rate of 100 per minute. The material removal rate due to repeated impacts is to consider the surface stresses due to indentation by a spherical particle. The radial tensile stress S(r), in the surface of an elastic half space subjected to a point load P, is given by $S(r) = P(1-2v)/(2 \pi r^2)$.

where r is the radial distance on the surface from the loading point and v is Poisson's ratio. The fatigue crack growth rate due to the surface tensile stress can be estimated by assuming that the stress acts on an edge crack. [4].
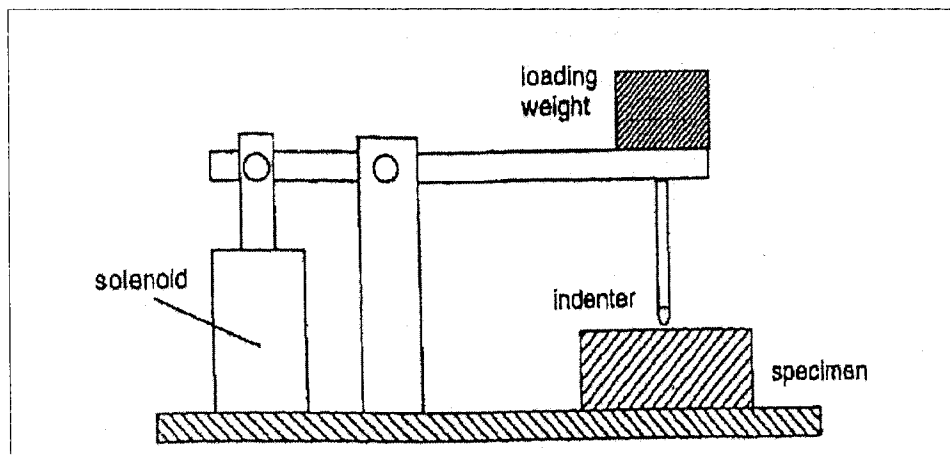
**Figure 6.4: Schematic diagram of the repeated indentation test apparatus constructed and used by Arnold and Hutchings [4].**

The results of the standard test methods including those discussed above often transfer poorly to industrial conditions. In order to simulate industrial conditions newly developed or modification for the standard test methods are necessary. The slurry erosion test method, used by Clark and co-workers, seemed reasonably close to the conditions at the AMC demonstration plant [3]. In order to maximise the simulation of AMC conditions, further modification of the slurry erosion tester were made. A brief description is given in the next section. A schematic diagram of the device is shown in Figure 6.5.

## 6.2 Description of the equipment

Principally, the slurry erosion tester consists of slurry tank, agitator shaft and agitator blades as shown in figure 6.5. In order to maintain a fixed, constant speed for the agitator blades, a 5 kW three phase electric motor coupled with reduction gear box was attached to the agitator shaft at top end. A set of typical hydrofoil impeller blades was attached to the bottom end of the agitator shaft. Specimen holders were attached to the agitator shaft via horizontal shafts which were set 150 mm above the position of the agitator blades. Two spherical roller bearings, attached to the fixtures, were incorporated in the design to support the agitator shaft. The entire equipment was attached and supported by a structural steel-frame. The slurry tank was placed on the centre of the frame-table. The tank was freely movable for convenient handling of the slurry and the samples.

76
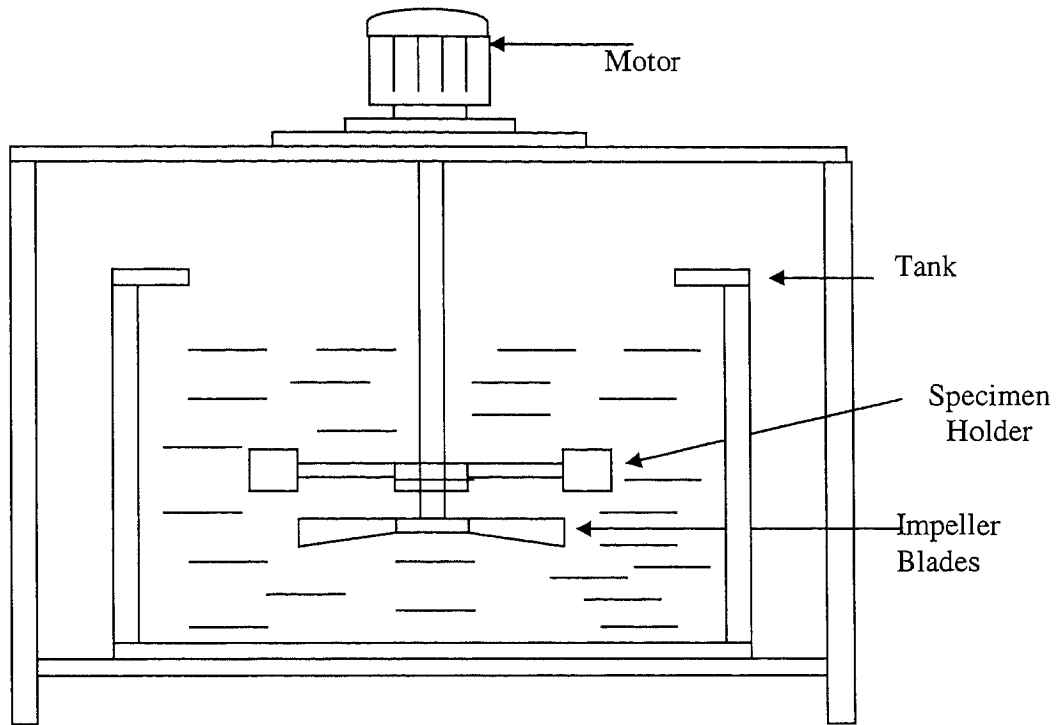
**Figure 6.5: Schematic diagram of the slurry erosion test apparatus.**

The test specimens consisted of strips of bromobutyl rubber wrapped around cylindrical specimen holders. The specimen holders were 60 mm in diameter and 50 mm in length. The strips were made of blocks 94.2 mm x 50 mm x 6 mm in dimension. Each test specimen was wrapped around the specimen holder tightly by using two hose clamps at both ends of the specimen holder. This was done so that the rubber would be exposed to a range of particle impingement angles.
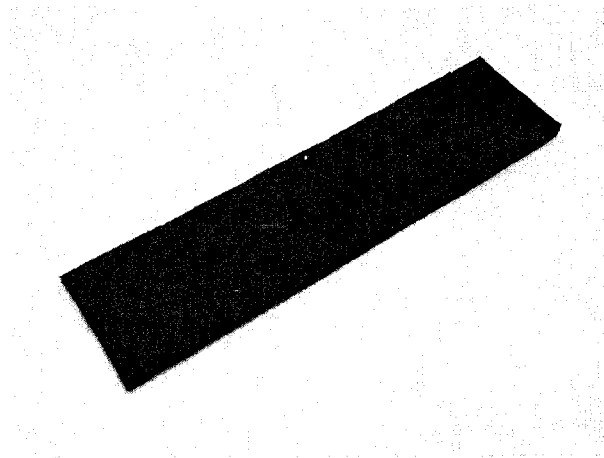
**Figure 6.6: A photograph of bromobutyl rubber test specimen.**

## 6.3 Design and materials selection

### 6.3.1 Slurry tank

The slurry tank was designed so that experiments with 1000 liters of magnesite slurry could be carried out safely. The diameter and the height of the tank was 1200 and 1150 mm respectively. A polyethylene tank, of wall thickness 6mm, was used for this project. A photograph of the test apparatus is shown in Figure 6.7.
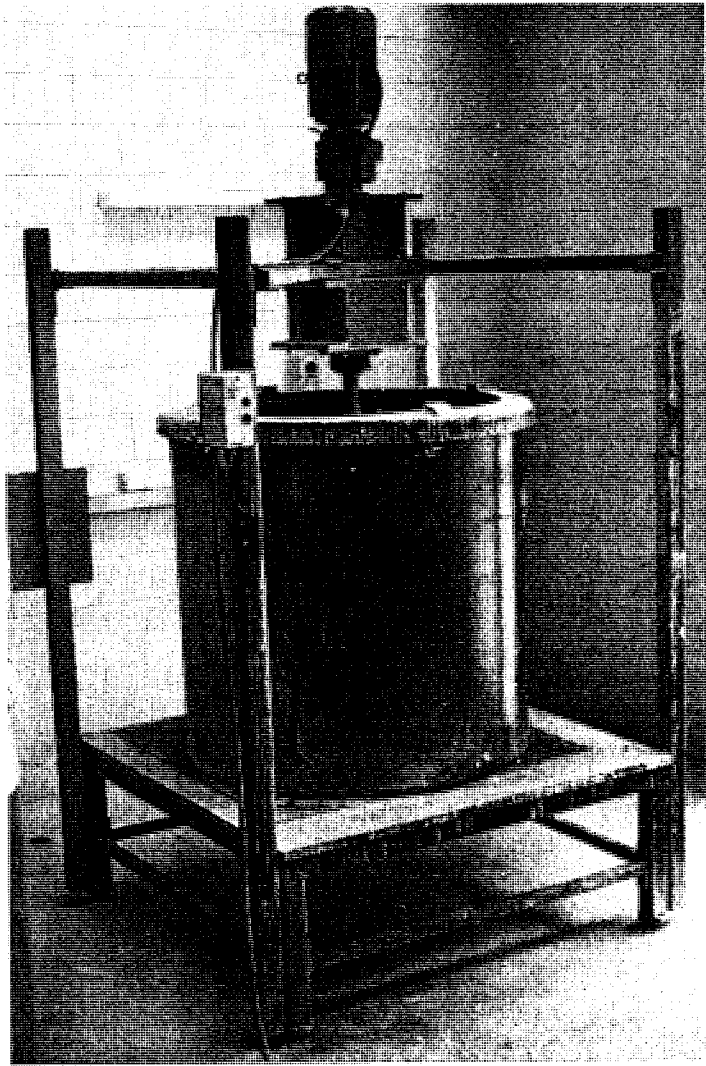
Figure 6.7: Photograph of the slurry erosion test apparatus.

## 6.3.2 Agitator shaft and impeller blades

The agitator shaft was a stainless steel hollow bar with outer and inner diameter 50 mm and 25 mm respectively. The length of the agitator shaft was 1500 mm and stainless steel-316 material was selected because of its hardness and corrosion resistance compared to mild steel.

A set of hydrofoil type impeller blades with a diameter of 450 mm was chosen in order to keep the magnesite particles suspended in the slurry. The impellers blades were also made of stainless steel. The detailed design of the impeller blades, power requirement for the agitator shaft and the slurry tank was performed according to the instructions available in the Slurry System Handbook [5].

## 6.3.3 Motor selection

In order to keep the magnesite particles suspended in the slurry, a three phase 5.5 kW motor was used following calculations for the power requirements of the impeller blades, horizontal shafts and specimen holders. Detailed calculations and assumptions have been included in Appendix A.

## 6.3.4 Specimen holders and arms

The specimen holders were 60 mm in diameter and 50 mm in length. The horizontal shafts were 197.5 mm and 272.5 mm in length respectively, in order to obtain two different specimen velocities. The hollow horizontal shafts were also made of stainless steel with outer and inner diameter 40 mm and 20 mm respectively. The specimen velocity of the specimens was measured using the relation between linear and angular velocity ($v = \omega\, r$).
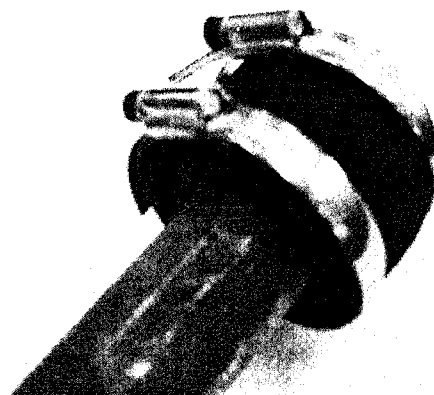


**Figure 6.8: Photograph of a cylindrical specimen holder wrapped with a bromobutyl rubber specimen attached to the horizontal shaft.**

## 6.4 Experimental design & procedure:

### 6.4.1 Sieving and slurry preparation:

Magnesite particles with a 40 mm average diameter were supplied by Queensland Magnesia (QMAG), a subsidiary of AMC. The as-received magnesite particles were crushed using primary and secondary jaw crushers. The crushed magnesite was screened to four different size ranges. These were 9.50 to 6.70 mm, 6.70 to 4.75 mm, 4.75 to 3.35 mm and 3.35 to 2.36 mm. The nominal particle sizes of these size ranges were 8.10 mm,

5.72 mm, 4.05 mm and 2.85 mm. Particle sizes below 2.36 mm were not used in the testing.

Slurries were made by mixing the magnesite particles with tape-water. For each particle size, slurries were made at three different levels of weight fractions such as 1%, 5% and 10% respectively. The experiments were carried out at room temperature (approximately $25^0$C) and for each test 1000 litres of magnesite slurry was used.

For each particle size, six tests were carried out. For the first test, 10 kg of magnesite particles were mixed with 990 litres of tap water into the tank to prepare the slurry of 1% weight fraction. Magnesite particles were then, in turn, added to make the slurries of 5% and 10% weight fraction for the $2^{nd}$ and $3^{rd}$ test. Slurry of 10% weight fraction was continued to use $4^{th}$, $5^{th}$ and $6^{th}$ test. The same procedures were followed for all particle sizes. Six tests were carried out with each particle size range.

## 6.4.2 Test material

Most of the experiments presented in this thesis were performed using bromobutyl rubber. The Linatex grade-B bromobutyl rubber was used and was supplied by Queensland Industrial Agencies, Rockhampton. The physical properties of the bromobutyl rubber in Table 6.1 were vendor's specifications.

Table 6.1: Physical properties of bromobutyl rubber supplied by Queensland Industrial Agencies.

| Serial | Properties | Test method | Quantity |
|---|---|---|---|
| 1 | Colour | - | Black |
| 2 | Polymer | - | Halogenated Butyl Rubber |
| 3 | Hardness | ISO48-1979 | 55 IRHD |
| 4 | Tensile Strength | ISO 37-1977 | 10.0 MPa |
| 5 | Elongation at Break | ISO 37-1977 | 580% |
| 6 | Tension Set | ISO 2285-1981 | 15% |
| 7 | Tear Strength | ISO 34-1979 Method C | 40 N/mm |
| 8 | Specific Gravity | - | 1.42 |
| 9 | Temperature Range | - | $-40^0$C to $+120^0$C |

## 6.4.3 Wear testing procedure

The wear testing was commenced with a particle size range 9.50-6.70 mm and was followed with the rest of the particle size ranges in decreasing order.
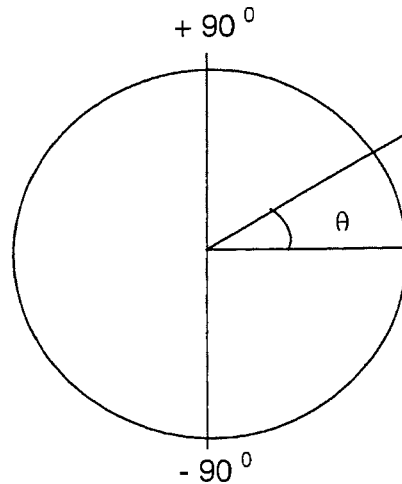


**Figure 6.9:** A sectional view of the specimen holder wrapped with the bromobutyl rubber specimen, where θ is the nominal angle of attack of the magnesite particles with respect to the horizontal line.

Rubber specimens were tightly wrapped around the specimen holders with hose clamps in order to prevent removal of the specimens in the turbulent slurry. Specimen holders were then added to the end of the horizontal shafts. Magnesite particles and tap water were then poured into the tank to produce the specified slurry concentration. The testing schedule for the particle size range 9.50 to 6.70 mm is detailed in Table 6.2. Similar schedules were followed for particles size ranges 6.70 to 4.75, 4.75 to 3.35 and 3.35 to 2.36 respectively.

**Table 6.2: Test schedule for the particles size range 9.50 to 6.70 mm.**

| Test serial | Mean particle size (in mm) | Test duration (in hours) | Specimen velocity (in m/s) | Slurry concentration (wt%) |
|---|---|---|---|---|
| 1 | 9.50 to 6.70 | 50 | 5.50 | 01 |
| 2 | 9.50 to 6.70 | 50 | 5.50 | 05 |
| 3 | 9.50 to 6.70 | 50 | 5.50 | 10 |
| 4 | 9.50 to 6.70 | 100 | 5.50 | 10 |
| 5 | 9.50 to 6.70 | 200 | 5.50 | 10 |
| 6 | 9.50 to 6.70 | 50 | 7.01 | 10 |

Once the test was complete, the turbulent slurry was allowed to settle for approximately one hour. Eroded specimens were replaced with new specimens for next test. The tested specimens were initially washed using tap water. A soft foam scrubber and hand washing soap were used to remove the remaining magnesite from the specimens.

## 6.4.4 Rubber characterization

After testing, the samples were examined visually with an optical microscope to map out the wear pattern. A Surtronic 3+ profilometer was also used to quantify wear by measurement of surface roughness. The surface roughness, Ra was measured as a function of the nominal angle of the attack of the particles. Sections of the worn rubber surfaces were examined in a Scanning Electron Microscope (SEM) for the features relevant to the failure mechanisms.

## 6.4.5 Particle characterization

The worn particles were collected after the testing and were conditioned for examination. Visual examination was performed and a particle size distribution was determined in order to establish how much the particles had degraded during the testing process. The degradation of particle size was calculated by determining the proportion of the worn magnesite particles that passed through the smaller sieve of the initial particle size range [6].

## 6.5 References

1. ASTM Standard, 2004, "Metals Test Method and Analytical Procedures - Wear and Erosion; Metal Corrosion", Vol. 03.02, pp.461
2. Iwai, Yoshiri and Nambu, Kazuyuki 1997, "Slurry wear properties of pump lining materials," Wear, Vol. 210, pp. 211-219.
3. Clark, H. McI. and Wong, K.K., 1995, "Impact angle, particle energy and mass loss in erosion by dilute slurries" Wear, Vol. 186-187, pp. 454-464.
4. Arnold, J.C. and Hutchings, I. M., 1993, "Erosive wear of rubber by solid particles at normal incidence," Wear, Vol. 161, pp. 213-221.
5. Baha E. Abulnaga, P.E.,2002, "Slurry systems handbook," chapter 7, section 9, Mcgraw-Hill, pp.7.40-7.50.
6. Akan, S. H., Druskovich, D. and Clegg, R. E., 2004, "Slurry erosive wear of bromobutyl rubber lining material in the leaching circuit of mineral processing industries," 1st International Tribological Conference, December 1-3, 2004, Singapore National University, Singapore, pp. B 92-93.

Chapter 7

# Experimental Results

## 7.1 General observations

Testing of the samples was carried out as described in Chapter 6. Examination of the worn rubber samples indicated that measurable amounts of volumetric wear had not occurred. This is likely to have been due to the relatively short period of testing and the fact that this test was not an accelerated test, but mimicked relatively closely the industrial situation. Although accelerated tests produce measurable results quite quickly, they do not necessarily correctly reflect the failure modes experienced in industry (see section 6.2). Furthermore, as discussed below, the important mechanisms of wear in these rubbers was probably not most sensitively measured by volumetric wear measurements.

Wear measurements reported in this thesis were made on the basis of three measurement techniques: (a) visual studies of the worn regions, (b) surface roughness measurements using a profilometer and (c) morphological studies of the worn surfaces using scanning electron microscopy. The results of these studies are reported below.

## 7.2 Visual inspection

As a first stage of the examination, the test samples were examined visually and with a low power stereo microscope in order to determine the wear pattern of the bromobutyl rubber specimens tested using the slurry erosion tester apparatus. In the worn regions, roughening of the surface was observed, and the density of roughening appeared uneven on the tested specimen surface.

The test samples consisted of strips of bromobutyl rubber that were wrapped about a mandrel. Observations on the samples were made at the surface of the rubber samples as a function of angle. The leading edge of the sample was at 0° (refer to Figure 7.1). Although, a fluid dynamics analysis of this system was not carried out, it is expected that the material at 0° would tend to suffer impact of particles at an angle perpendicular to the surface (described here as 0 ° impact). As the angle increases, the nominal angle of impact of the particles will increase also, so that at 90° the particles will simply graze the

surface of the rubber. It is acknowledged that the analysis provides an oversimplified view of the likely trajectories of the slurry particles as the flow of particles and fluid near the sample will be affected by the shape of the mandrel with fluid parting and flowing about the mandrel. Also, because of the vigorous mixing of the tank by the impellor there will be a significant component of axial flow in the tank, which will affect the general flow patterns within the tank. Nonetheless, this approach provides a useful frame of reference for the analysis of these results.

In all samples examined, wear was observed only between $-90^0$ to $+90^0$ of the specimen (refer to Figure 7.1). No wear was visible on the other half of the specimen surface. For most of the cases, relatively low level of wear was observed at the middle of the specimen (at an angle of $0^0$ with the horizontal line) towards the direction of the rotation.
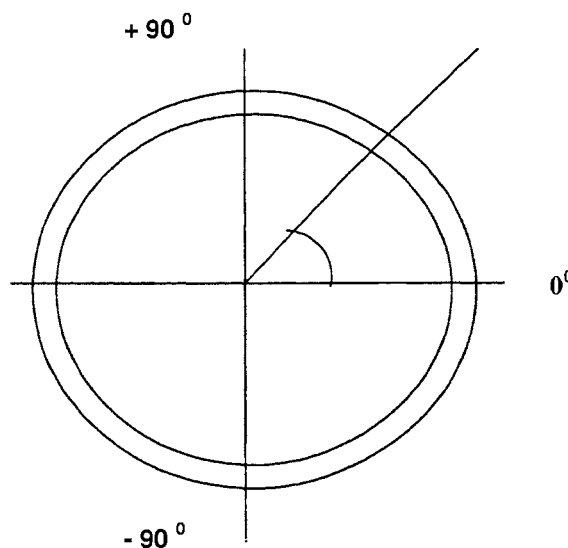


**Figure 7.1: Brmobutyl rubber specimen wrapped around a specimen holder.**

The greatest degree of wear was found on the region of the specimen surface between 0 to $+/- 90^0$. The wear pattern of each specimen appeared to be symmetrical. Wear on the area of the specimen surface adjacent to $+/- 90^0$ was found to be low.

Increased roughening was observed for rubber specimens tested at level of slurry concentrations 1, 5 and 10% respectively for various particle size ranges. Variation of roughness due to particle size was not apparent as was observed with slurry

concentration. However, the difference was observed through careful observation. A little increase in roughening was observed due to various erosion duration for particle size ranges 9.50 to 6.70, 6.70 to 4.75, 4.75 to 3.35 and 3.35 to 2.36 mm. Surprising results were that low roughening was observed with high specimen velocity (7.01 m/s) and high roughening was observed with low specimen velocity.

Examination of the surfaces with a low power stereo microscope showed that surface pits and holes were present in the worn regions. The presence of these surface pits was confirmed by scanning electron microscopy and the importance of these defects is discussed below.

## 7.3 Surface roughness measurement

Wear is most commonly measured as weight or volume loss of the materials and is often expressed as mm lost per unit flow or time. However, as discussed above, this method was inappropriate to measure the wear produced on the surfaces studied here. The principal reason for this was that the weight or volume loss of tested rubber was very small compared to the original materials before being used in the experiment. Hence, surface roughness measurements were used to give some measure of the damage occurring on the specimen surfaces. A Surtronic 3+, profilometer was used to obtain experimental data for this work. The equipment was capable of measuring a number of surface roughness parameters such as Ra, Rq and Sm. Cut-off length used throughout the surface roughness measurements was 0.80 mm. Ra is the most used and internationally recognized parameter of roughness. It is the arithmetic mean of the departures of the profile from the mean line. Surface roughness of a virgin rubber specimen was measured in order to compare roughening with tested rubber (as shown in Figure 7.2).
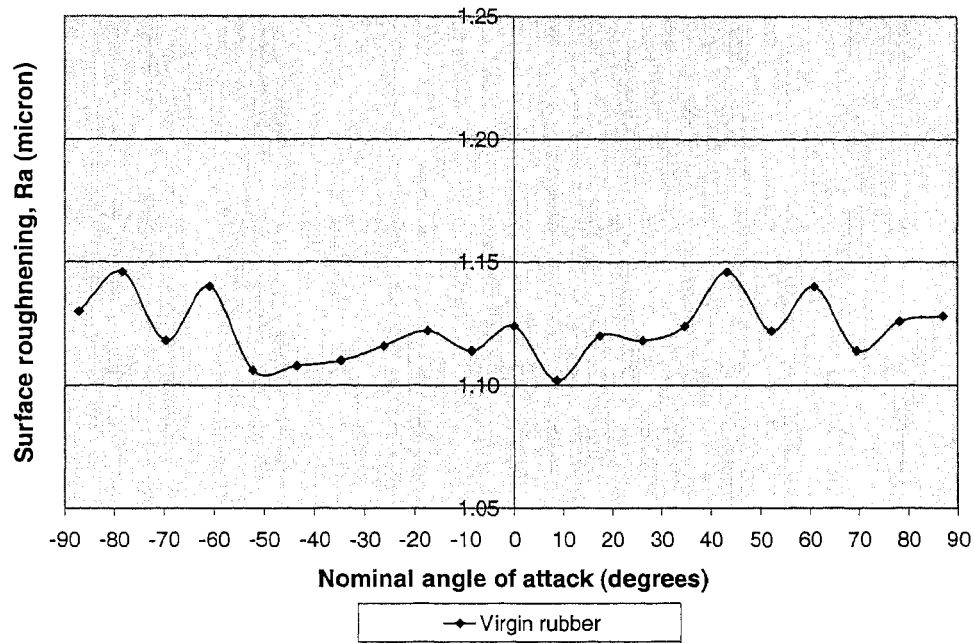
Figure 7.2: Surface roughness of a virgin rubber specimen against nominal angle of attack.

Surface roughness is used as a measure of damage, based on the theory that wear will cause the formation of pits and grooves in the surface. If the initial texture of the rubber was relatively smooth, then increasing amounts of wear should produce increasing levels of damage on the rubber surface and this should translate to increased surface roughness. In this study, surface roughness, Ra, is plotted as a function of nominal angle of attack.

For each sample measurements were taken five times at intervals $8.5^0$ in the range of $-87^0$ to $+87^0$ (refer to Figure 7.1). Each point on the graph represents an average of five roughness measurements on the sample. The effects of various test parameters on the surface roughness results are discussed below.

### 7.3.1 Nominal angle of incidence

In slurry erosion, the angle between the direction of motion of an impinging solid particle and the normal to the surface at the point of impact is considered as angle of incidence [4]. According to this definition, the nominal angle of attack would be regarded as angle of incidence. As discussed above, the nominal angle of incidence represents the angle about the mandrel and will be different from the actual angle of incidence of the particles.

Nonetheless it is a convenient way of examining the effect of angle of attack on wear rates.
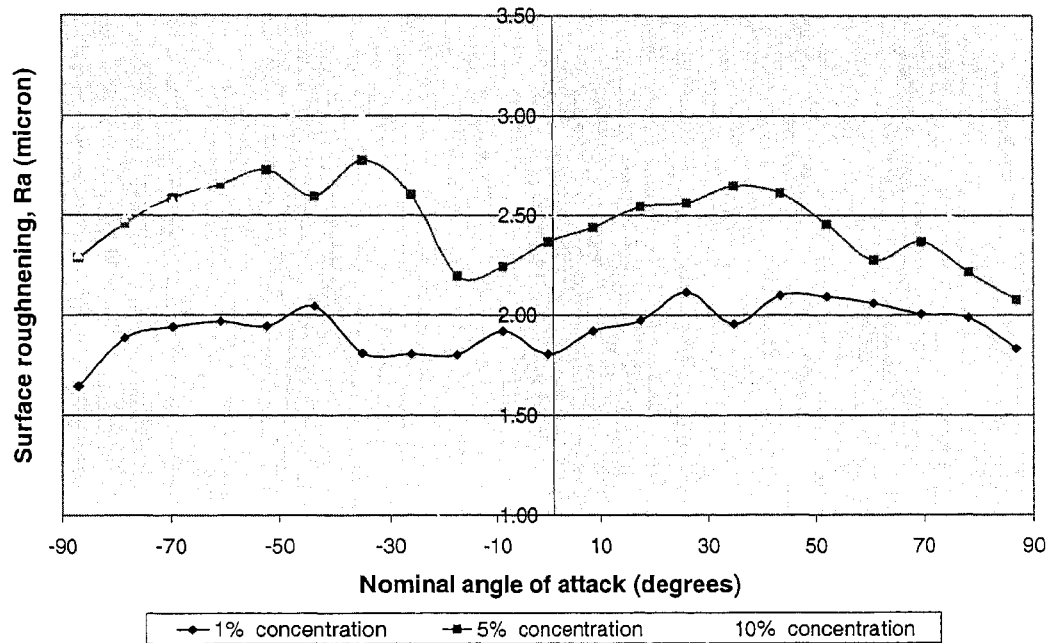


Figure 7.3 Surface roughness of bromobutyl rubber samples against nominal impingement angle at 1%, 5% and 10% slurry concentration for magnesite particle size range 6.70 to 4.75 mm.

Figure 7.3 shows the variation of surface roughness against nominal angle of attack of particles. The results indicate that the degree of roughening, in most cases, increased initially and then decreases. The maximum roughening was observed approximately at angles ranging from +/-30 to +/- $70^0$. According to the information in Figure 7.3, the roughness was observed at approximately at an angle of attack +/- $40^0$. These results are consistent the work of Ahn et al. [5] who studied the effect of silica based slurry on aluminium metal and Finnie [6] who investigated the effect of angle of attack on maximum wear rates in ductile and brittle solids. Similar results were found for most of the bromobutyl rubber specimen tested in magnesite slurry regardless of test parameters. A detailed list of the results is shown in Appendix B.

## 7.3.2 Particle size

Figure 7.4 shows the variation of surface roughness of bromobutyl rubber samples tested in magnesite slurry for particle size 8.10, 5.72, 4.05 and 2.85 mm respectively. These are the calculated nominal particle sizes for size ranges 9.50 to 6.70, 6.70 to 4.75, 4.75 to

3.35 and 3.35 to 2.36 mm. In this series of tests, the magnesite slurry concentration was kept at 10% and the tests were carried out for 50 hours.
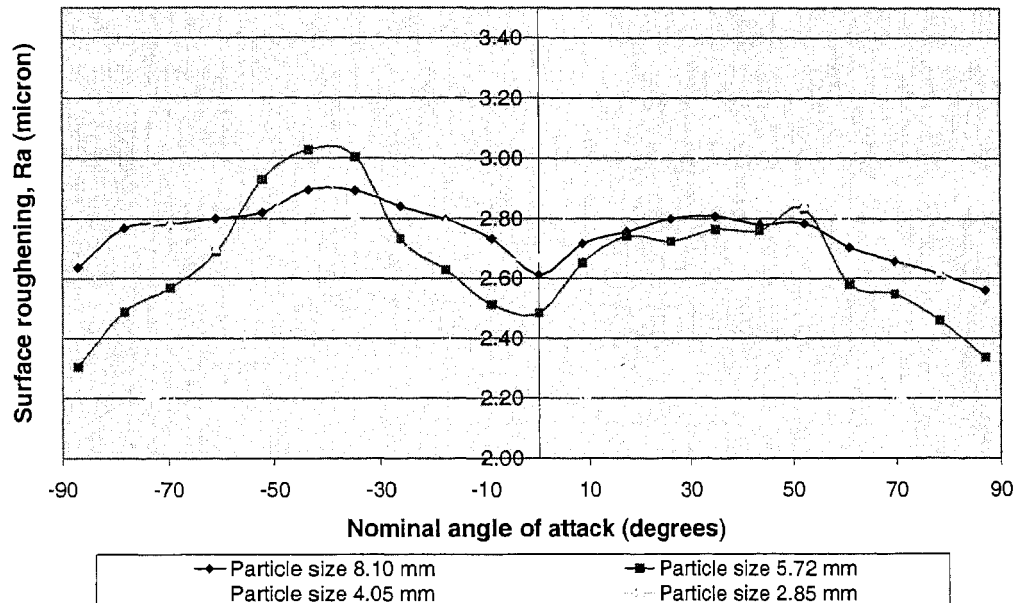


Figure 7- 4 Variation of surface roughening of bromobutyl rubber at constant slurry concentration (10%) for nominal particle size 8.10, 5.72, 4.05 and 2.85 mm.

The results indicate that the surface roughening increased with increasing particle size in general, although the effect appeared to saturate above 4.05 mm, with little increase in surface roughening. These results were consistent with the work of a number of researchers in slurry erosion [1-3], who found a relationship between particle size and wear rates.

## 7.3.3 Slurry concentration

Figure 7.5 shows the results of surface roughness measurements against the nominal impingement angle for three individual rubber samples at 1%, 5% and 10% slurry concentration. Each sample was tested for 50 hours using the largest size range (9.50 to 6.70 mm) particles. Similar results were obtained (see Appendix B) for the magnesite slurries of particle size range 6.70 to 4.75, 4.75 to 3.35 and 3.35 to 2.36 mm.
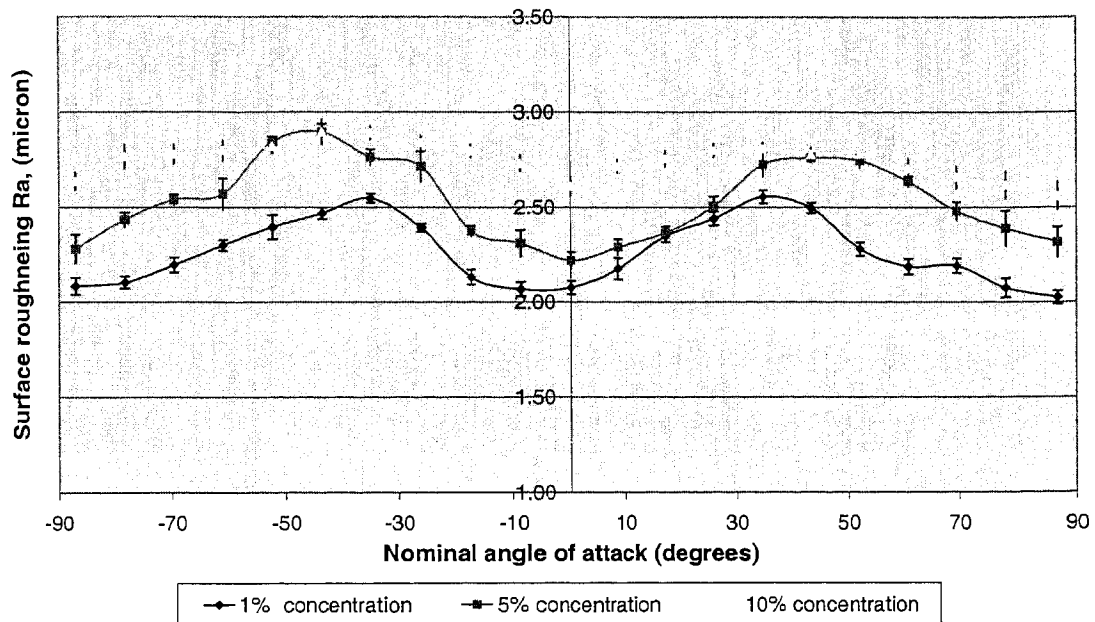
Figure 7-5: Surface roughness of three bromobutyl rubber samples against nominal impingement angle at 1%, 5% and 10% slurry concentration for nominal particle size 8.10 mm. The average Ra for virgin rubber was 1.13.

The results indicate that the roughening of the surface increases with increasing slurry concentrations. The maximum roughening occurs approximately at $40^0$ impingement angle (as shown in Figure 7.5). These results are consistent with the work of Ahn et al. [5] and with the work of Finnie [6]. Iwai and Nambu [3] showed that the wear rate of rubber is a function of solid concentration in slurry.

According to the results obtained in Figure 7.3 and in Figure 7.5, the surface roughness at $0^0$ nominal impingement angles was reasonably low. At this angle, the foremost part of the rubber sample remained toward the direction of the rotation of the agitator blades. The roughening at this location was predicted to be higher than for any other points on the same rubber surface. This prediction was not verified in this study. The trend of surface roughening from $0^0$ to $+/-40^0$ was found to increase. Opposite trend of roughening appeared in the range of $+40^0$ to $+90^0$ and $-40^0$ to $-90^0$. From $+/-90^0$ to $0^0$ nominal impingement angle, the downward trend of the surface roughening tends to be continued.

### 7.3.4 Erosion time

Figure 7.6 shows the variation of the surface roughness of tested bromobutyl rubber with erosion period of 50, 100 and 200 hours respectively. Slurry concentration was maintained constant (10%) and three individual rubber specimens were used. The particles used in these experiments were in the range of 9.50 to 6.70 mm.
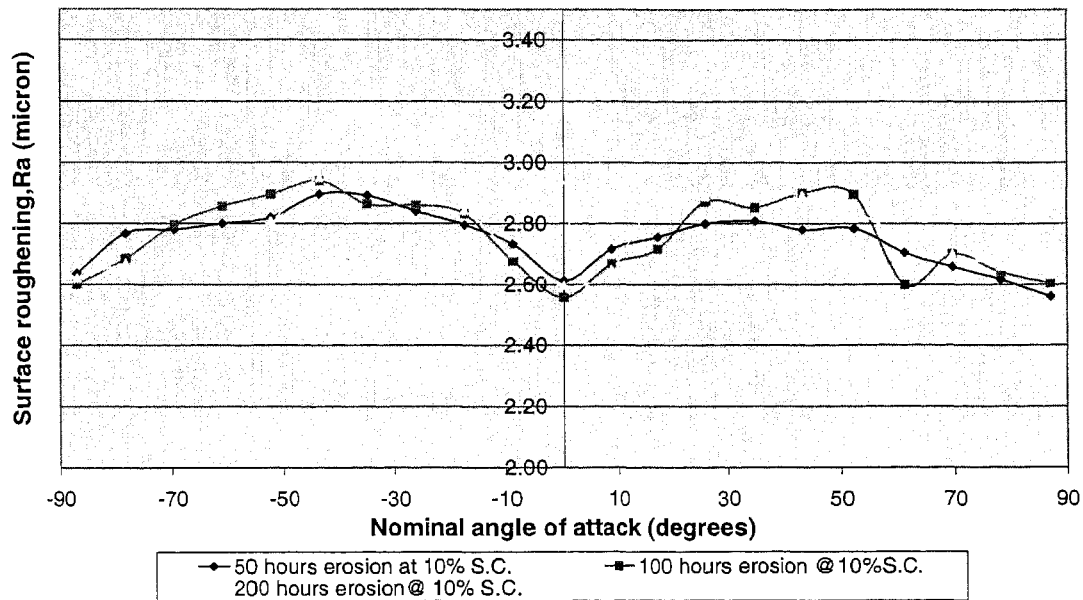
**Figure 7- 6: Surface roughness of tested bromobutyl rubber samples for 50, 100 and 200 hours of erosion time by 8.10 mm particle size in constant slurry concentration (10%).**

The results indicate that only small increases in surface roughening occurred with increasing erosion period. The roughening that occurred for 100 and 200 hours of erosion was found marginally higher than roughening that occurred after 50 hours. The results obtained here are consistent with the results of Lynn et al. [8] who used 1.2 wt.% suspensions of silicon carbide (in diesel oil) to erode P110 steel. Similar results were obtained using magnesite slurries of particles size range 6.70 to 4.75, 4.75 to 3.35 and 3.35 to 2.36 mm. Evidence for the results are available in Appendix B.

Hill et al. [1] found increased volume loss with increasing erosion period for a number of elastomers including polyurethane using the dry rubber sand wheel test apparatus. A similar trend with erosion period was also reported by Mesa et al. [9]. It is expected that erosion should be a function of erosion time as considerably higher quantity of kinetic energy of particles was transferred to the eroding materials.

This study indicates that after 50 hrs of abrasion, there is little increase in the degree of roughening occurring to the rubber surface. At the same time it was observed that the magnesite particle shape became rounded during testing. As the same abrasive was used throughout each test, this may indicate that most of the roughening of the

92

surface occurred in the first stages of wear and less roughening occurred once the particles became rounded.

### 7.3.5 Specimen velocity

Researchers in slurry erosion have concentrated on the effect of particle velocity on the eroding surface. None of them so far have emphasized the importance of specimen velocity. In this particular work, attention was given to exploring the wear of bromobutyl rubber due to the variation of the specimen velocity. The linear specimen velocity such as 7.01 and 5.50 m/s was maintained using specified horizontal shafts.

Figure 7.7 shows the surface roughness profiles for specimen velocities of 7.01 and 5.50 m/s respectively. The results indicate that the surface roughness decreased with increasing specimen velocity.
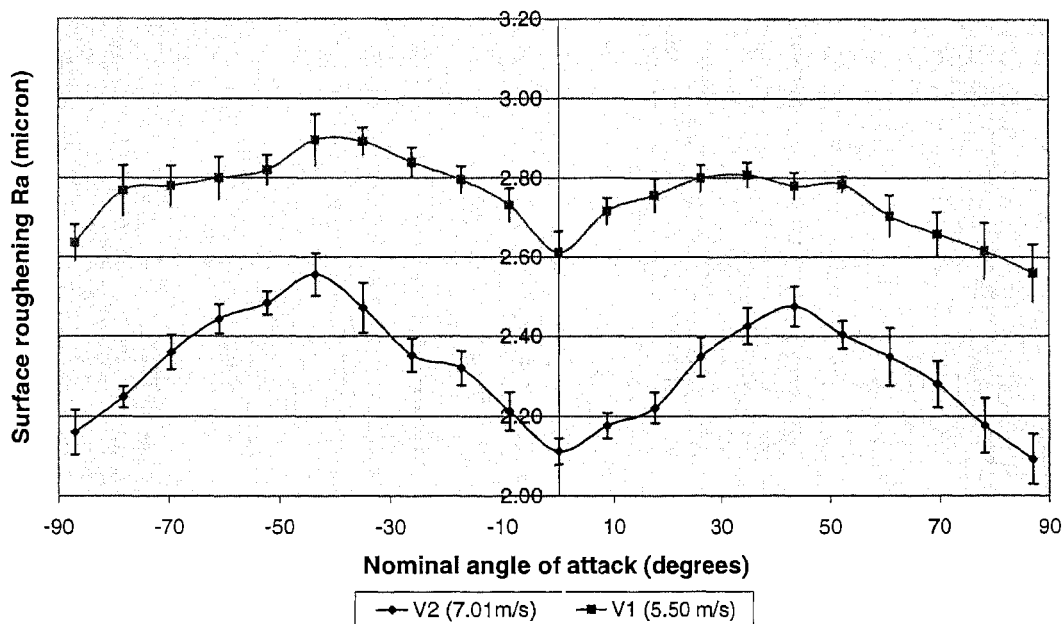


Figure 7- 7: Surface roughness of tested bromobutyl rubber samples for specimen-tip velocity 7.01 and 5.50 m/s at a constant slurry concentration by 8.10 mm size particles.

## 7.4 SEM studies

Figures 7.8 to 7.10 show SEM images of bromobutyl rubber following slurry erosion at 1, 5 and 10 % slurry concentration for the particles size range 9.50 to 6.70 mm. At a lower slurry concentration (1%), the formation of a number of holes and cracks were observed. The occurrence of these significantly increased with increasing slurry

concentration (as shown in Figures 7.9 to 7.10). These results are consistent with the results of Iwai and Nambu [1] who measured wear of rubber materials in silica sands slurry erosion using a slurry jet test apparatus. At the highest concentration (10%), significant damage had occurred on the rubber surface. This was possibly due to increased particle impacts on rubber surface as the slurry concentration continued to increase [1, 3].
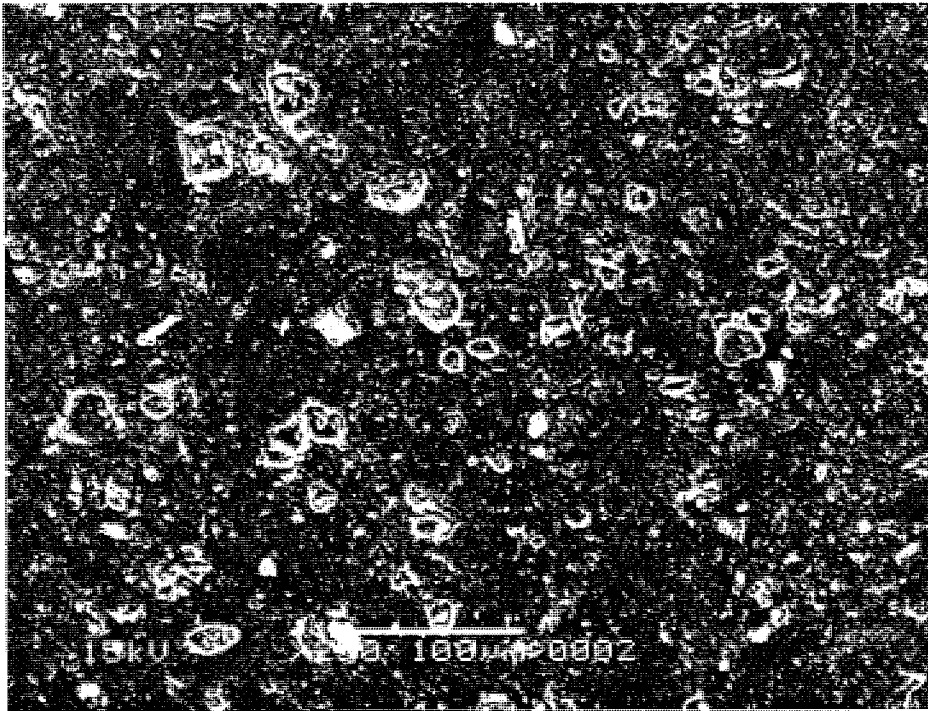


Figure 7.8: SEM micrograph of damage produced on rubber specimen tested at 1% slurry concentration.
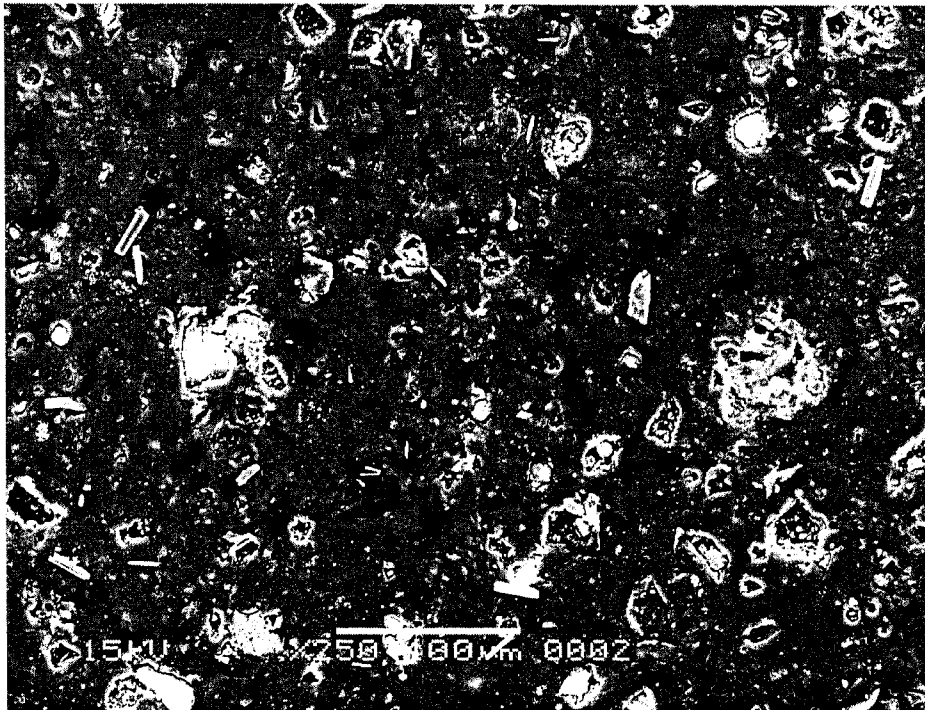
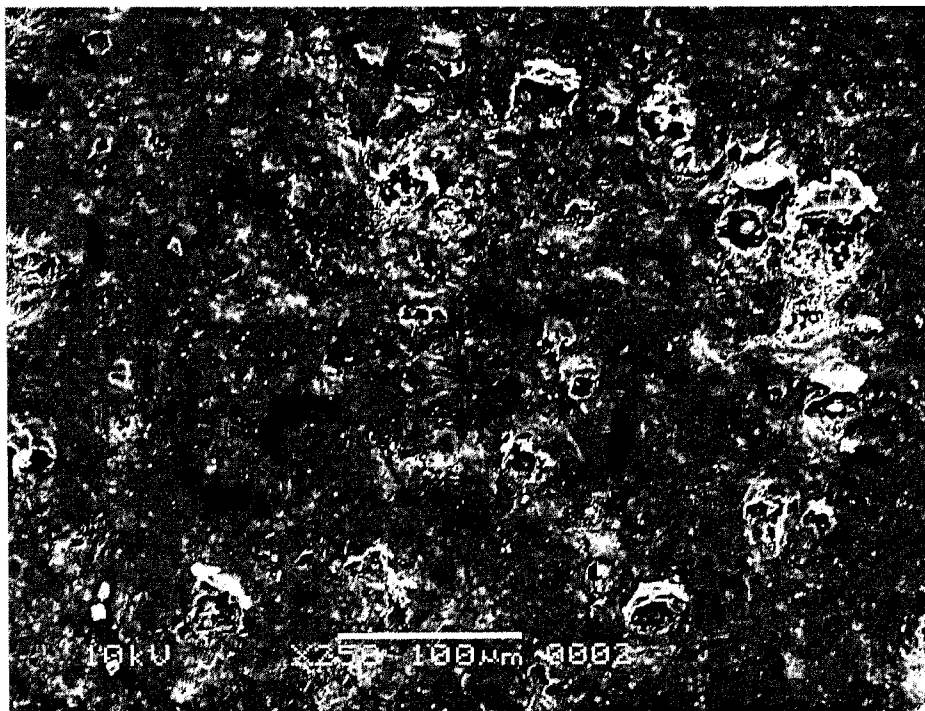Figure 7.9: SEM micrograph of damage produced on rubber specimen tested at 5% slurry concentration.



Figure 7.10: SEM micrograph of damage produced on rubber specimen tested at 10% slurry concentration.

95

Similar results were observed for particles size range 6.70 to 4.75, 4.75 to 3.35 and 3.35 to 2.36 mm respectively. The detailed information regarding these results was placed in the Appendix B of this thesis.

Figures 7.11 to 7.13 show the variation of damage produced on bromobutyl rubber surfaces due to erosion at 50,100 and 200 hours respectively from particle size range 9.50 to 6.70 mm under constant slurry concentration (10%). The SEM results indicated that the degree of damage decreased with increasing erosion time. The damage produced for the rubber sample tested for 100 hours was found relatively low compared to the rubber sample tested for 50 hours (see Figures 7.11 to 7.12). The eroding damage for the rubber sample tested after 200 hours was found to be significantly lower compared to the rubber sample tested for 50 and 100 hours respectively (as shown in Figures 7.11 to 7.13). Similar results were also observed for particles size range 6.70 to 4.75, 4.75 to 3.35 and 3.35 to 2.36 mm respectively and these results have been placed in the Appendix B.
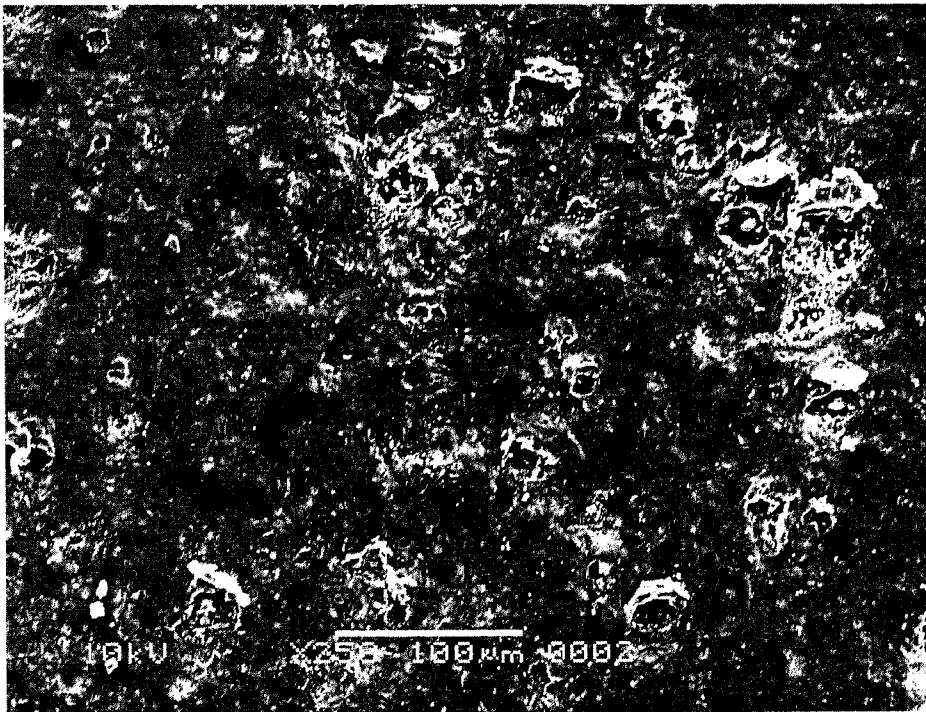


Figure 7.11: The variation of damage produced on bromobutyl rubber samples tested for 50 hours in erosion by particles size range 9.50 to 6.70 mm at 10% slurry concentration.
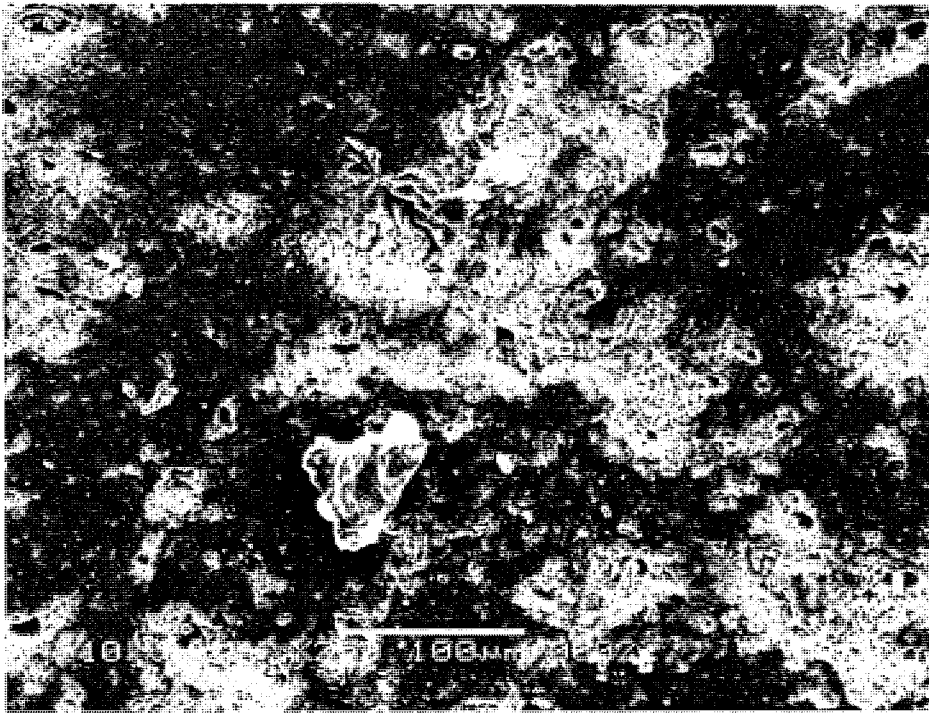
Figure 7.12: The variation of damage produced on bromobutyl rubber samples tested for 100 hours in erosion by particles size range 9.50 to 6.70 mm at 10% slurry concentration
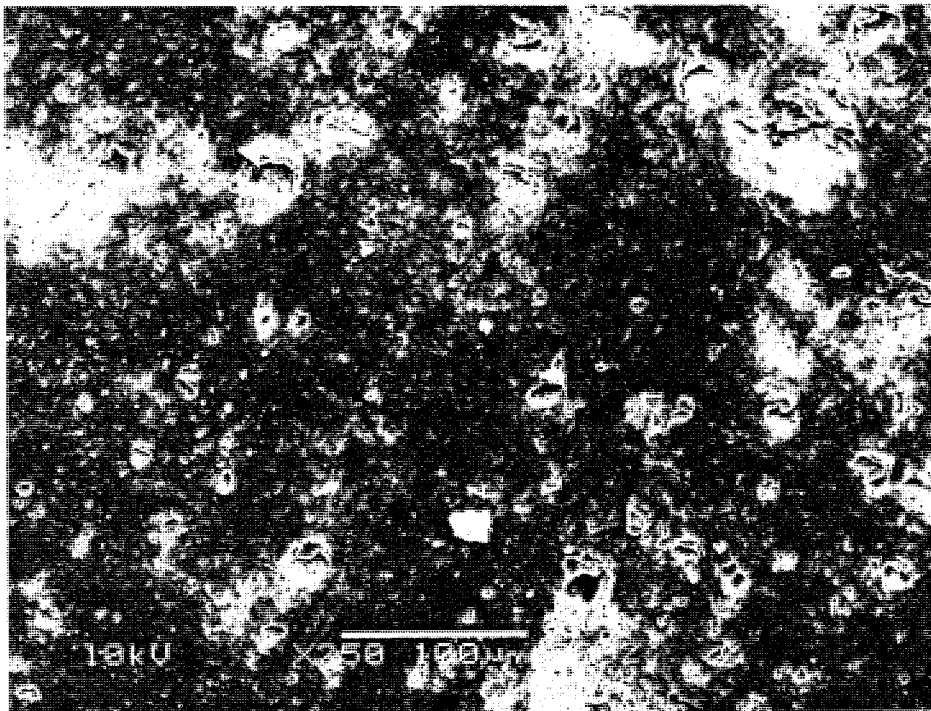


Figure 7.13: The variation of damage produced on bromobutyl rubber samples tested for 200 hours in erosion by particles size range 9.50 to 6.70 mm at 10% slurry concentration

During testing it became apparent that particle shape was important to the wear characteristics of the rubber. Samples tested with fresh and sharp particles tended to wear more rapidly than samples tested with worn particles. As mentioned earlier (refer to test schedule, Chapter 6), the magnesite particles were added cumulatively up to 10% concentration while testing. The same concentrated slurry was used for rest of the tests of each particle size range. Hence in the later tests more worn particles were present in the magnesite slurry. As a result, less damage was produced on rubber specimens tested later despite being eroded for a longer period. These results are consistent with our previous results obtained by SEM studies [7] but not with our present results obtained measuring surface roughness of bromobutyl rubber. The results were also inconsistent with the results of Iwai and Nambu [3].

Figures 7.14 to 7.17 represent the damage produced by particle size range 9.50 to 6.70, 6.70 to 4.75, 4.75 to 3.35 and 3.35 to 2.36 mm respectively at 10% slurry concentration. The degree of cracking and subsequent holes formation appeared to be related to the size of the particles. From visual and SEM studies it was observed that the larger particle sizes tended to lead to greater damage than for the finer particle sizes. The results are consisted with the observation of a number of workers in wear [1-3]. The larger particles have greater kinetic energy than smaller particles and hence tend to cause greater damage.
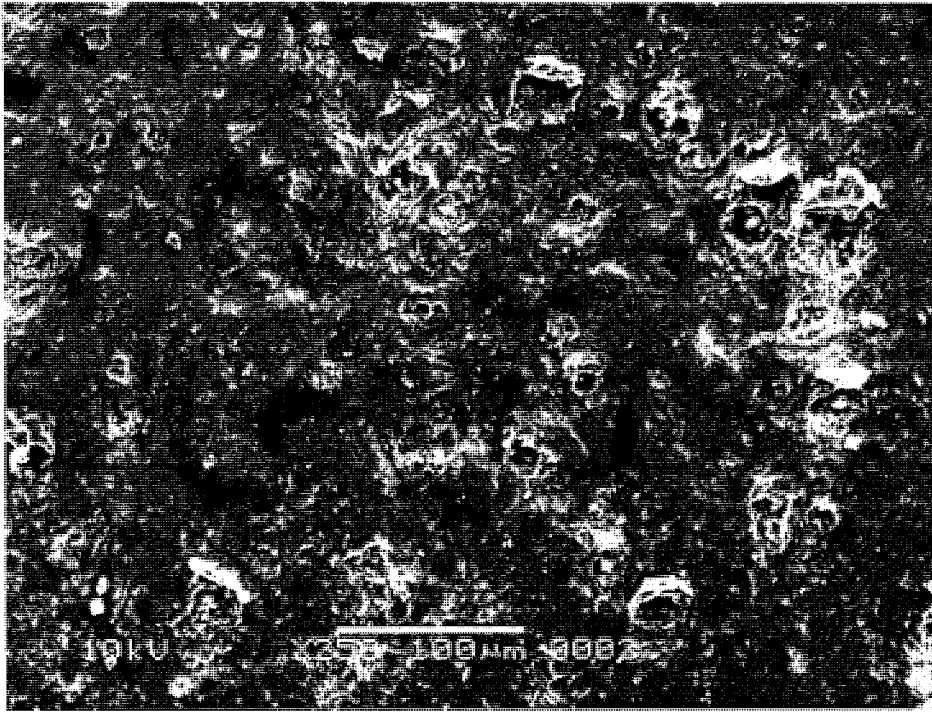
Figure 7.14: Damage produced on bromobutyl rubber samples tested in magnesite with 10% concentration by particles size range 9.50 to 6.70 mm.
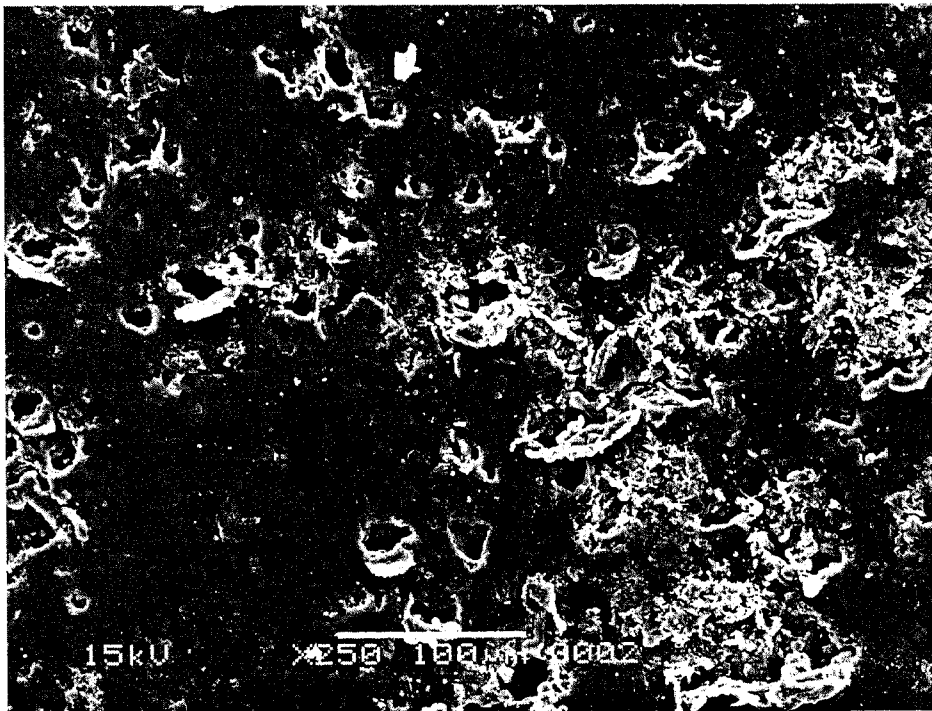


Figure 7.15: Damage produced on bromobutyl rubber samples tested in magnesite with 10% concentration by particles size range 6.70 to 4.75 mm.
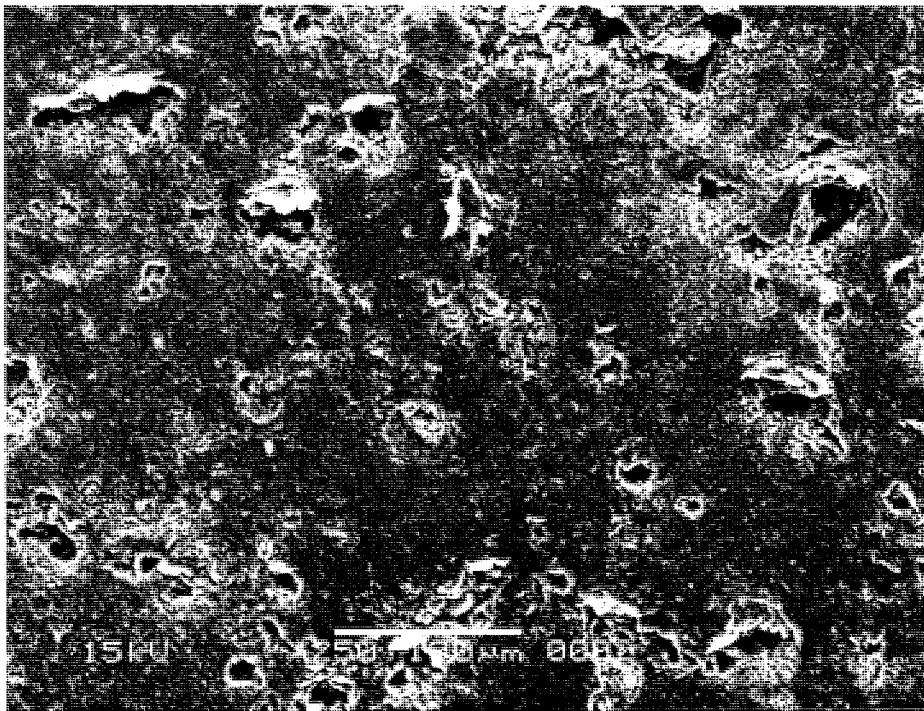
Figure 7.16: Damage produced on bromobutyl rubber samples tested in magnesite with 10% concentration by particles size range 4.75 to 3.35 mm.
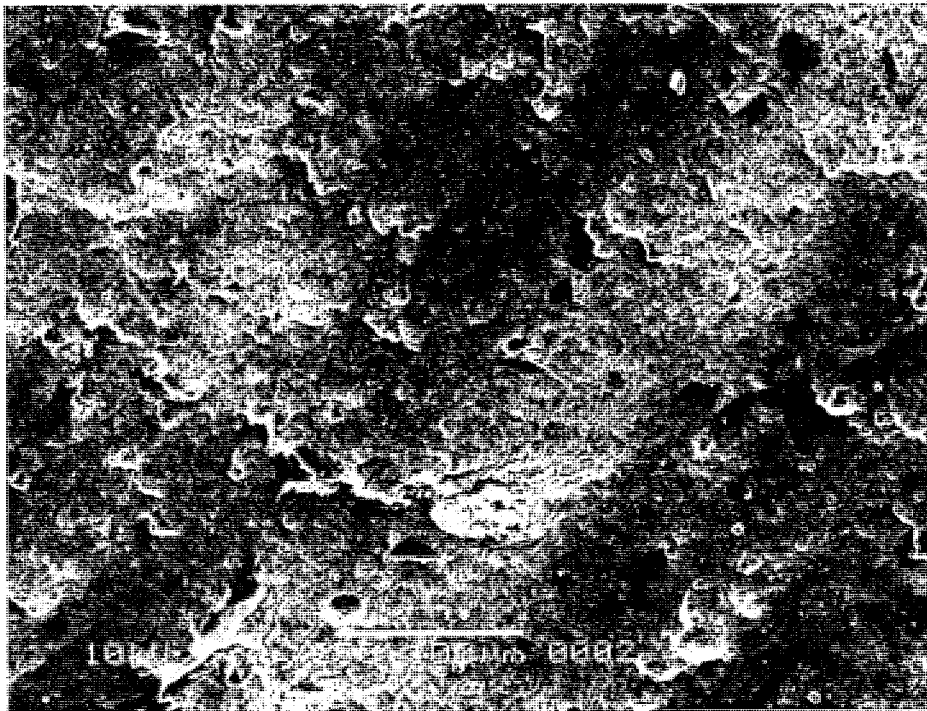


Figure 7.17: Damage produced on bromobutyl rubber samples tested in magnesite with 10% concentration by particles size range 3.35 to 2.36 mm.

Figures 7.18 to 7.19 represent the damage produced on bromobutyl rubber surfaces due to specimen-tip velocity 7.01 and 5.50 m/s in magnesite slurry for particle size range 9.50 to 6.70 mm. The results indicated that the severity of damage was higher for lower specimen velocity and was lower for higher specimen velocity. Although the results are consistent with our previous results, it is not consistent with the kinetic energy transferred to the eroded rubber specimen [7].

A significant quantity of relatively less worn particles was present in the magnesite slurry when the test with specimen velocity 5.50 m/s was carried out. Consequently, more rounded particles were present in the slurry during the test with specimen velocity 7.01 m/s. As a result, damage produced for lower tip-velocity (5.50 m/s) was significantly higher than damage produced for higher tip-velocity possibly due to sharpness of the particles. According to the test schedule and the observation, the sharpness of the particles tended decrease in the later tests. The sharpness depends on the shape of the particles [10].
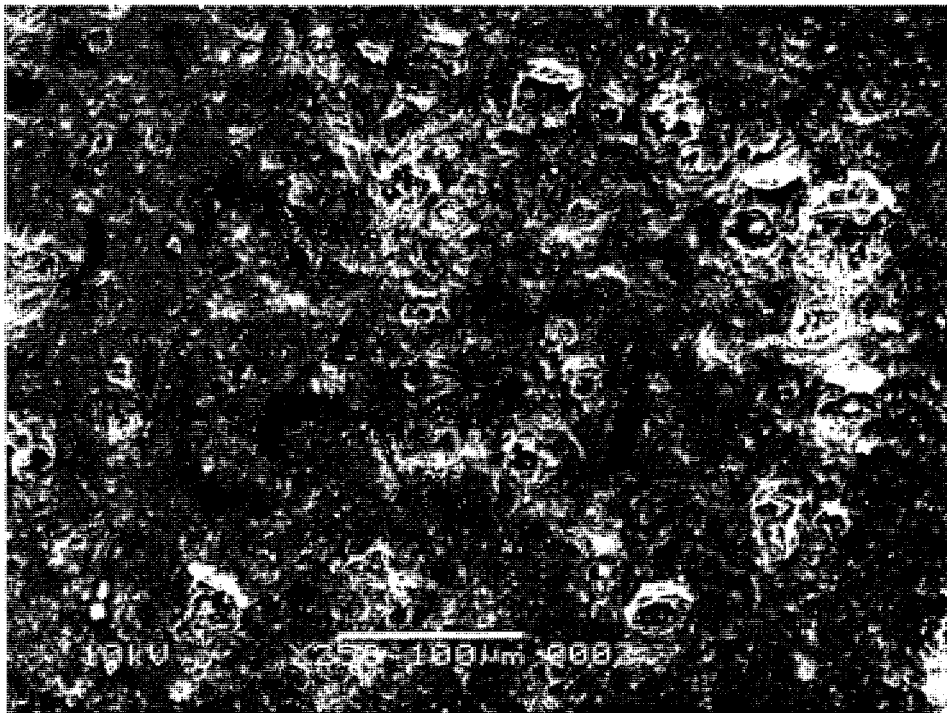


Figure 7.18: SEM micrograph of rubber specimen tested at 5.50 m/s specimen velocity (with 10% slurry concentration, 50 hours duration period and particles size range 9.50 to 6.70 mm)
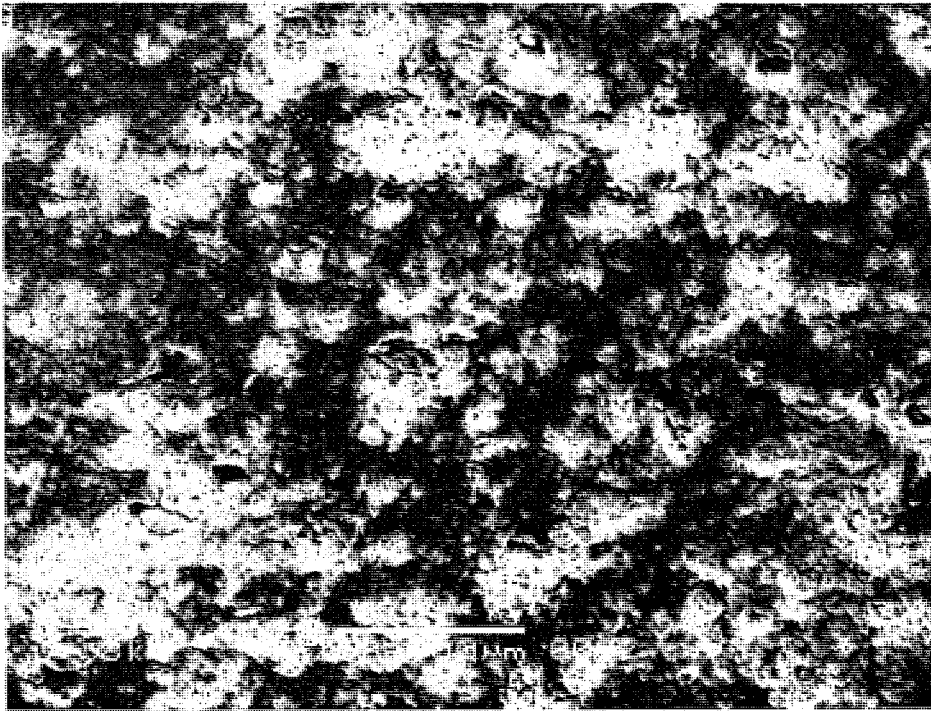
Figure 7.19: SEM micrograph of rubber specimen tested at 7.01 m/s specimen velocity (with 10% slurry concentration, 50 hours duration period and particles size range 9.50 to 6.70 mm)

## 7.5 Particle analysis

During testing, it became clear that the mechanical action of the agitator and mixer were sufficient to cause degradation of the particles. Following testing the worn particles were analysed to determine how much degradation had occurred. Figure 7.20 illustrates the mass degradation of magnesite particles used in the slurry test apparatus. The percentage mass degradation was calculated by determining the proportion of the slurry particles that passed through the smaller screen in the initial size range of particle.
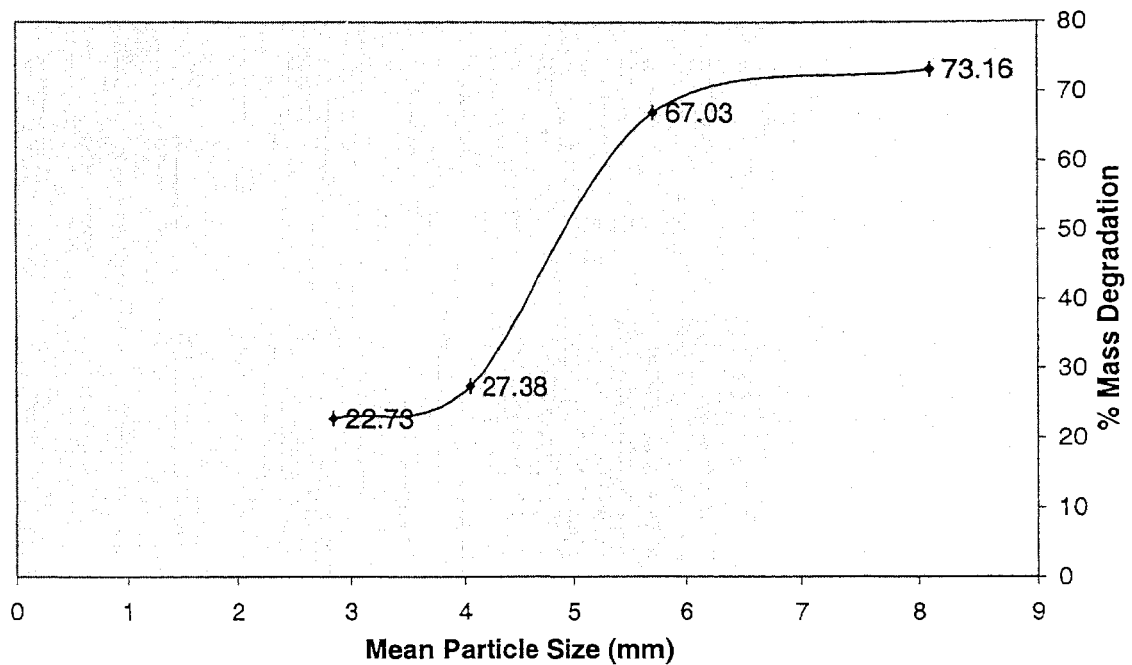


Figure 7- 20: The variation of mass degradation of magnesite particles used in the slurry-pot erosion tester.

The greatest degree of degradation had occurred for the largest size range (9.50 to 6.70 mm) particles which were 73% (as shown in Figure 7.20). This means that 73% mass of the particles passed through the smaller screen (6.70 mm) in the size range 9.50-6.70 mm. For the sample with initial particle size range of 3.35 to 2.36 mm, the lowest degree of degradation had occurred which was 22.73% (refer to Figure 7.20). Similarly, only 22.73% of the mass of the particles passed through the 2.36 mm screen after testing. This indicated that the smaller particles were more resistant to degradation that the larger particles.

Figure 7.21 shows the images of magnesite particles before and after slurry testing. The initial shape of the particles was fairly angular (refer to figure 7.21a). Following testing, the particles became well rounded as a result of repeated impact in the agitated slurry (refer to Figure 7.21b). Although the particle size decreased due to wearing, many of the worn particles were of a similar mass to the unworn particles [7].
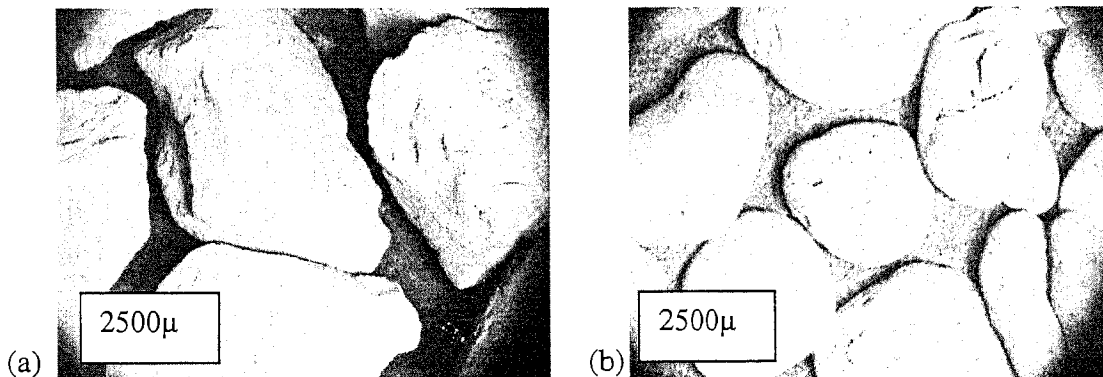


**Figure 7.21: The shape of the magnesite particles (a) before testing (b) after testing.**

A number of cracks and pores were visible in most of the worn particles. This could be due to a number of reasons such as impact, shape and impurities in the particles.

## 7.6 References

1. Hill, D.J.T., Killen, M.I. and Whittaker, A.K., 1997, "Laboratory wear testing of polyurethane elastomers," Wear, Vol. 208, pp. 155-160.
2. Clark, H. McI. and Wong, K.K., 1993, " A model of particle velocities and trajectories in a slurry pot erosion tester," Wear, Vol. 160, pp. 95-104.
3. Iwai, Yoshiri and Nambu, Kazuyuki 1997, "Slurry wear properties of pump lining materials," Wear, Vol. 210, pp. 211-219.
4. ASTM Standard, 2004, "Metals Test Method and Analytical Procedures - Wear and Erosion; Metal Corrosion", Vol. 03.02, pp.461

5. Ahn, Yoomin ; Yoon, Joon-Yong ; Baek, Chang-Wook ;Kim, Yong-Kweon, 2004, "Chemical mechanical polishing by colloidal silica-based slurry for micro-scratch reduction, Wear, Vol. 257, pp. 785-789.

6. Finnie, I., 1995, "Some reflections on the past and future of erosion," Wear, Vol. 186-187, pp. 1-10.

7. Akan, S. H., Druskovich, D. and Clegg, R. E., 2004, "Slurry erosive wear of bromobutyl rubber lining material in the leaching circuit of mineral processing industries," 1st International Tribological Conference, December 1-3, 2004, Singapore National University, Singapore, pp. B 92-93.

8. Lynn, R. S., Wong, K. K. and Clark, H. McI., 1991, "On the particle size effect in the slurry erosion," Wear, Vol. 149, pp. 55-71.

9. Mesa, D. H., Toro, A., Sinatora, A., and Tschiptschin, A. P., 2003, "The effect of testing temperature on corrosion-erosion resistance of martensitic stainless steels," Wear, Vol. 255, pp. 139-145.

10. Kaya, E.; Hogg, R.; Kumar, S.R.; "Particle shape modification in communication", KONA, No. 20, pp. 188-195.

Chapter 8

# Experimental Discussions

The wear of material is commonly measured as loss of mass or volume of the original material over a period of time or a unit of wearing distance. However, in the tests carried out in this study, relatively low wear was generated on the surface of rubber specimens tested using the slurry erosion tester. Because the wear rate was very slow and the rubber tended to absorb unknown quantities of moisture, wear was impossible to quantify as loss of mass or loss of volume. As a result, alternative methods of characterizing the wear were sought and one of these was to examine the effects of wearing behaviour on the surface roughness of the rubber. Surface roughening of the specimens was measured using Surtronic 3+ surface roughness profilometer. The surface roughness of bromobutyl rubber was measured against a number of test parameters such as slurry concentration, erosion time, specimen velocity, and particle size and incidence angle. In this chapter, we discuss the results of the surface roughness measurements, the particle mass degradation tests and SEM images to determine how effective this method of study into wear is and to discuss some of the effects of test parameters on wear behaviour. The wear mechanisms are also discussed in the light of SEM studies.

## 8.1 Surface roughness measurement

The measurement of abrasive wear in the laboratory is difficult for a number of reasons. First, wear rates can be slow in the materials of interest and long periods of time may be needed to observe measurable quantity of wear. Second, the results of standardized tests generally transfer poorly to industrial experience. The wear mechanisms are often complex and difficult to reproduce in the laboratory. The wear of tested rubber specimens was measured using a surface roughness profilometer as discussed above. The results are discussed here mainly on the basis of the test parameters.

### 8.1.1 Particle size

The surface roughening of bromobutyl rubber was measured for particle size range 9.50 to 6.70, 6.70 to 4.75, 4.75 to 3.35 and 3.35 to 2.36 mm (refer to Figure 8.1).

The results indicate that the surface roughness was highest for the largest particles (size range 9.50 to 6.70 mm) and was lowest for the smallest particles (size range 3.35 to 2.36). In general, larger particles contain more kinetic energy than smaller particles when travelling at the same speed and hence damage produced on the rubber surface due to transfer of kinetic energy is greater for larger particles [8]. Surface roughness tended to increase with increasing particle size except for particles size range 4.75 to 3.35 mm. A number of reasons were suspected for this and these were discussed in the experimental results section of this report. Apart from this, our results were consistent with the work of a number of researchers who considered that changes in particle size affect the wear rate of target materials [1-3]. Arnold and Hutching also found the steady-state erosion rate higher with larger particles.
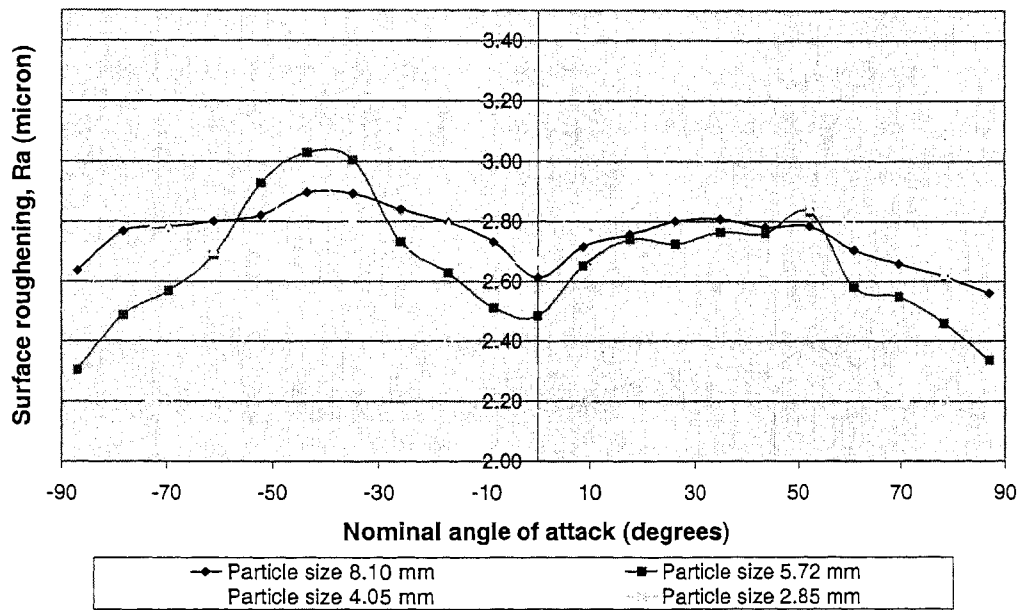


**Figure 8.1: Variation of surface roughening of bromobutyl rubber at constant slurry concentration (10%) for particles size range 9.50 to 6.70, 6.70 to 4.75, 4.75 to 3.35 and 3.35 to 2.36 mm.**

One of the most important issues not fully understood is the difference in surface roughening among particle size ranges. Although there was a significant change in surface roughness between the 2.85 and 4.05 mean particle sizes, the effect appeared to plateau (refer to Figure 8.1). The slurries used to produce Figure 8.1 were a mixture of new and worn particles and the differences in roughening characteristics may reflect this

rather than the effects of particle size. This suggests that control of particle shape is important for the study of wear in these materials.

## 8.1.2 Particle impingement angle

In slurry erosion, knowledge of the flow of fluid and particles about the test piece is important to fully understand the mechanics of erosion. As discussed earlier, we have not been able to fully characterize the fluid flow behaviour in this system. As a result, the discussion of the effect of impact angle is based on nominal angle of attack, which is the angle between the horizontal and the normal to the surface of the specimen. The results can be refined as more knowledge of the fluid flow behaviour is gained, but this is out of the scope of this thesis.

The effect of particle impact angle can be quantified by the impingement angle. Hence, the impingement angle of particles has been one of the key parameters in studying erosion. It has also been an important indicator for the cutting and cutting and deformation wear models developed by Finnie and Bitter [4-6].

The results indicate that surface roughening was greatest at an angle of incidence or nominal angle of attack of approximately $+/- 40^0$ (as shown in Figures 8.1 to 8.4) This suggests that wear is greatest where the particles strike the rubber at a significant angle. Rubber is relatively resistant to wear when the angle of impingement is perpendicular to the surface [13]. This is because the energy of the particle is absorbed by elastic deformation of the rubber. At angles in the range of 30 to $70^0$, the particles tend to cut the rubber surface as they are dragged across the surface and this appears to be the case here. The results are also consistent with the work of a number of researchers including Nambu *et al.* [3] who determined the wear rate of a number of rubber materials for various impingement angle.

## 8.1.3 Slurry concentration

Slurry concentration has also been recognized as one of the important factors relating to the wear of materials. In processes where chemical reactions are involved, the slurry concentration is constrained by the process requirements. However, in some cases, slurry concentration may be adjusted in order to reduce the wear of materials.
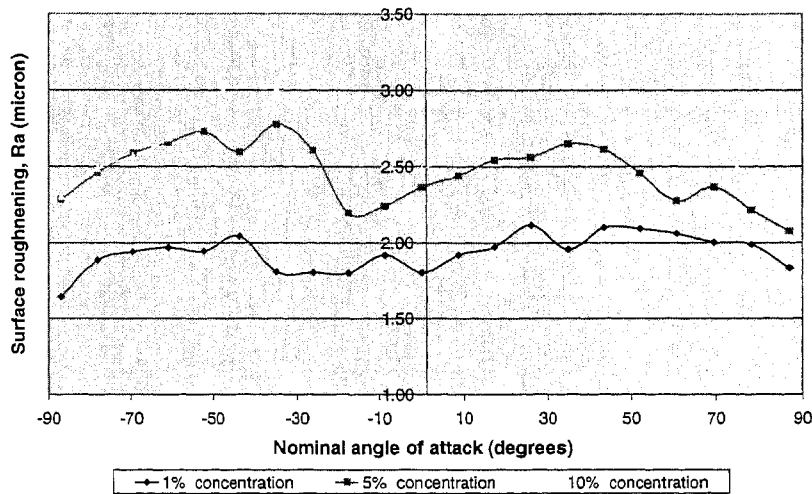
Figure 8.2: Surface roughness of three bromobutyl rubber samples against nominal impingement angle at 1%, 5% and 10% slurry concentration for magnesite particles size range 6.70 to 4.75 mm.

The greatest damage on the rubber specimen occurred for the highest slurry concentration (10%) but with the lowest slurry concentration (1%) the initiation of damage was also observed, as can be seen in Figure 8.2. A higher slurry concentration means that the number of particle impacts per unit time was higher than that for a lower concentration. Since the kinetic energy of particles imparted into the surface of the rubber is dependent on the number of particle impacts, the highest concentration would be expected to be responsible for the greatest damage.

One major limitation in the tests carried out was that only concentrations at level of 1, 5 and 10 % were performed. Iwai and Nambu determined that the wear rate of rubber material is proportional to the sand concentration to some power [3]. This indicates that after a critical level of slurry concentration damage will not be influenced by slurry concentration. The reason for this could be that a higher concentration of particle may affect the fluid flow behaviour about the specimens and the effects of particle impacts may saturate.

## 8.1.4 Erosion time

In general, slurry erosive wear of materials is a slow and time consuming process. The quantitative results (as shown in Figure 8.3) obtained in the tests indicate that roughening due to erosive wear is slightly increased with increasing erosion time (except for a few points along the specimen surface), but roughening rate is not proportional to

time. It should be remembered that surface roughness is not a direct measure of the wear rate and should not be confused with weight loss measurements. It may be that the wear rate was increasing with increasing time, but the surface roughness may not have altered during this process.
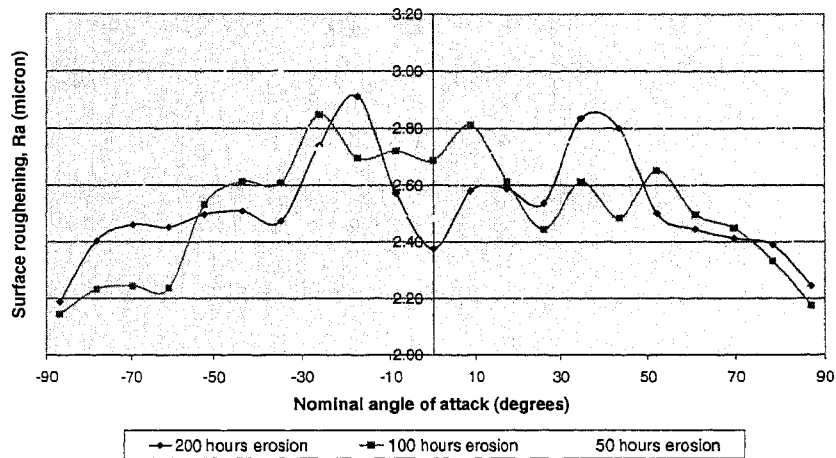


Figure 8.3: Surface roughness of tested bromobutyl rubber samples for 50, 100 and 200 hours of erosion time by 5.72 mm particle size in constant slurry concentration (10%).

In their studies, Mesa *et al.* found specific mass loss of a number of steel materials as a function of erosion duration [9]. A similar observation was made by Bijwe *at el.* using a number of composite materials [10]. Iwai and Nambu also reported increasing volume loss of materials such as polyurethane, elastomer and rubber with increasing time [3]. This indicates that duration is an important factor in erosion for most of the materials. Although the results in this work are consistent with the work of the above mentioned researchers, the differences in surface roughening were not significant as would have been expected. Mixing of worn and unworn particles reported as in the previous section may be the reason. Since erosion is a progressive and relatively slow process, selection of test duration such as 50, 100 and 200 hours were not enough to generate significant quantity of wear. Possibly even after 200 hours, there has been insufficient time for this rubber to wear significantly.

## 8.1.5 Specimen velocity

An interesting result was that the surface roughening of bromobutyl rubber was found highest with the lowest specimen velocity (refer to Figure 8.4). Specimen

velocities of 5.50 and 7.01 m/s were performed using different arm length (agitator shaft to specimen holder) in the tests. In these tests, the slurry concentration (10%) and erosion duration (50 hours) were maintained constant. Mostly fresh particles were used for specimen velocity 5.50 m/s and relatively worn particles were used for specimen velocity 7.01 m/s. Fluid behaviour due to different specimen velocities was unknown. One complicating factor was that the same slurries were used in the two tests and hence the results may reflect changes in particle morphology, rather than the effects of velocity [8].
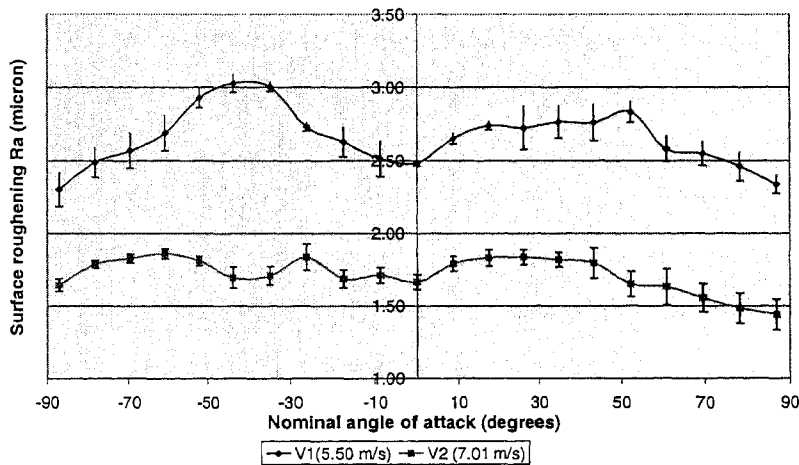


**Figure 8.4: Surface roughness of tested bromobutyl rubber samples for specimen-tip velocity 7.01 and 5.50 m/s at a constant slurry concentration by 5.72 mm size particles.**

The degradation of particles appeared to be reasonably low and hence the change in kinetic energy due to mass was insignificant. This was attributed to the fact that the greatest damage occurred when new and sharp particles were used even though with the lowest specimen velocity.

Interestingly, the SEM studies of these specimens showed that there appeared to be more damage on the surface of the specimens tested at 7.01 m/s. This may be because the rubber was smeared and worn smooth by the higher velocity.

## 8.2 SEM studies

One out of two rubber specimens tested in each test was examined using scanning electron microscopy. The investigation revealed the wear mechanisms of bromobutyl

rubber in magnesite slurries. Some qualitative agreement and disagreement were also encountered with the SEM studies and are discussed here.

## 8.2.1 Particle size

Little difference in damage due to the different particle size ranges was found in the SEM micrographs compared with the observed differences in surface roughness. Some difference in rubber damage was distinguished in the SEM images (as shown Figure 7.2 in Chapter 7). However, these differences were less significant compared to the reported results of a number of researchers in the field of slurry abrasive wear [1-3]. This was due to the fact that the damage can be apparent after a critical value of kinetic energy of particles is consumed by rubber. As the test apparatus was not designed according to computational fluid dynamic modelling, the concentration of particle and liquid flow were impossible to optimise. These significantly can influence the differences in rubber damage identified using the surface roughness tester and the scanning electron microscopy. However, as the slurry concentrations were similar to those in the industrial setting, the results are more likely to reflect the industrial failures.

## 8.2.2 Slurry concentration

SEM micrographs showed that increased damage on the rubber surface occurred with increasing slurry concentration (refer to Figure 8.5). This suggests that the number of impacts of the magnesite particles per unit time were more likely with high slurry concentration. A similar observation was quantified by Iwai and Nambu [3] who worked on the wear of a number of rubber materials subjected to the impact of silica particles.
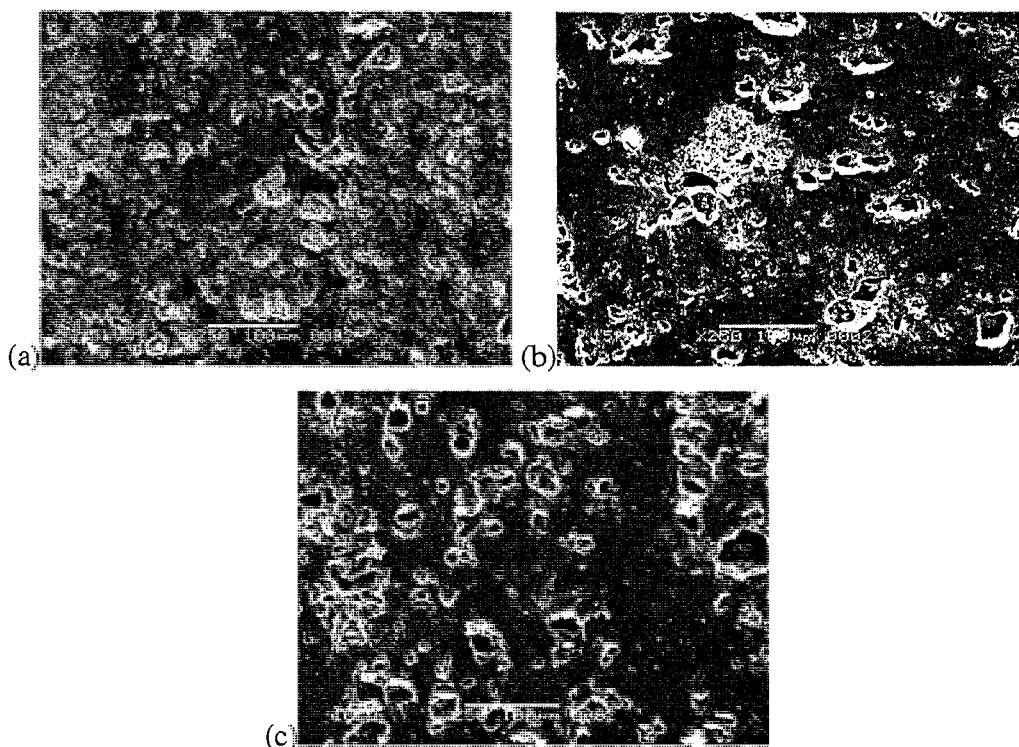
**Figure 8.5: Damage to bromobutyl rubber as a result of slurry concentration at (a) 1, (b) 5 and (c) 10 % by particles size range 4.75 to 3.35 mm.**

Although the similar results were seen in slurries with particles ranging from 9.50 to 6.70, 6.70 to 4.75, 4.75 to 3.35 and 3.35 to 2.36 mm, the critical value of slurry concentration was not yet identified as only three values of 1, 5 and 10% concentrations were tested.

## 8.2.3 Erosion time

Most of the researchers in the field of wear have concluded that duration of erosion is a critical factor in wear [3, 8-10]. Little increase in surface roughening with increasing erosion period was found using surface roughness profilometer. However, the SEM micrographs in this case demonstrated different results. Decreasing damage to rubber surfaces appeared with increasing erosion period as shown in Figure 8.6.
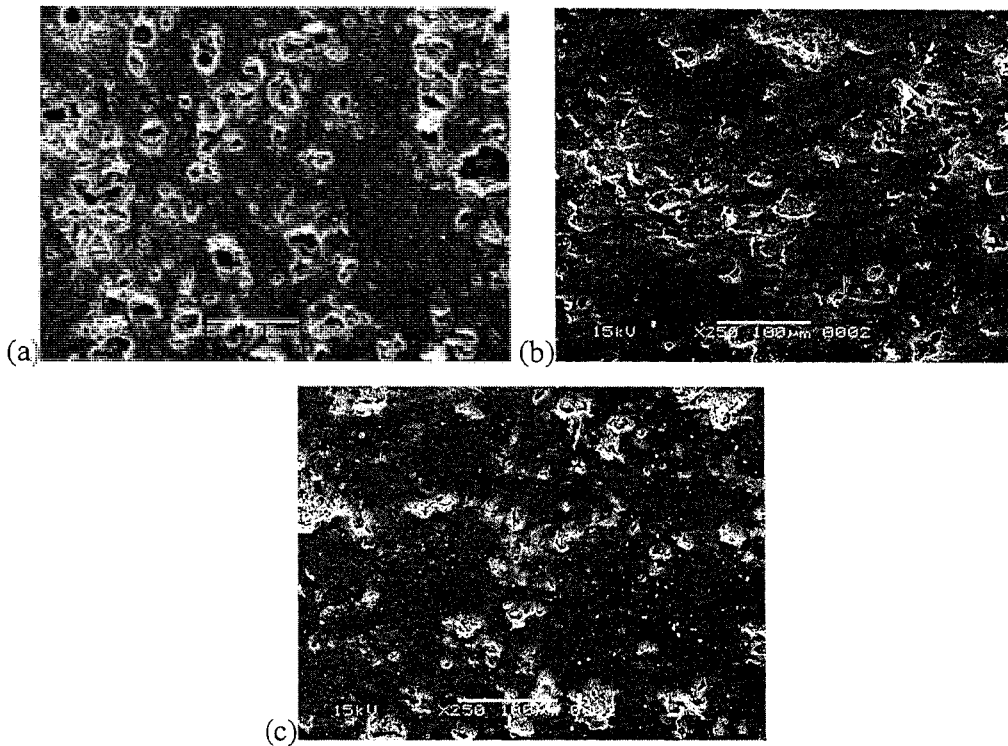
Figure 8.6: Surface damage to bromobutyl rubber due to erosion duration at (a) 50, (b) 100 and (c) 200 hours by particles size range 4.75 to 3.35 mm.

Increasing number of particle impacts are likely on rubber surface with increasing duration of erosion [3]. In this particular case, surface damage appeared surprisingly less despite numerous particle impacts with longer period of erosion. One of the main factors here may be the contact area between particle and material surface. For unworn particles, contact area between particle and material surface is significantly lower than worn particles. As a result, intensified stresses were produced on the rubber surface due to less contact area of unworn particles with short period of erosion. It was mentioned in chapter 7 that the same slurry was used for the tests of 50, 100 and 200 hours respectively. In these tests increased duration of erosion was unable to generate much damage as was expected.

## 8.2.4 Specimen velocity

Although the same slurry was used with specimen velocity such as 5.50 and 7.01 m/s, the damage was significantly less on rubber surface for specimen velocity 7.01 m/s. Interestingly this is the opposite of the effect observed in the surface roughness tests. This may be due to smearing of the rubber at the higher velocity.
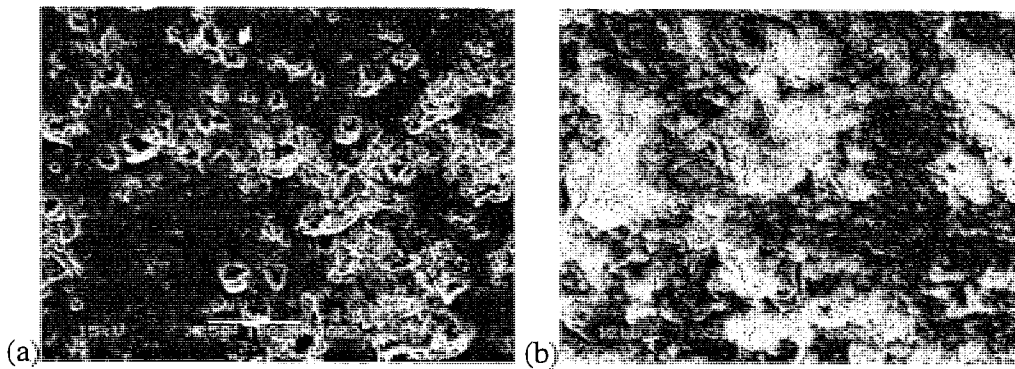
114

**Figure 8.7: Variation in surface roughness due to specimen velocity (a) 7.01 m/s and (b) 5.50 m/s in magnesite slurries having particle size range 6.70 to 4.75 mm.**

Particles in the tests carried out with specimen velocity 5.50 m/s were less worn than tests carried out with 7.01 m/s. As a result, the asperity of particles significantly reduced as particles become rounded in the later tests. This suggests that asperity of particles should be considered in slurry erosion and asperity depends on the shape of the particles involved in erosion.

## 8.2.5 Wear mechanism

A number of wear mechanisms such as micro-plowing, micro-cutting and microfracture may occur in slurry erosion [14]. The mechanisms of micro-plowing and micro-cutting are considered here. Using SEM images, it is possible to identify qualitatively the dominant mechanism that operates during slurry erosion process [15].

Determination of the impacting angle between the particle and the target surface is difficult to understand without a computational fluid dynamic study incorporating turbulent slurry conditions. However, some useful information can be gained from these studies. We define the impacting angle as the angle between the incident particle and the normal to the surface. At relatively high impacting angle, a cutting mechanism is dominant due to high tangential velocity of the particle while plowing mechanism is dominant at relatively low angle of attack. Magnesite is a relatively soft mineral with Mohs hardness ranging from 3.5 to 5.0. So the effect of cutting and plowing actions of the particles, on the resilient rubber surface, may not be occurred till the rubber becomes fully plastic.

The impact of particles on the rubber surface causes a pattern of tensile, compressive and shearing stresses within the rubber. These repeated stresses can cause

115

the rubber material to lose its elasticity and increase in hardness over time. Although wear resistance of metallic materials increase with hardness the rubber material may exhibit opposite trend. Hence the rubber material becomes easier for solid particles to erode. With continuous agitation erosion damage such as cracks and holes can be initiated on the rubber surface as was evidenced by SEM studies in chapter 7. Cracks can grow perpendicular to the surface and may penetrate deep into the rubber. The density of cracks increases with increasing number of impact of particles. The material at intersections of these cracks can be detached by further impact of particles and this can form the main erosion mechanism [13]. This mechanism does not rely on a general loss of material, but can result from a relatively rapid cracking of the rubber. In this case, ultimate failure of the coating rubber in the AMC leaching circuit occurred in a period of three to eight months. This tends to favour a cracking mechanism, where the cracks grow through the rubber surface and eventually lead to the failure of the agitator blades.

## 8.3 Particle analysis

The degradation of magnesite particles affected the surface damage of the bromobutyl rubber and this was a major complicating factor in this study. Although the particles decreased in size due to wear, the differences in mass between worn and unworn particles appeared to be insignificant and this indicates that the difference in kinetic energy between worn and unworn particles would not be significantly different. So, the major effect of the particle degradation was removing asperities and rounding the shape of the particles. This indicates that the damage to the bromobutyl rubber was not only the result of the kinetic energy of the particles but was also strongly influenced by the sharpness of the particles.

Most of the researchers in slurry erosion assumed that the particles were spherical in shape. However, in practice a number of shapes such as angular, spherical and round could be in existence in the slurry particles. Particles having spherical shape may not be dominant in all the cases. This is why the effect of particle shape in wear has not received much research attention to date. Arnold identified that the assumption that particle shape was spherical and constant may be one of the major causes of discrepancy between the erosion models and the experimental data [11]. Various types of surface damage can

result from different shapes of the particle. Bell and Roger suggested considering the nature of the particle in slurry erosion. The importance of particle shape has gained increasing attention in recent years. Kaya *et al.* described the significant role of particle shape in the applications of slurry abrasives and slurry rheology. Their investigation indicated that the shape of particles was controlled by the nature of the material, the type comminution devices used and the residence time in the grinding circuit [12].

## 8.4 Effect of acid and temperature on the failure

One of the complicating factors with this failure was that the agitator blades were immersed in a concentrated acid solution at 70°C during the period of the wearing of the rubber. It is possible that there has been some synergistic effect between the wear and the acid environment. Indeed, our study showed that immersion in acid at 70°C tended to increase the hardness of the rubber over material only immersed in water. As discussed previously, increases in hardness tend to decrease the resistance of rubber to cracking and this would have increased the likelihood of cracking of the rubber. Hence, the acid may have increased the rate at which cracking and erosion occurred.

Cracking is a particularly severe form of failure in the case of this rubber. If a crack were to form and penetrate the rubber, the acid would be allowed to come in contact with steel. If this occurred, then the steel would corrode, particularly along the interface between the rubber and the steel. This would increase the delamination of the rubber and accelerate the failure of the blades.

## 8.5 References

1. Hill, D.J.T., Killen, M.I. and Whittaker, A.K., 1997, "Laboratory wear testing of polyurethane elastomers," Wear, Vol. 208, pp. 155-160.
2. Clark, H. McI. and Wong, K.K., 1993, " A model of particle velocities and trajectories in a slurry pot erosion tester," Wear, Vol. 160, pp. 95-104.
3. Iwai, Yoshiri and Nambu, Kazuyuki 1997, "Slurry wear properties of pump lining materials," Wear, Vol. 210, pp. 211-219.
4. Finnie, I., Stevick, G. R. and Ridgely, J. R., 1992, "The influence of impingement angle on the erosion of ductile metals by angular abrasive particles," Wear, Vol. 152, pp. 91-98.
5. Bitter, J.G.A., 1962, "A study of erosion phenomena," Part 1, Wear, Vol. 6 pp. 5-21.
6. Bitter, J.G.A., 1963, "A study of erosion phenomena," Part 2, Wear, Vol. 6 pp. 169-190.

7.  ASTM Standard, 2004, "Metals Test Method and Analytical Procedures - Wear and Erosion; Metal Corrosion", Vol. 03.02, pp.461.

8.  Akan, S. H., Druskovich, D. and Clegg, R. E., 2004, "Slurry erosive wear of bromobutyl rubber lining material in the leaching circuit of mineral processing industries," 1st International Tribological Conference, December 1-3, 2004, Singapore National University, Singapore, pp. B 92-93.

9.  Mesa, D. H., Toro, A., Sinatora, A., and Tschiptschin, A. P., 2003, "The effect of testing temperature on corrosion-erosion resistance of martensitic stainless steels," Wear, Vol. 255, pp. 139-145.

10. Bijwe, Jayashree and Fahim, M., 2001, "Friction and wear behaviour of polyetherimide composites in various wear modes," Wear, Vol. 249, pp. 715-726.

11. Bell, J.F. and Rogers, P. S., "Laboratory scale erosion testing of wear resistant glass-ceramic", Materials Science and Technology, Vol. 3, pp. 807-813.

12. Kaya, E.; Hogg, R.; Kumar, S.R.; "Particle shape modification in communication", KONA, No. 20, pp. 188-195.

13. Arnold, J.C. and Hutchings, I. M., 1993, "Erosive wear of rubber by solid particles at normal incidence," Wear, Vol. 161, pp. 213-221.

14. Gates, J.F.,2003, "Material selection for wear," A seminar handout on Materials Selection at Gladstone, Australia, pp.1-11.

15. Harsha, A.P. & Tewari, U.S., 2003, "Two-body and three-body abrasive wear behaviour of polyaryletherketone composites," Wear, Vol. 22, pp. 403-418.

Chapter 9

# Conclusions and Future Directions

## 9.1 Conclusions

Considering the large volume of work in this thesis, conclusions are given separately in the following sections.

### 9.1.1 Failure analysis

A comprehensive investigation, including XRD and SEM studies as well as particle and slurry chemical analysis, was carried out in order to determine the failure process. SEM studies revealed the wear mechanisms. A number of factors influencing the failure process were also identified and described here.

Damage such as scratches, small holes and cracks were observed by visual inspection. SEM studies revealed that the wear mechanisms of micro-plowing and micro-cutting were present in the failure mode. The failure was attributed to erosion or cracking of the rubber layers, leading to exposure of the underlying steel to the acid environment. The SEM studies suggested that failure occurred as a result of progressive fatigue crack growth in the rubber surface due to repeated impact of particles. These cracks grew and eventually exposed the mild steel blade to the corrosive medium which accelerated the failure of agitator blades rapidly.

XRD analysis showed that the presence of silica in particles of magnesite ore over 600 microns in size was insignificant and the silica that was present was concentrated in the particles less than 600 microns in size.

### 9.1.2 Rubber degradation test method

Chemical degradation was examined as a change in (shore A) hardness of rubber during immersion. Both in water and in acid the hardness of the rubber decreased initially. In acid, this was followed by a slight increase in hardness, whereas for samples tested in water, the hardness continued to decrease.

Inclusion of foreign elements such as chlorine was evidenced by the EDS analysis of tested rubber in acidic solution. This may have caused further cross-linking of the

rubber to make the rubber brittle which could accelerate damage to rubber during erosion. Surface morphology of virgin and tested rubber was compared. Visible damage was not identified except the indentation marks caused by the pocket durometer.

### 9.1.3 Slurry erosion test method

As measured by surface roughness and surface morphology studies, wear rates increased as a function of slurry concentration, erosion duration and particle size (except for particles size range 4.75 to 3.35 mm). Although surface roughness measurements were able to give some insight into the wear behaviour of the rubber, it does not give absolute values for wear rates.

The surface roughness measurements indicated that there was less roughening of the surface as velocity increased, although SEM examination of the surface seemed to suggest an increase in damage. It was concluded that the increase in velocity tended to smooth the surface of the rubber, although this result may be complicated by the effect of particle rounding.

For particle incidence angle, peak roughening occurred at approximately at $40^0$ for most of the cases. This was caused by particle flow conditions around the specimen holder. This was concluded to be the angle at which maximum cutting was occurring.

### 9.1.4 Modeling

A model was proposed based on the principle of synergistic effect of particles in the magnesite slurries. The model has not yet been validated due to lack of experimental data. Following modifications of the slurry erosion test apparatus data could be available to validate the model.

### 9.2 Further direction

The future direction for this work can be divided into three major areas: experimental results for slurry erosion test apparatus, improving degraded rubber characterisation and improving erosion modelling. Through the use of advanced techniques the slurry erosion test method could significantly be improved. Therefore, the experimental results not only affect the mass transfer of magnesite particles in the slurries but also the erosion rate.

Further modification of the rubber degradation test method also could develop experimental results. In this present rubber degradation method, specimens were not in motion in the chemical solution as was in the AMC leaching circuit. Not only that, tested rubber specimens were characterized to determine (shore A) hardness only of rubber. A number of properties such as tensile stress, compression set and tear strength were not characterized which could be affected by rubber degradation.

Although the erosion model here has not yet been validated, further improvement of the model is necessary particularly applying CFD code. The assumptions for the model need to be changed in order to obtain better fluid dynamic results.

Appendix A

# Design of slurry erosion test apparatus

## A.1: Agitator shaft

Materials:316 Stainless steel
Very tough and ductile material
Expensive but more suitable for our operation.

Ultimate strength Fu = 515 MPa
Yield Strength Fy = 205 MPa
Endurance Strength Fe = 240 MPa

Power (Rated) transmitted by shaft 5.5 KW.
Assuming a loss of 10% through gear and bearing, net power transmitted to shaft is 4.95 KW.

$P = Tw/100$
N = 190 RPM
T = 1000*4.95/(2*3.14*190/60) = 248.99 N.m

For AISI 316 stainless steel endurance strength 240 MPa
Using maximum shear stress theory and a basic safety factor of 2.0

Allowable shearing stress $F_s$ = 240/(2*2) = 60 M Pa

From torsion formula for hollow bar, $F_{s\,(max)}$ = (16Td)/ (3.14 x $(d^4 - d_i^4)$).

**Torsional deflection**

$\theta$ = TL/GJ, where L = 1480 mm
J = $\pi$ $(d^4 - d_i^4)$/32 = 4.02*$10^6$ $mm^4$
G = 74 GPa and torque T = 248.99 N.m.

So, torsional deflection $\theta$ = $0.00923^c$ = $1.66^0$

**Permissible $\theta$ = $3^0$/m >$01.66^0$/ m**

## A.2: Power requirement for agitator blades

Actual tank inlet height = 1150 mm

| | | | | |
|---|---|---|---|---|
| Tank diameter D = | 1200 | mm | | |
| Tank height H = | 1000 | mm | (To be used) | |
| Impeller diameter $D_a$ = | 450 | mm | 17.71 | inch |

Average particle (nominal)

| | | | | |
|---|---|---|---|---|
| diameter $d_g$ = | 6.175 | mm | | |
| Density of Magnesite $\rho_{MgCO3}$ = | 3000 | kg/m3 | | |
| | | | (at 50% weight solid | |
| $\rho_{slurry}$ = Density of slurry | 1500 | kg/m3 | concentration) | |
| Specific gravity of Slurry | 1.5 | | | |
| Number of sets of propeller n = | 1 | | | |

**Budrick's Equation $V_t = 8.925[(1 + 157 d_g^3)^{1/2} - 1]/d_g$**

Terminal velocity of the particle         $V_t$ =         73.02   mm/s         14.4   ft/min
from Budryck's Equation at average particle diameter dg = 6.175 mm

Corelation factor         Fw =         1.85         (at 50% weight solid concentration)

Design particle velocity Vd =         Fw*Vt         135.08   mm/s         26.59   ft/min

For impeller diameter to tank diameter ratio $D_a/H$ =                 0.45

Scale of agitation 6 (Provides concentration uniformity of the solids to 90% of the fluid's batch height)

From figure 7.41 in Slurry Systems Handbook.

We get $\phi$ =         3.5*10^10 =   35000000000

But $\phi = (N^{3.75} D^{2.81}) / Vd$

So by calculation we get N =                 180   rpm

$N^3$ =         5875350.50

Tip velocity of blades (at 180 rpm) $V_{tip}$ =( 2 π N/60) * R (R = 450 mm)

By calculation $V_{tip}$ = 4.24 m/s at 180 rpm
Power required for propeller at 180 rpm
Power = $((D_a /394) * (\rho_{slurry} *N^3 * n)^{.2})^{(1/.2)}$ = 1.6
kW

For tip velocity $V_{tip}$ = 6m/s, required rpm for the impeller N =                 255   rpm
So, power required for the impeller at 255 rpm

Power = $((D_a /394) * (\rho_{slurry} *N^3 * n ).2)^5$ horse power

**So, by calculation, Power =                 4.6   kW**
**Considering miscellaneous losses during operations 5.5 kW motor was selected.**

## A.3: Motor selection
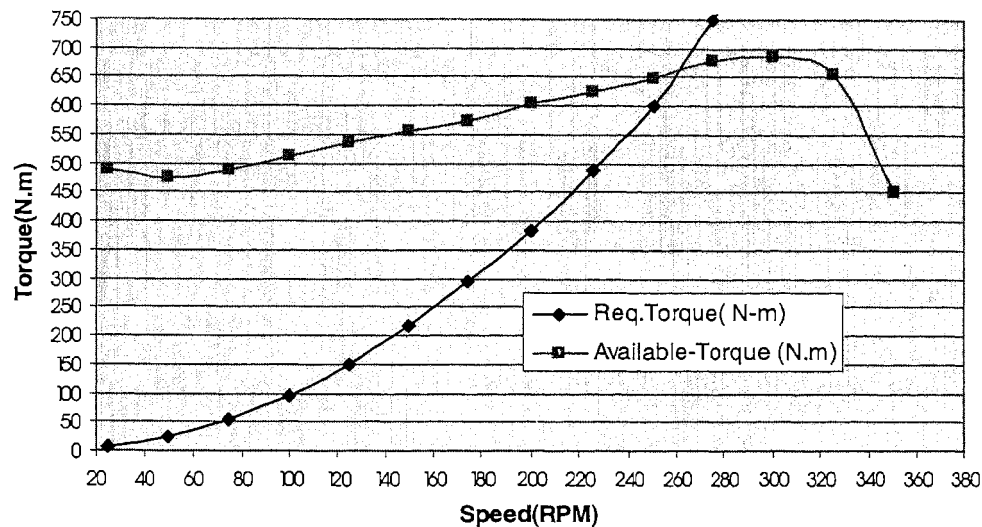


Figure A.1: Torque analysis for a 5.5 kW motor.

## A.4: Test schedule

| Test serial | Particle size range (in mm) | Nominal particle size (in mm) | Test duration (in hours) | Specimen velocity (in m/s) | Weight fraction (in percentage) |
|---|---|---|---|---|---|
| 1 | 9.50 to 6.70 | 8.10 | 50 | 5.50 | 01 |
| 2 | 9.50 to 6.70 | 8.10 | 50 | 5.50 | 05 |
| 3 | 9.50 to 6.70 | 8.10 | 50 | 5.50 | 10 |
| 4 | 9.50 to 6.70 | 8.10 | 100 | 5.50 | 10 |
| 5 | 9.50 to 6.70 | 8.10 | 200 | 5.50 | 10 |
| 6 | 9.50 to 6.70 | 8.10 | 50 | 7.01 | 10 |

Table A.1: Test schedule for particles size range 9.50 to 6.70 mm.

| Test serial | Particle size range (in mm) | Nominal particle size (in mm) | Test duration (in hours) | Specimen velocity (in m/s) | Weight fraction (in percentage) |
|---|---|---|---|---|---|
| 1 | 6.70 to 4.75 | 5.72 | 50 | 5.50 | 01 |
| 2 | 6.70 to 4.75 | 5.72 | 50 | 5.50 | 05 |
| 3 | 6.70 to 4.75 | 5.72 | 50 | 5.50 | 10 |
| 4 | 6.70 to 4.75 | 5.72 | 100 | 5.50 | 10 |
| 5 | 6.70 to 4.75 | 5.72 | 200 | 5.50 | 10 |
| 6 | 6.70 to 4.75 | 5.72 | 50 | 7.01 | 10 |

Table A.2: Test schedule for particles size range 6.70 to 4.75 mm

| Test serial | Particle size range (in mm) | Nominal particle size (in mm) | Test duration (in hours) | Specimen velocity (in m/s) | Weight fraction (in percentage) |
|---|---|---|---|---|---|
| 1 | 4.75 to 3.35 | 4.05 | 50 | 5.50 | 01 |
| 2 | 4.75 to 3.35 | 4.05 | 50 | 5.50 | 05 |
| 3 | 4.75 to 3.35 | 4.05 | 50 | 5.50 | 10 |
| 4 | 4.75 to 3.35 | 4.05 | 100 | 5.50 | 10 |
| 5 | 4.75 to 3.35 | 4.05 | 200 | 5.50 | 10 |
| 6 | 4.75 to 3.35 | 4.05 | 50 | 7.01 | 10 |

Table A.3: Test schedule for particles size range 4.75 to 3.35 mm.

| Test serial | Particle size range (in mm) | Nominal particle size (in mm) | Test duration (in hours) | Specimen velocity (in m/s) | Weight fraction (in percentage) |
|---|---|---|---|---|---|
| 1 | 3.35 to 2.36 | 2.85 | 50 | 5.50 | 01 |
| 2 | 3.35 to 2.36 | 2.85 | 50 | 5.50 | 05 |
| 3 | 3.35 to 2.36 | 2.85 | 50 | 5.50 | 10 |
| 4 | 3.35 to 2.36 | 2.85 | 100 | 5.50 | 10 |
| 5 | 3.35 to 2.36 | 2.85 | 200 | 5.50 | 10 |
| 6 | 3.35 to 2.36 | 2.85 | 50 | 7.01 | 10 |

Table A.4: Test schedule for particles size range 3.35 to 2.36 mm.

Appendix B

# Experimental Results

## B.1: Surface roughness measurements
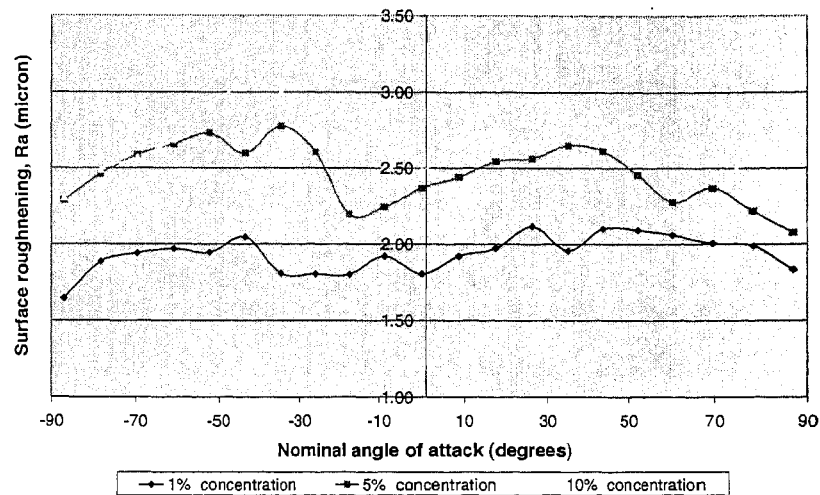


**Figure B.1:** Surface roughness of three bromobutyl rubber samples against nominal impingement angle at 1%, 5% and 10% slurry concentration for magnesite particles size range 6.70 to 4.75 mm.
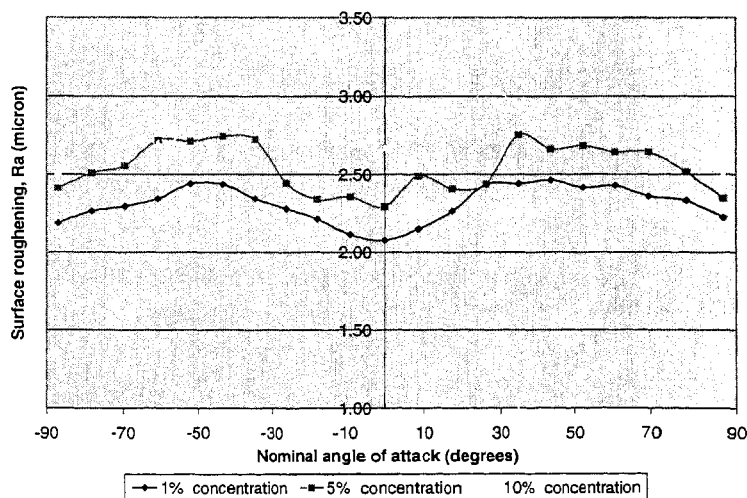


**Figure B.2:** Surface roughness of three bromobutyl rubber samples against nominal impingement angle at 1%, 5% and 10% slurry concentration for magnesite particles size range 4.75 to 3.35 mm.

126
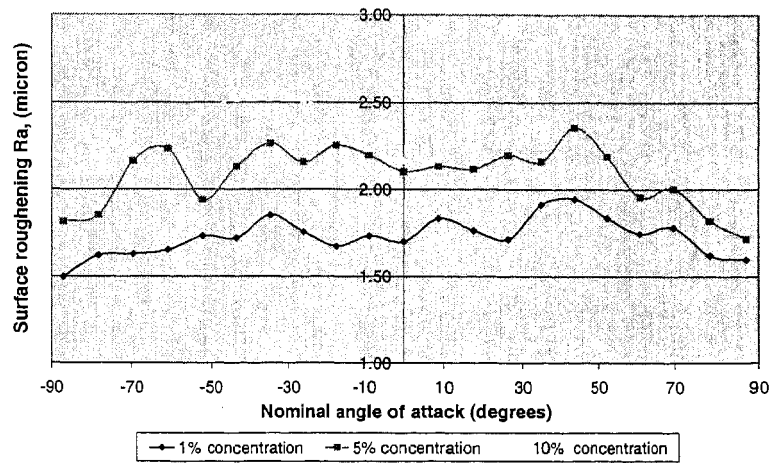
**Figure B.3:** Surface roughness of three bromobutyl rubber samples against nominal impingement angle at 1%, 5% and 10% slurry concentration for magnesite particles size range 3.35 to 2.36 mm.
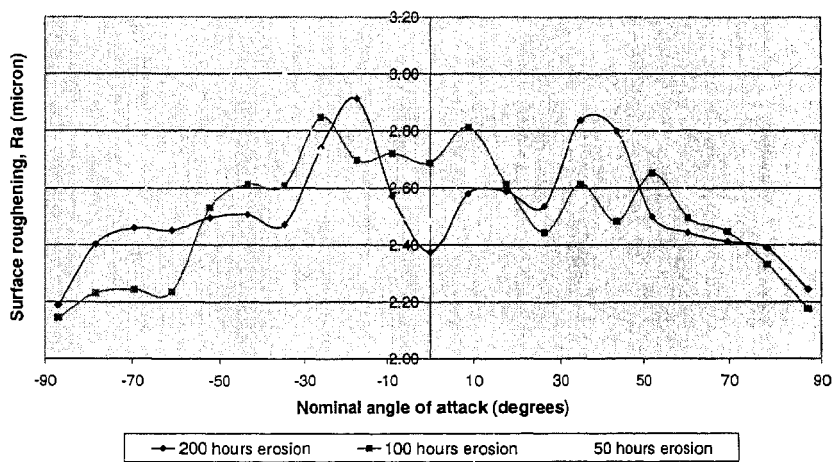


**Figure B.4:** Surface roughness of tested bromobutyl rubber samples for 50, 100 and 200 hours of erosion time by particles size range 6.70 to 4.75 mm at constant slurry concentration (10%).
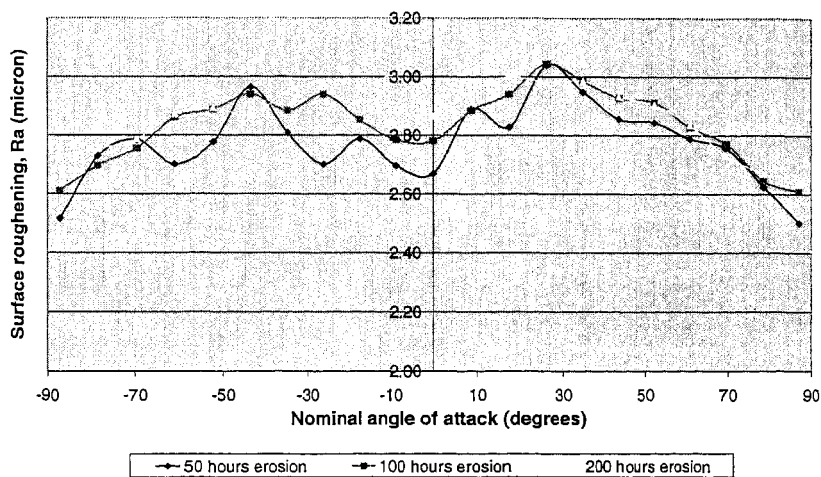
**Figure B.5:** Surface roughness of tested bromobutyl rubber samples for 50, 100 and 200 hours of erosion time by particles size range 4.75 to 3.35 mm at constant slurry concentration (10%).
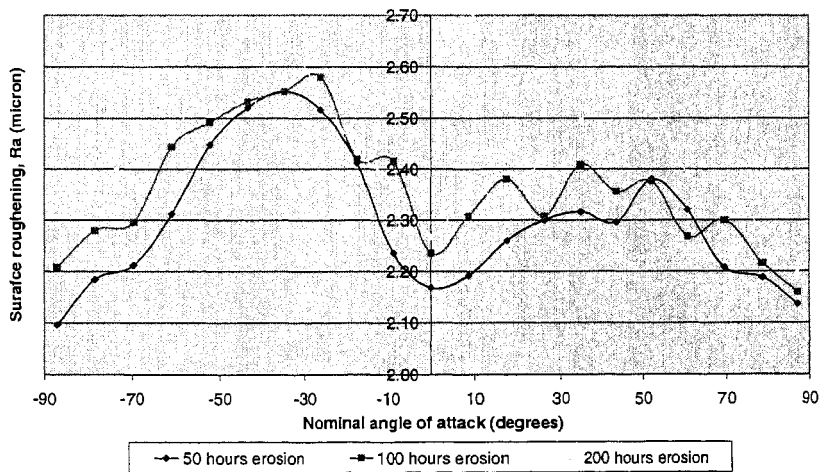


**Figure B.6:** Surface roughness of tested bromobutyl rubber samples for 50, 100 and 200 hours of erosion time by particles size range 3.35 to 2.36 mm at constant slurry concentration (10%).
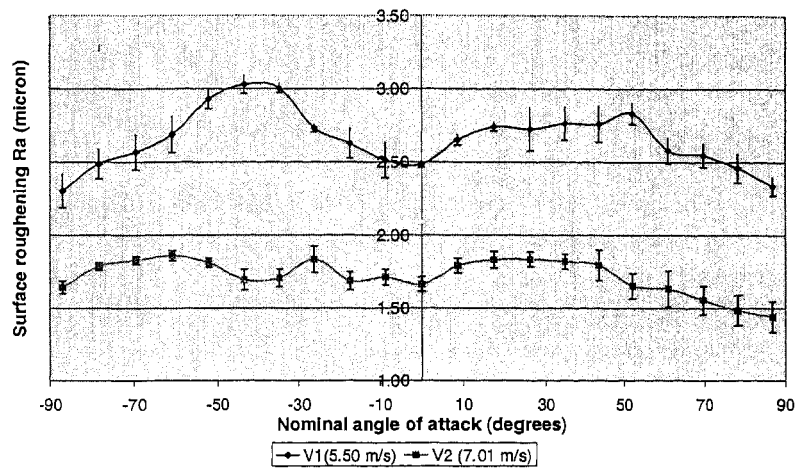
**Figure B.7: Surface roughness of tested bromobutyl rubber samples for specimen velocity 7.01 and 5.50 m/s at a constant slurry concentration by particles size range 6.70 to 4.75 mm.**
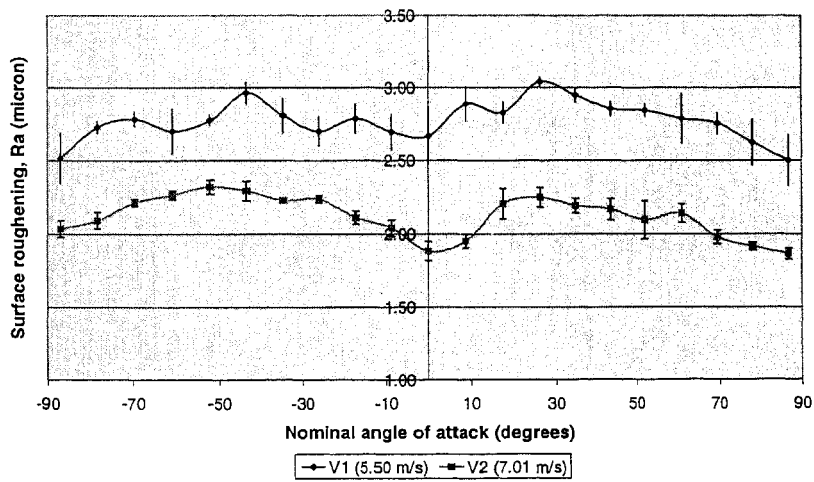


**Figure B.8: Surface roughness of tested bromobutyl rubber samples for specimen-tip velocity 7.01 and 5.50 m/s at a constant slurry concentration by particles size range 4.75 to 3.35 mm.**
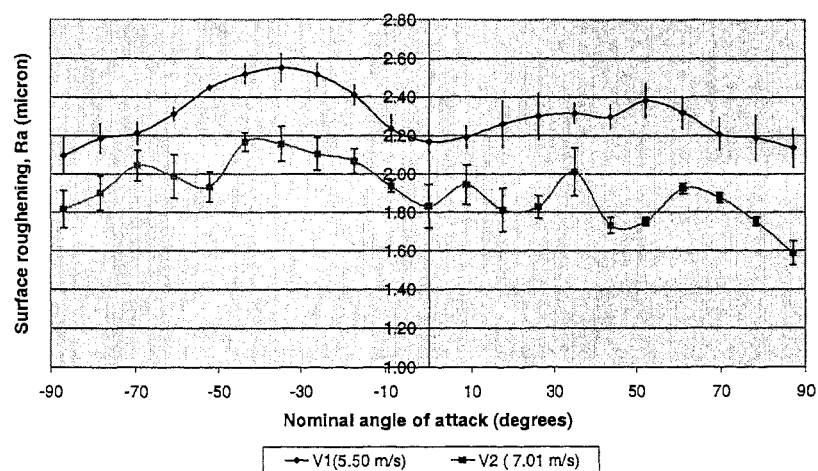
Figure B.9: Surface roughness of tested bromobutyl rubber samples for specimen-tip velocity 7.01 and 5.50 m/s at a constant slurry concentration by particles size range 3.35 to 2.36 mm.

## B.2: SEM studies



(a)

(b)
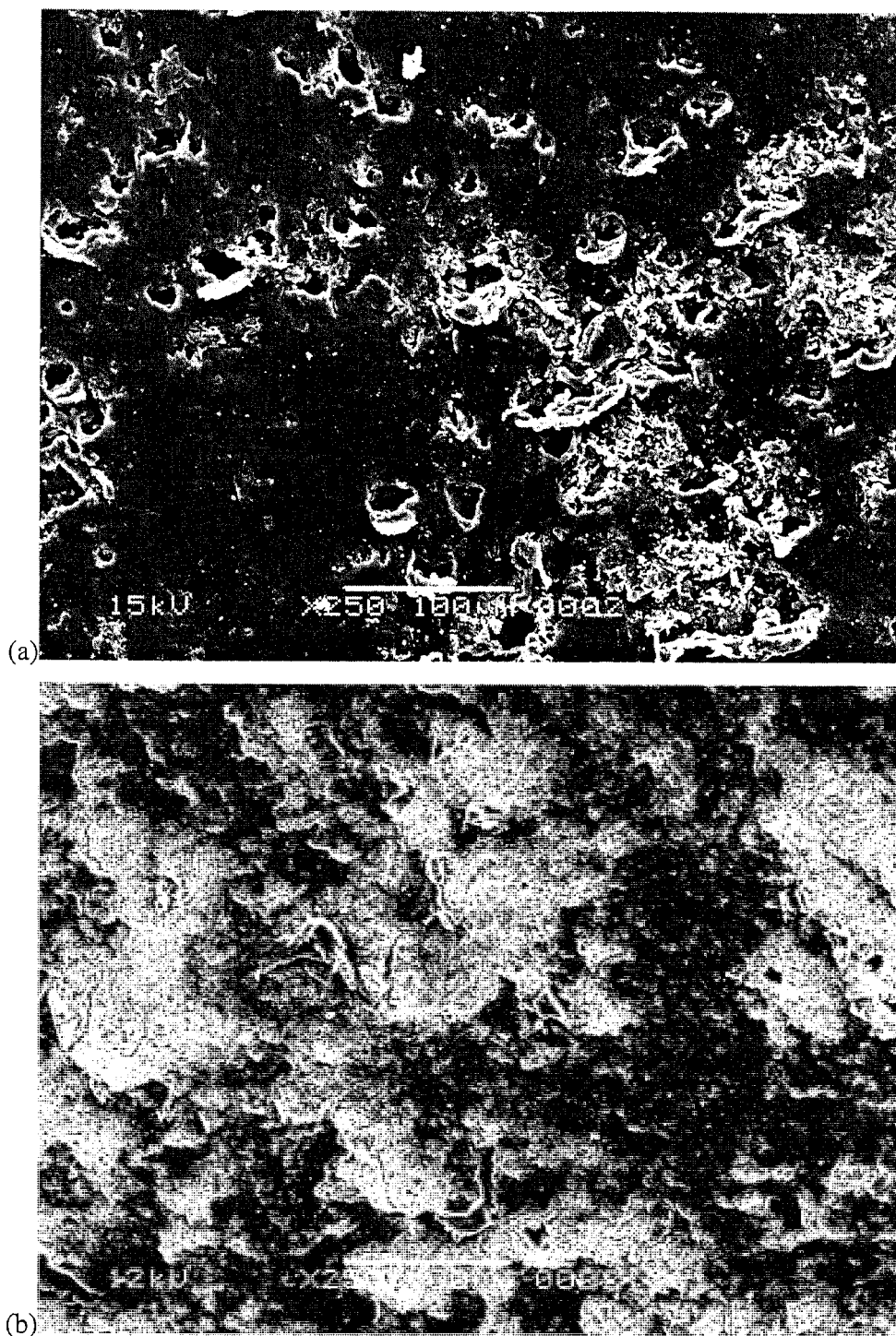
Figure B.10: Difference in damage to bromobutyl rubber due to specimen velocity (a) 5.50 m/s and (b) 7.01 m/s for particles size range 6.70 to 4.75 mm.
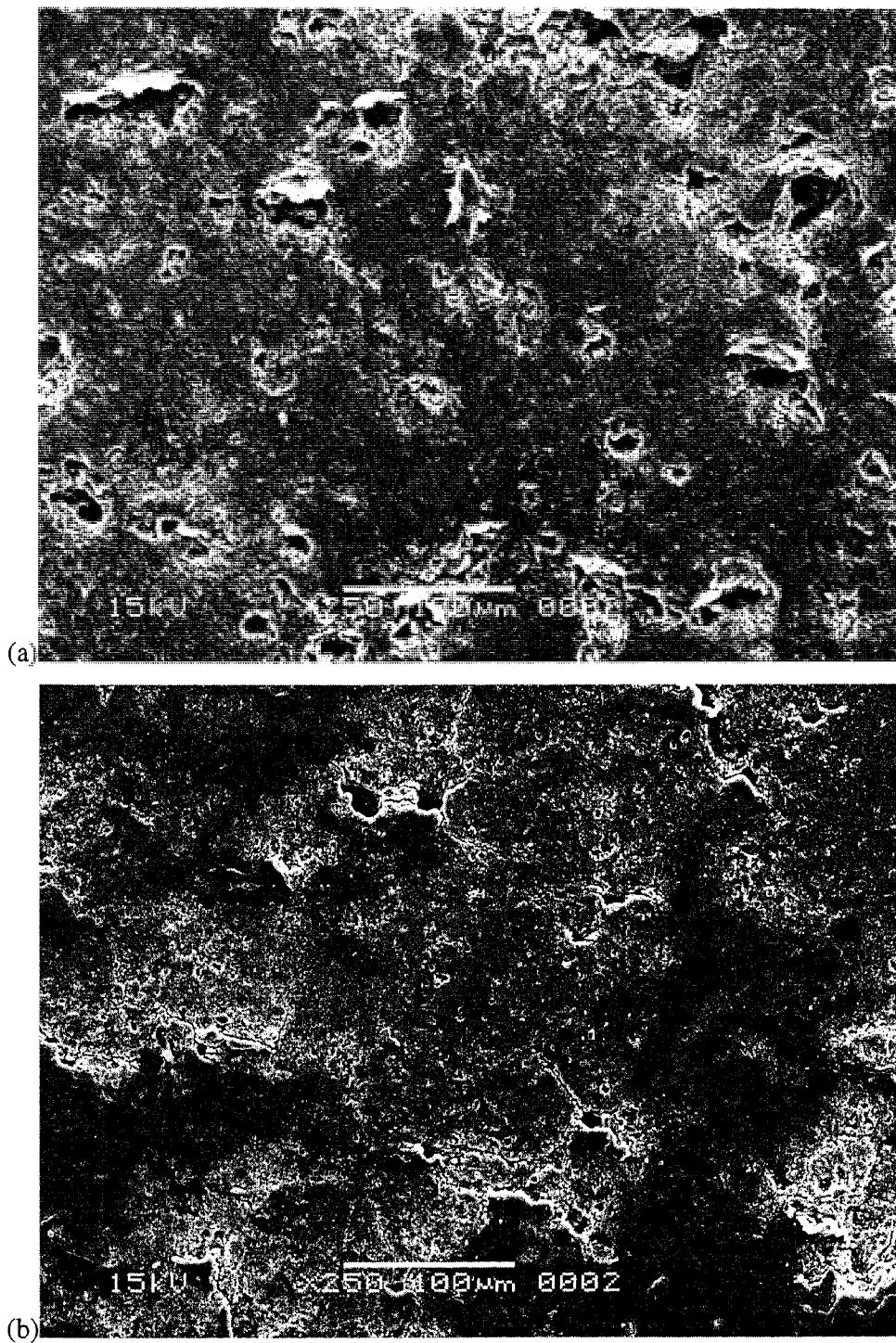
**Figure B.11: Difference in damage to bromobutyl rubber due to specimen velocity (a) 5.50 m/s and (b) 7.01 m/s for particles size range 4.75 to 3.35 mm.**
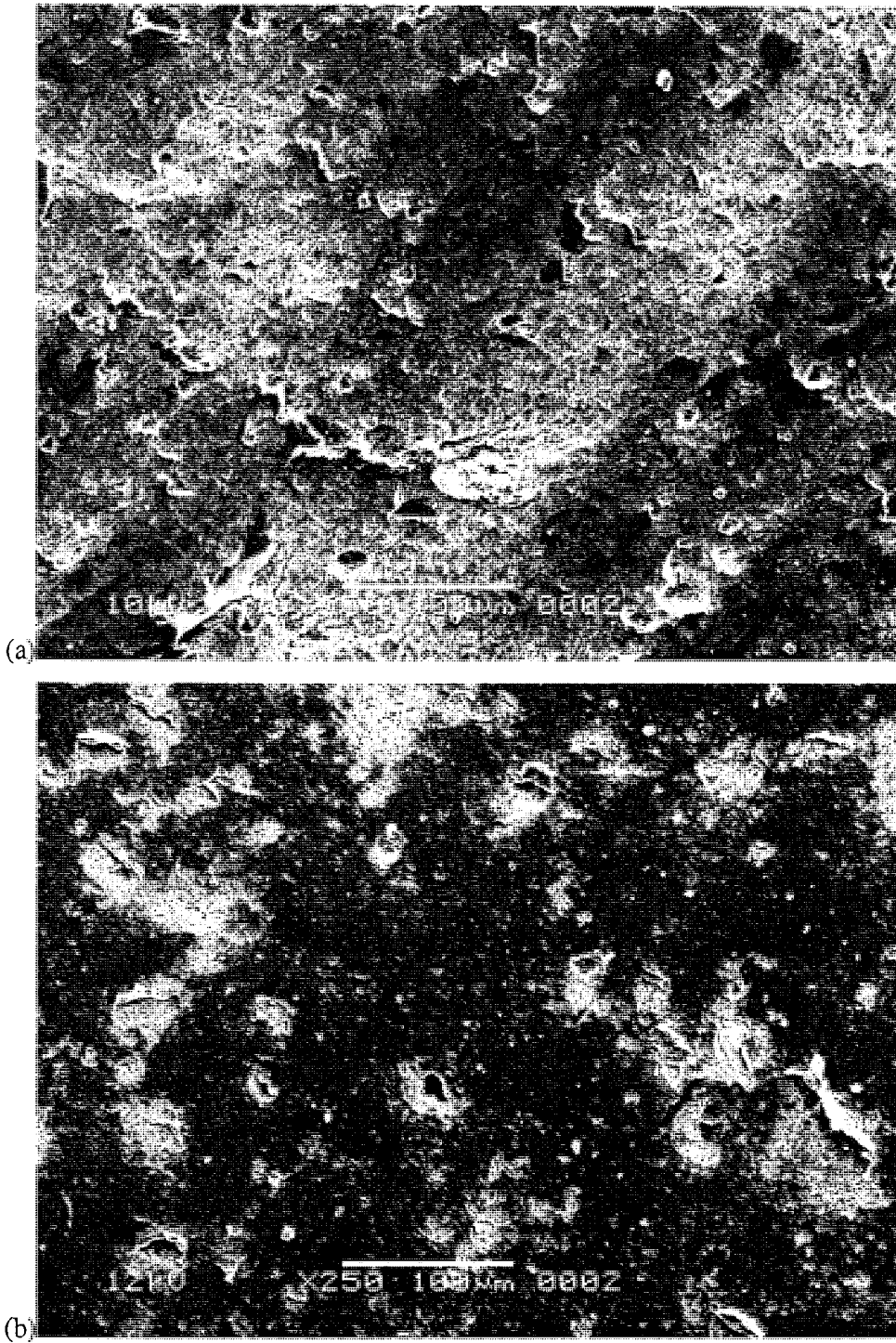
Figure B.12: Variation in surface roughness due to specimen velocity (a) 5.50 m/s and (b) 7.01 m/s for particles size range 3.35 to 2.36 mm.

(a)



(b)

(c)
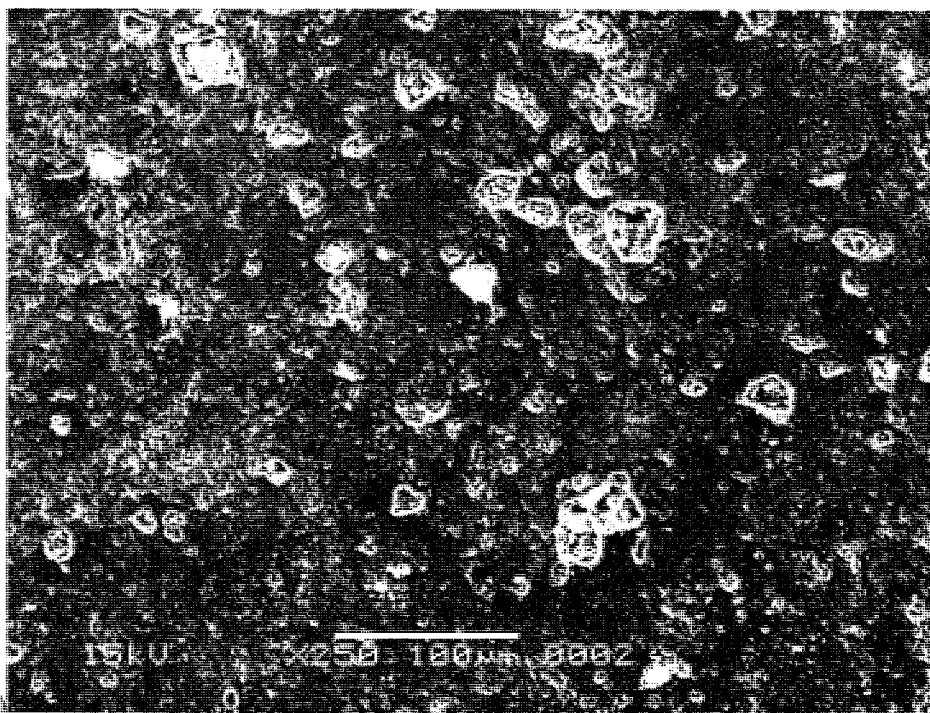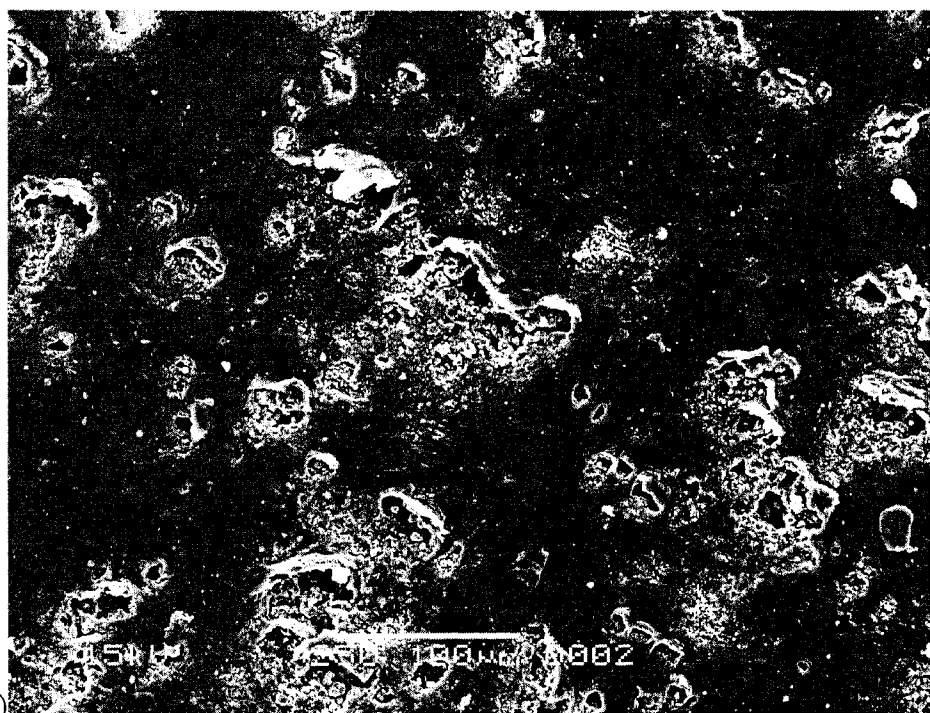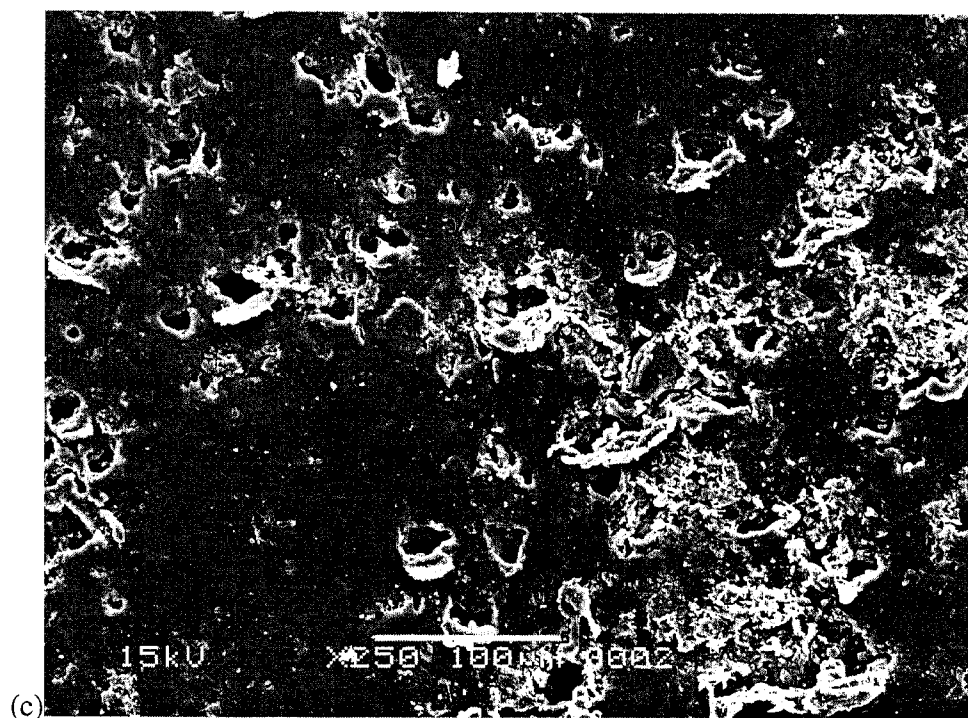
Figure B.13: Damage to bromobutyl rubber due to slurry concentration (a) 1% (b) 5% and (c) 10% for particles size range 6.70 to 4.75 mm.
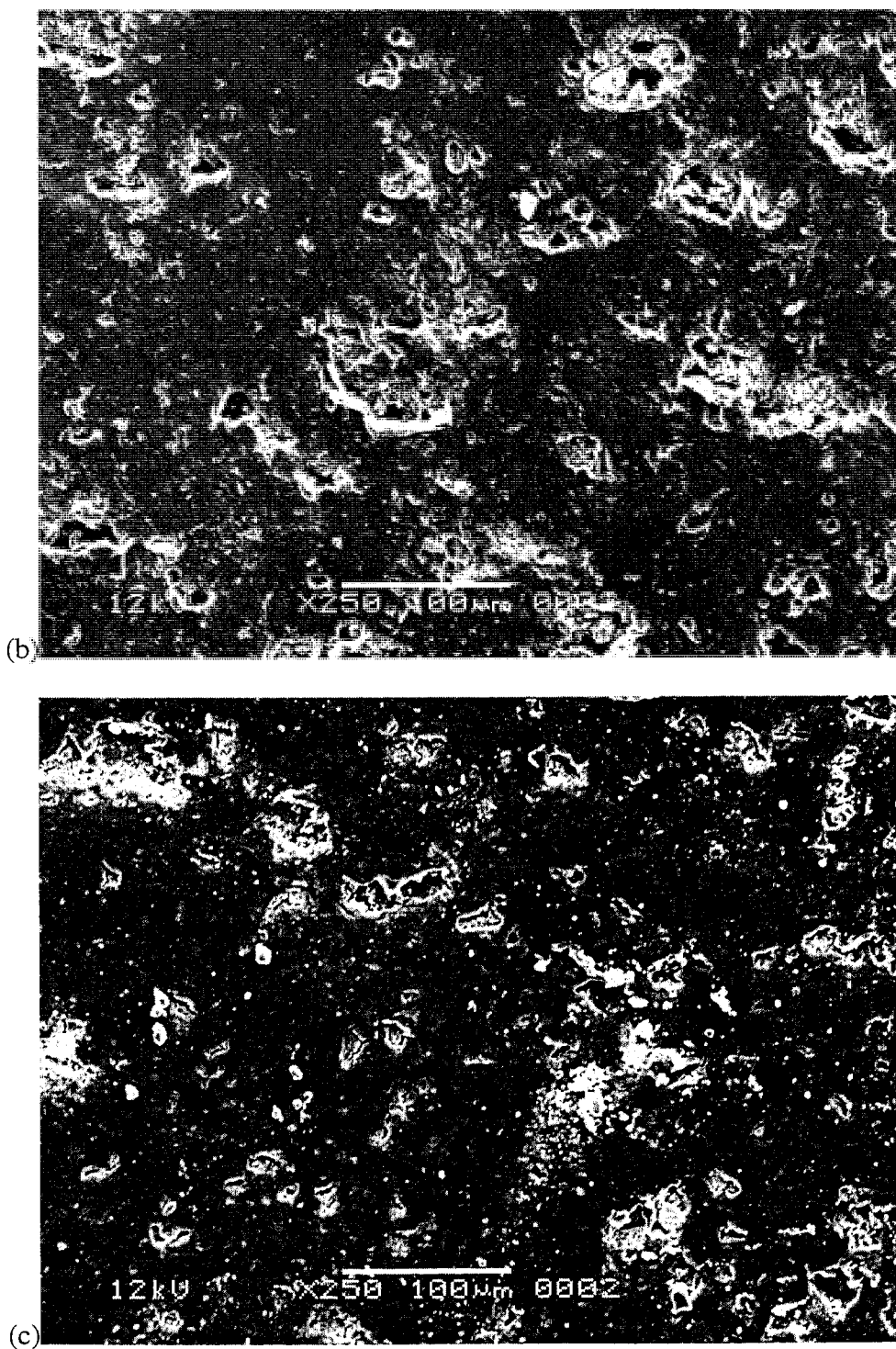


(a)
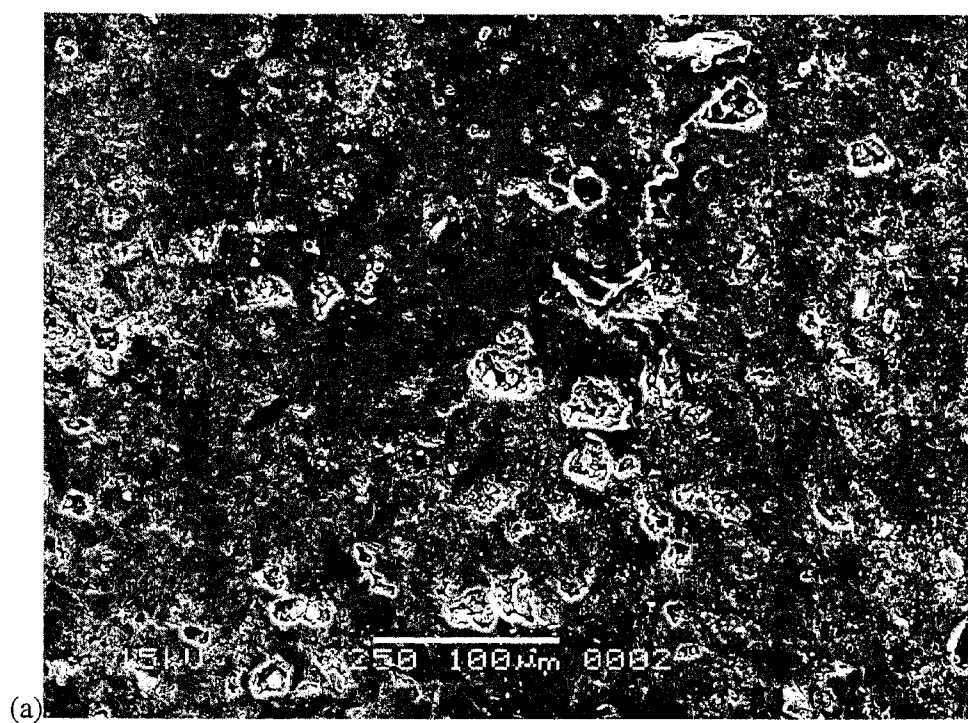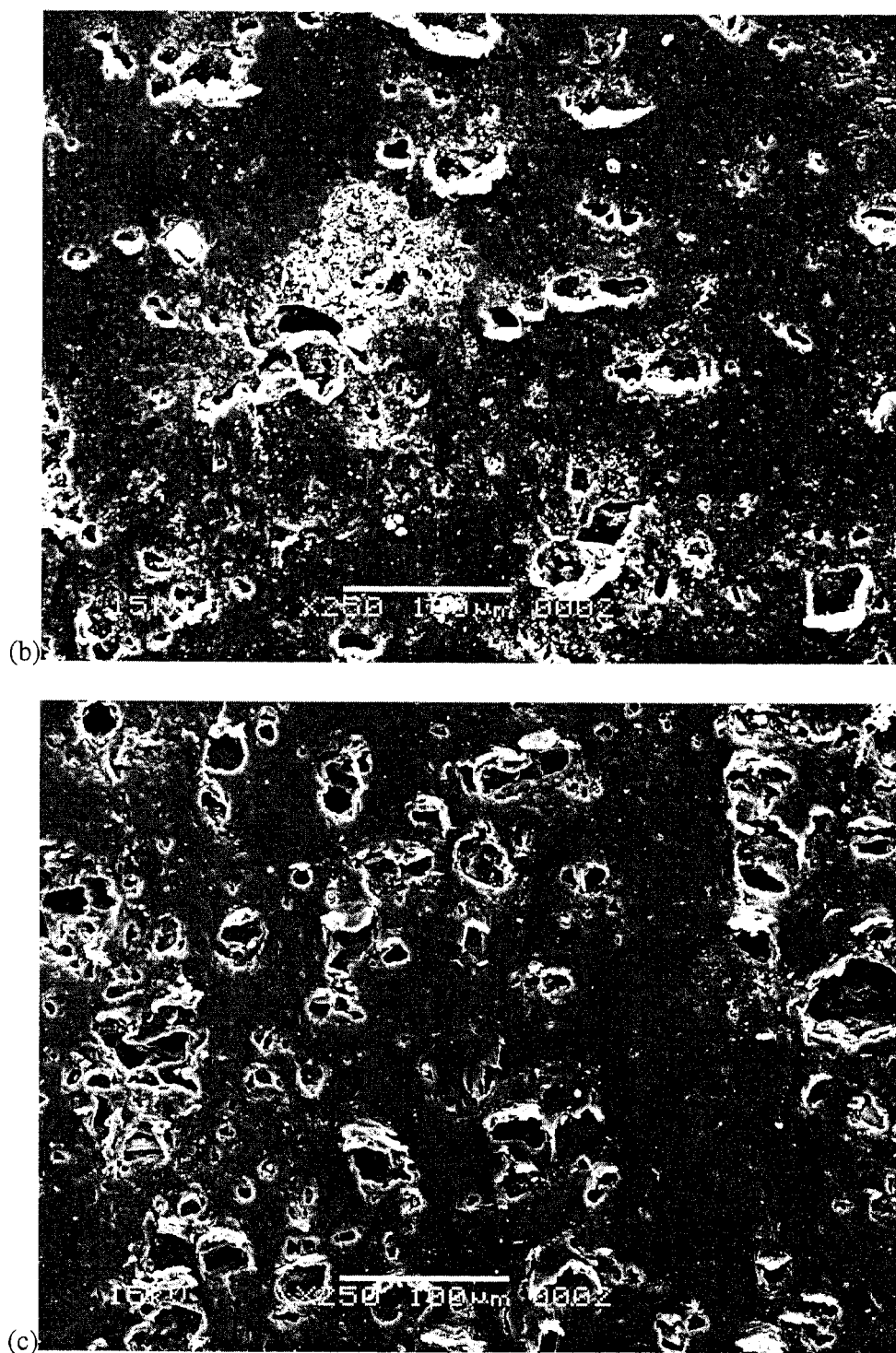
Figure B.14: Damage to bromobutyl rubber due to slurry concentration (a) 1% (b) 5% and (c) 10% for particles size range 4.75 to 3.35 mm.
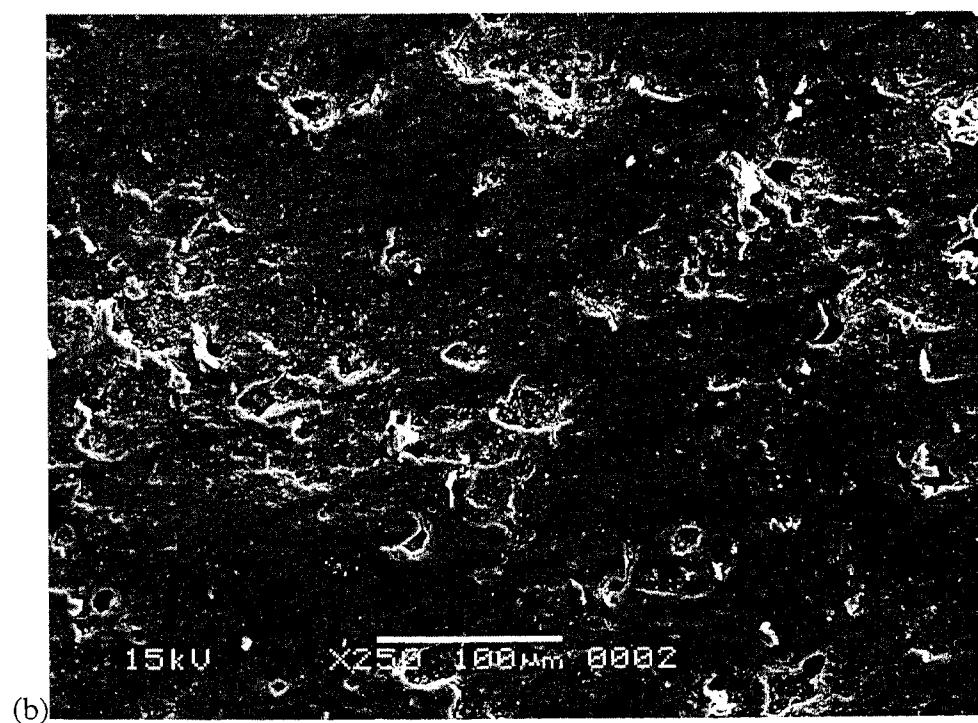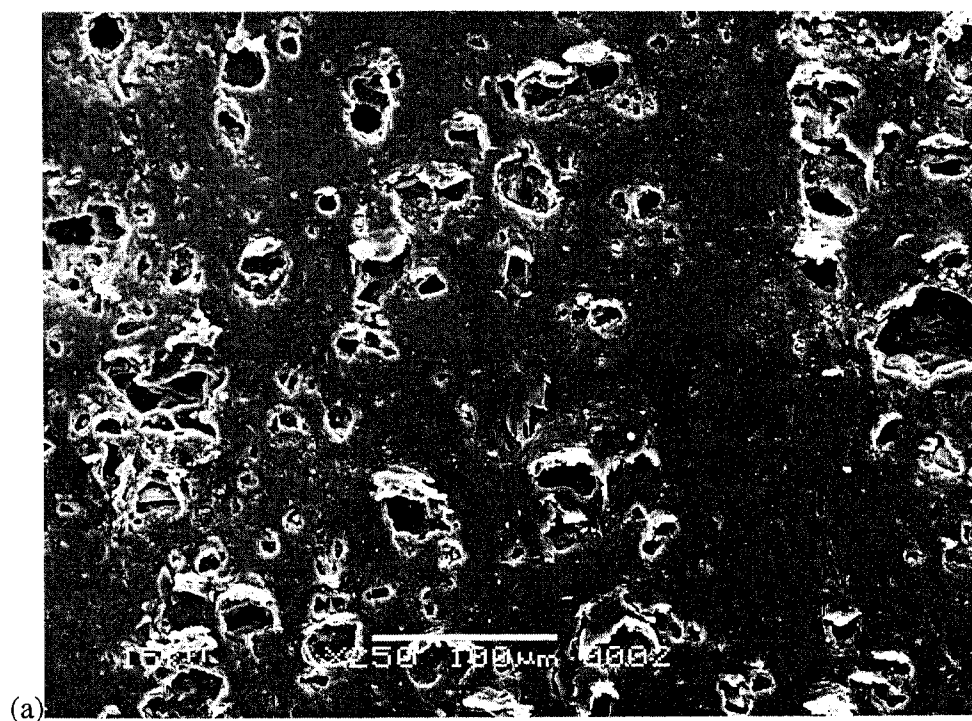
(a)



(b)

(c)
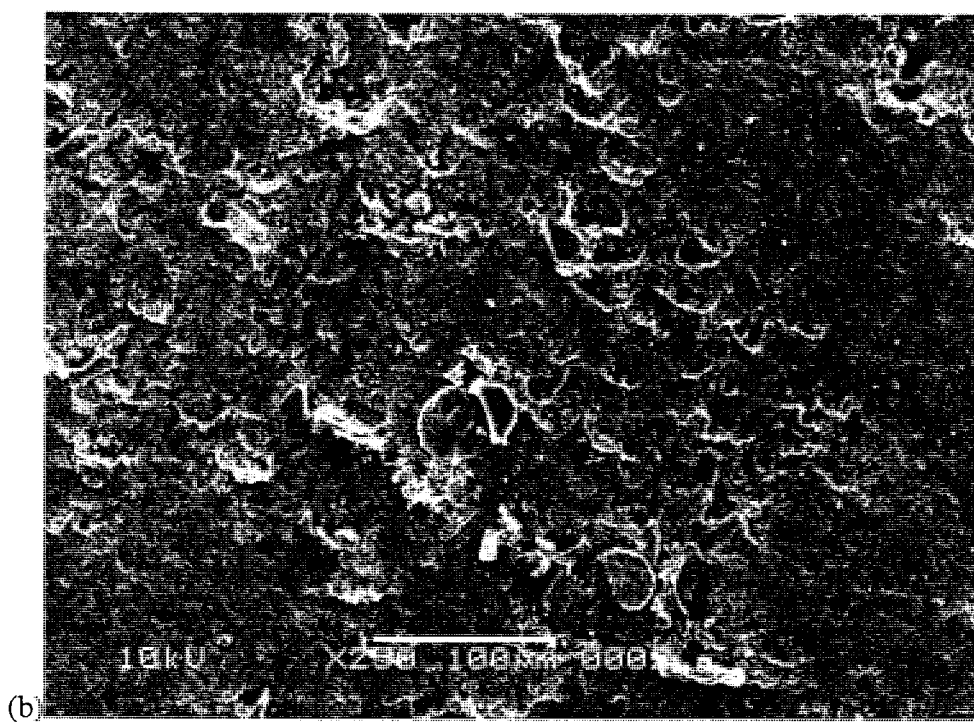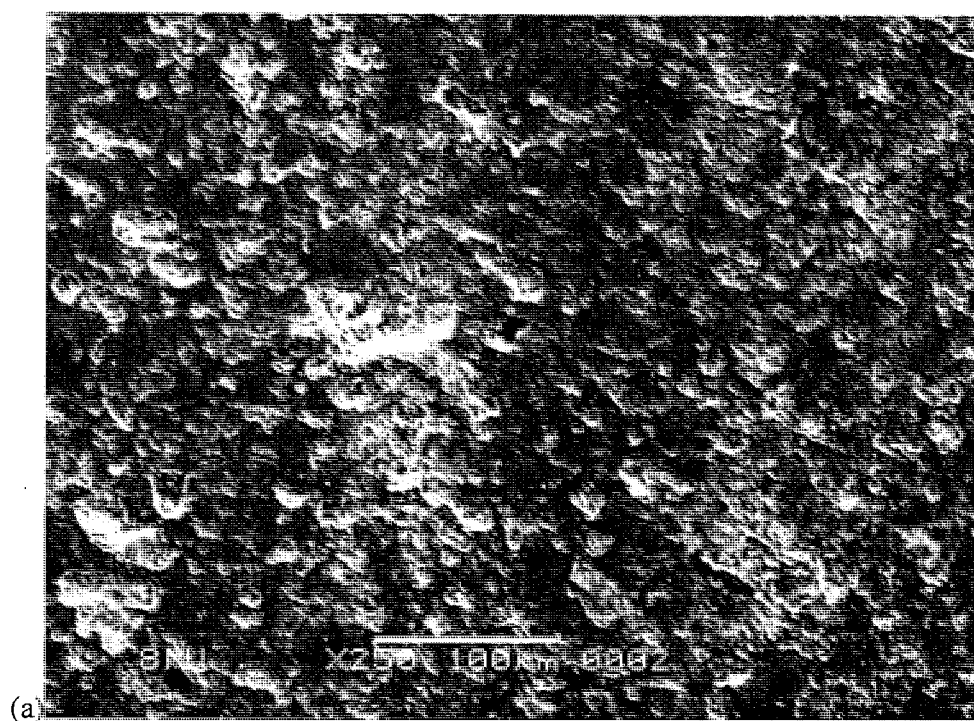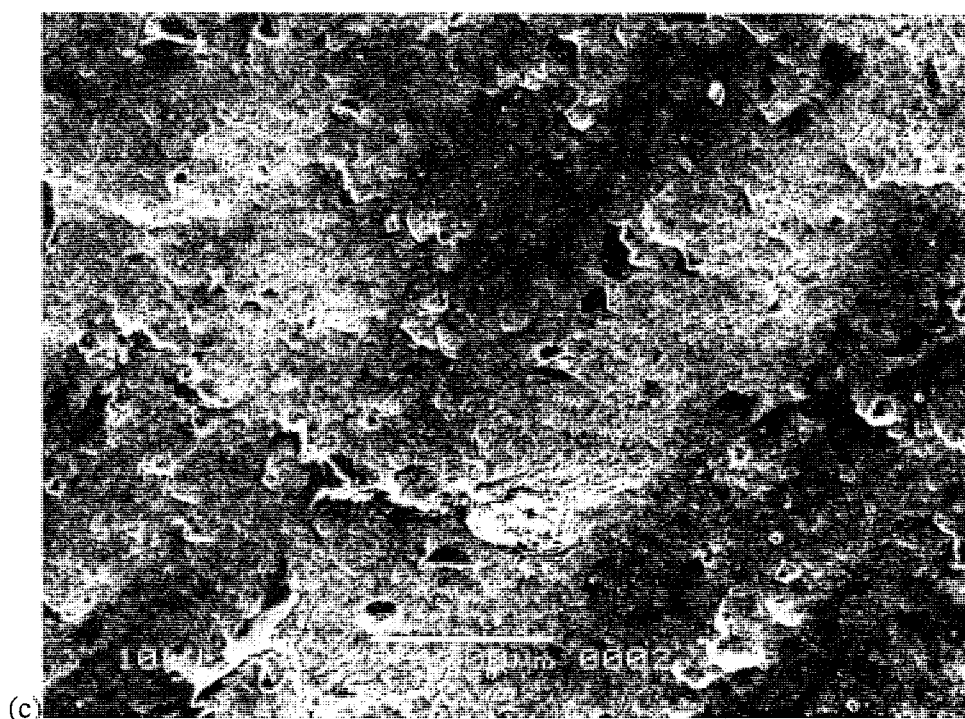
**Figure B.15:** Damage to bromobutyl rubber due to slurry concentration (a) 1% (b) 5% and (c) 10% for particles size range 3.35 to 2.36 mm.



(a)

(b)



(c)
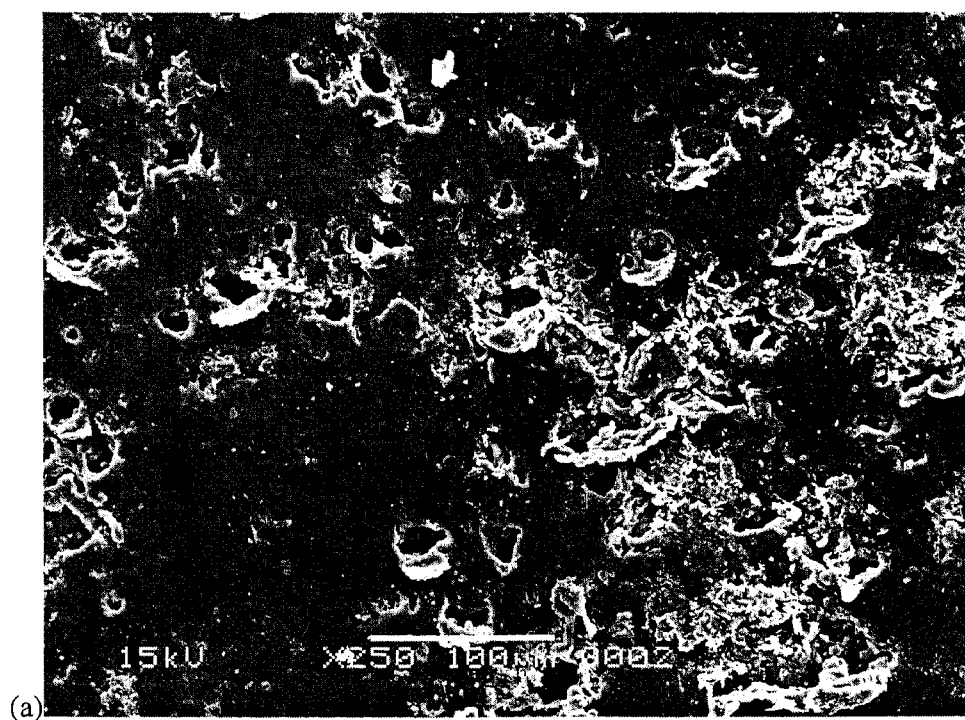
**Figure B.16:** Surface damage to bromobutyl rubber due to erosion duration (a) 50 hours (b) 100 hours and (c) 200 hours for particles size range 6.70 to 4.75 mm.
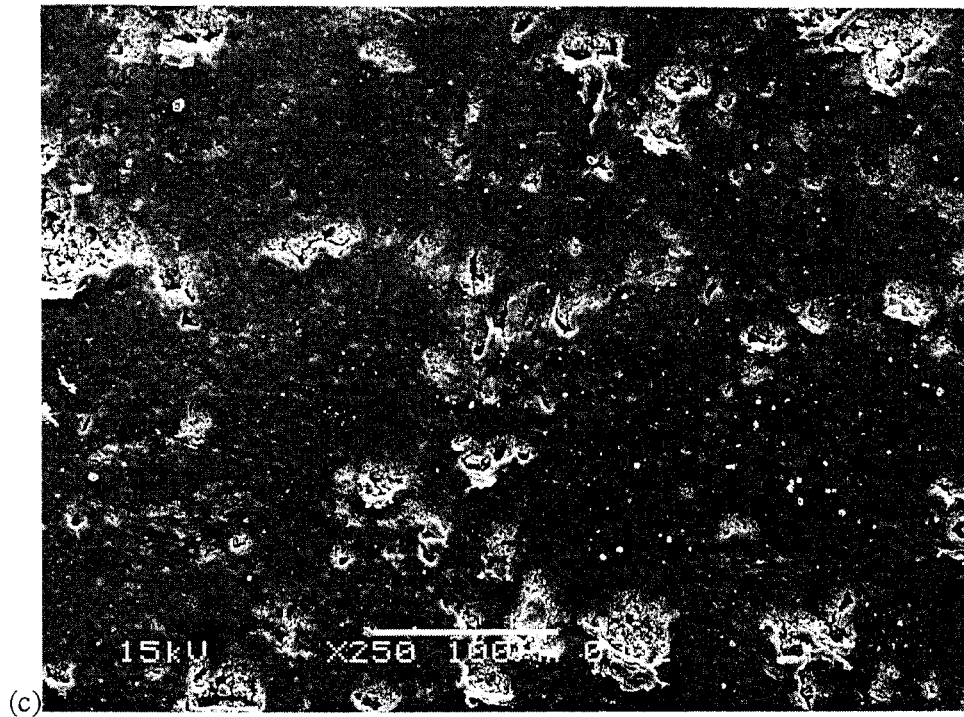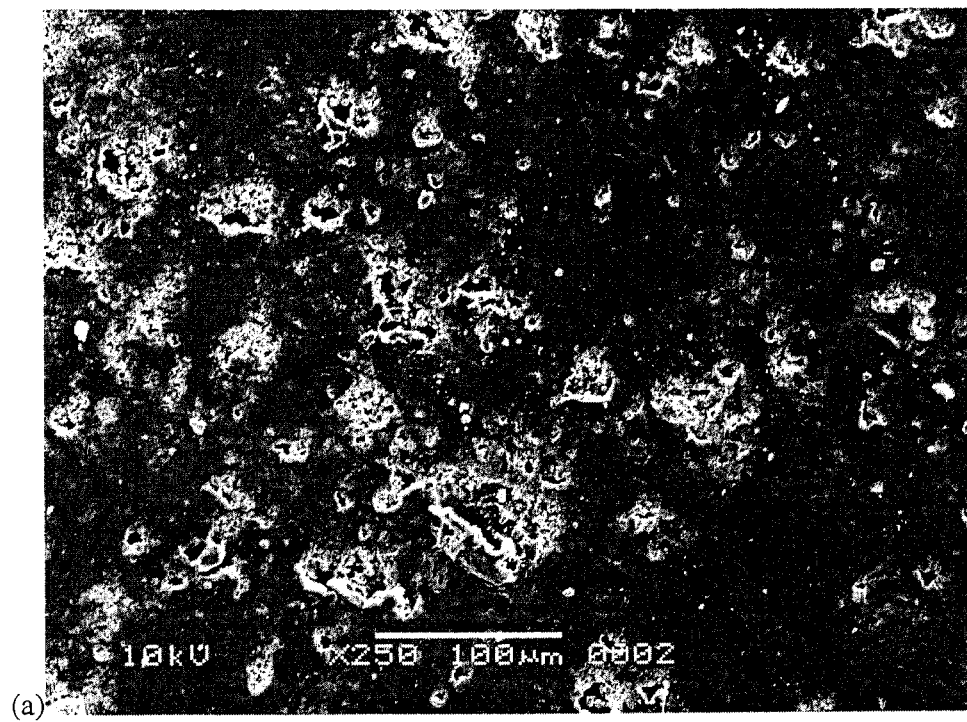
(a)

(b)

(c)

Figure B.17: Surface damage to bromobutyl rubber due to erosion duration (a) 50 hours (b) 100 hours and (c) 200 hours for particles size range 4.75 to 3.35 mm.
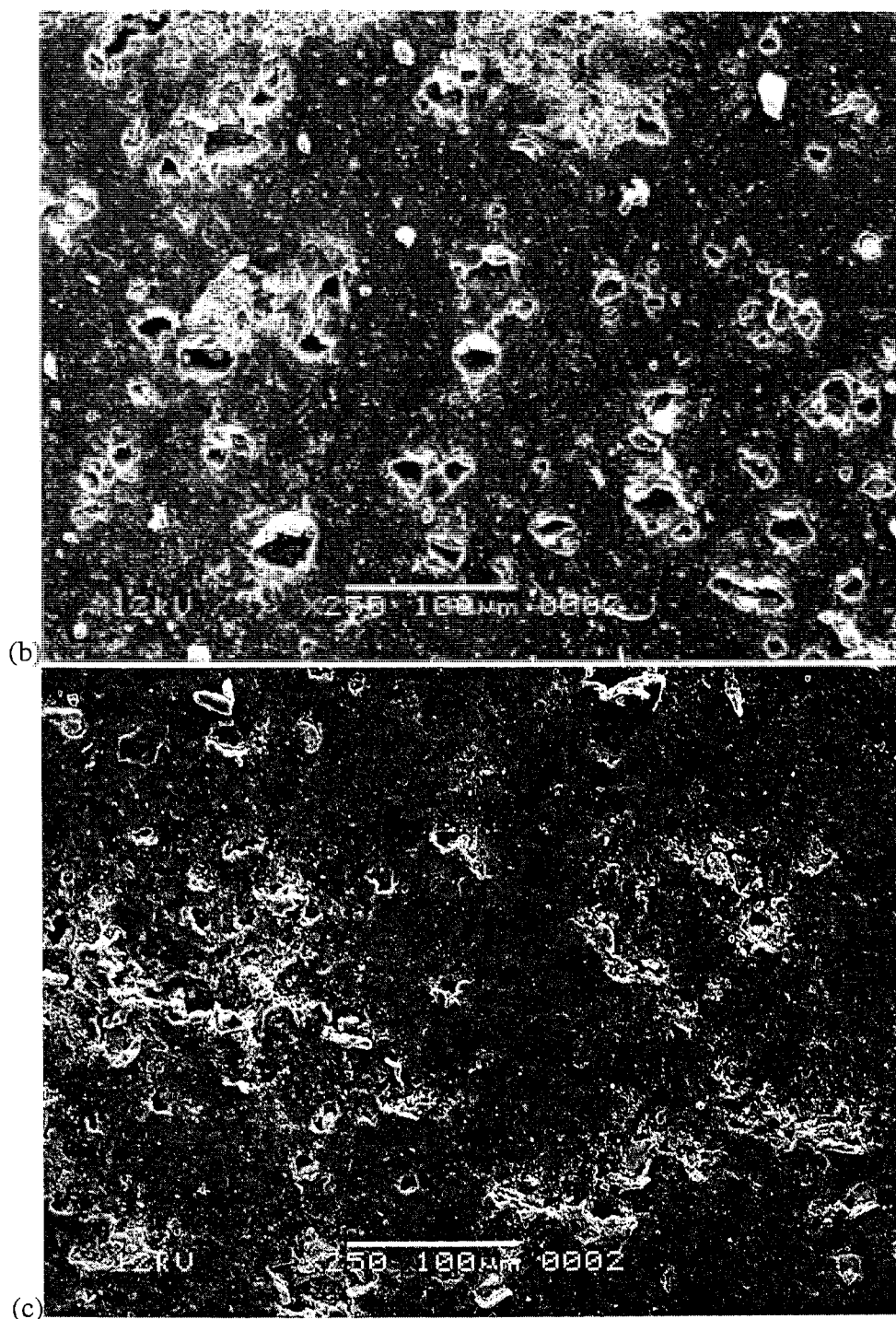


(a)

Figure B.18: Surface damage to bromobutyl rubber due to erosion duration (a) 50 hours (b) 100 hours and (c) 200 hours for particles size range 3.35 to 2.36 mm.